JOINT INSTITUTE FOR AERONAUTICS AND ACOUSTICS

National Aeronautics and
Space Administration

Ames Research Center

Stanford University

JIAA TR - 50

TRANSMISSION OF SOUND ACROSS A VORTEX LAYER ENCLOSING A CYLINDRICAL COLUMN OF JET

Raymond Luh and C.C. Chao

STANFORD UNIVERSITY
Department of Aeronautics and Astronautics
Stanford, California 94305

AUGUST 1982

DISPLAY 18/2/1

83N18407*# ISSUE 8 PAGE 1261 CATEGORY 71 RPT#: NASA-CR-169845 NAS 1.26:169845 SU-JIAA-TR-50 CNT#: NCC2-76 82/08/00 142 PAGES

UNCLASSIFIED DOCUMENT

UTTL: Transmission of sound across a vortex layer enclosing a cylindrical column

JIAA TR - 50

TRANSMISSION OF SOUND ACROSS A VORTEX LAYER ENCLOSING A CYLINDRICAL COLUMN OF JET

RAYMOND LUH AND C. C. CHAO

The work here presented has been supported by the National Aeronautics and Space Administration under NASA Grant NCC2-76.

ACKNOWLEDGMENT

The author wishes to express his deepest appreciation to Professor Chi-Chang Chao for his patience, encouragement and guidance throughout the course of this work. Thanks are due to Professor Harold Levine for the many discussions that were so very helpful and to Professor Krishnamurty Karamcheti for his overall guidance and support as well as for providing financial support through the Joint Institute of Aeronautics and Acoustics. The author also wishes to thank Professor Sotiris Koutsoyannis and Professor I-Dee Chang. Finally, warm thoughts go to the many colleagues (too many to mention by name) for making the author's stay at Stanford a very memorable one.

Present investigation was sponsored by NASA Ames Research Center under Grant NCC 2-76.

TABLE OF CONTENTS

I. INTRODUCTION

The problem of transmission of sound through shear layers has stimulated many investigations for quite some time. The simplest model considers a shear layer of zero thickness or an interface of two fluid media in relative motion known as the plane vortex sheet model. As early as 1944, Landau[19] investigated the stability of such compressible fluid motions which evidenced a discontinuity in tangential velocity at a plane surface. He demonstrated the stability of the vortex sheet, that is, the persistence of infinitesimal displacements from its equilibruim position provided that there is a sufficiently large velocity jump across the discontinuity. The nature of vortex sheet phenomena has acquired a greater importance in connection with theories of jet noise initiated by Lighthill[20] in 1951; specifically, it is appropriate to determine vortex sheet motions in the presence of an incident acoustical excitation. The problem investigated in this thesis concerns, in particular, the interaction of an implusive ring source with a curved vortex sheet which forms the boundary of a cylindrical jet flow.

During the late 1950's numerous studies of reflection and transmission of sound by a vortex sheet due to incident time periodic plane acoustic waves were undertaken; after some initial efforts in which a kinematic boundary condition at the sheet was improperly formulated, Miles[23] (1957) removed this defect and successfully determined the plane wave reflection coefficient. He confirmed Landau's results regarding the stability of small amplitude vortex sheet motions and furthermore drew

attention to the so called neutrally stable motions with large amplitudes of the sheet that do not tend to grow or decay. The designation of resonant mode is given to such a large amplitude excitations of the vortex sheet. Miles' study was paralleled by that of Ribner[28] (1958) who also included transmission as well as reflection in a similar problem; both their studies were relatively simple and significant as prototypes of more complex problems. Miles[24] (1958) also analyzed the displacement of an initially undisturbed plane vortex sheet following a suddenly imposed, spatially periodic velocity disturbance. The resulting stability criterion was shown to be in agreement with that appropriate to the prior time periodic case. Transient wave propagation problems are inherently more difficult than the steady state harmonic ones and it was not until 1969 that Friedland and Pierce[9] determined the reflected field due to an implusive line source embedded in a stationary half-space, separated by a vortex sheet from a moving half-space. Howe[13] (1970) examined a similar problem, locating an impulsive point source close to the vortex sheet and stressed the fact that a correct analysis must account for both the instability and resonance which are left out of the classical ray theory. Subsequently, in a series of papers published in the early 1970's, Jones and Morgan[14-16] and their associates[11-17] investigated various problems of sound-vortex sheet interaction due to line or point sources with time-periodic or impulsive nature and significantly clarified the propagation of instability waves.

Integral transform methods are employed for the analysis of the multi-variable (space-time) problems just mentioned; the technical diffi

culties, which arise predictably at the stage of inverse transformation of the solutions, are approached differently by various investigators. Causality can be ensured when the path of a time inversion integral is suitably located. This is accomplished for instance by Friedland and Pierce before analyzing the response integral with the help of Cagniard's technique which sequentially involves an integration variable change, a contour deformation, and an interchange of order of integration. Although they are able to derive an exact solution for the reflected wave, the physically more significant transmitted wave is set aside as being too difficult. Howe likewise adopts Cagniard's technique in his analysis and by restricting attention to the far field is able to deduce an explicit representation for the transmitted solution which incorporates the instability and resonance waves. Jones and Morgan elected to invert the space Fourier transform first. The solutions thus obtained do not satisfy causality, that is, disturbances may precede the excitation, unless a homogeneous (source free) solution which corresponds to instability waves is added. This additional term is neither a conventional nor a real generalized function, but a delta function with complex arguments or so-called ultra-distribution. It is, in fact, the ultra-distribution thus introduced which helps to clarify the role of instability waves in a transient problem. However, the final form of their solutions is usually too abstract for extracting quantitative estimates of the excitations under consideration.

More recently, Chao[13] (1977) employed the Cagniard's technique and also allowed for ultra-distribution in the inverse analysis; moreover he

was able to express in an exact manner the point source solution in terms of a single finite range integral and to characterize the solution without any integral in the line source case. The solutions which he arrived at are advantageous in that they enable the influence of a plane vortex sheet on an incident impulsive source of sound to be ascertained through uncomplicated numerical evaluations. The outcome confirms the following. First, areas on the vortex sheet reached by the sound waves will now act as source regions which generate transmitted as well as reflected waves in the respective media. Second, for Mach number $M < 2\sqrt{2}$, sound disturbances will cause the vortex sheet to become unstable, resulting in the propagation of instability waves. Finally, when $M > 2$, resonance or neutral stability waves are propagated. Both instability and resonance waves are shown to propagate downstream in a limited wedge-like region close to the vortex sheet.

The success shown by Chao's method has motivated the investigation of a more complicated vortex/source geometry considered in this thesis. Specifically, the configuration chosen involves a curved vortex sheet which forms the boundary between an external medium at rest and a cylindrical jet column, otherwise known as an axisymmetric jet. And for mathematical simplicity as well as practical interest, the source considered here assumes the shape of a circular ring (with negligible internal radius) whose plane is normal to the jet axis and is centered within the jet. Both fluids are assumed to have the same density and speed of sound to keep the details simple and all non-linearities including those of viscosity and heat conduction are neglected.

The stability of axisymmetric jets was first discussed by Batchelor and Gill[2] (1962) and then in a similar fashion by Crow and Champagne[16] (1970), with criteria that involved not only the jet speed but also the wavelength of the primary sound source. Their works were significant in strongly suggesting that instability in jets is temporal, i.e. time-wise, in nature. The mathematical problem of cylindrical vortex layer instability under the influence of a time periodic pressure fluctuation was first investigated by Tam[29] (1971) but his solution simplified to that of a plane vortex sheet due to the nature of his approximation. However, his work was significant in linking the instability predicted by the vortex sheet model with the strong directional acoustic radiations from supersonic jets observed in some experiments. Morgan[26] (1975) was actually the first to obtain a solution for the transmitted sound field in the motionless fluid outside an axisymmetric subsonic jet, due to a harmonic point source located off axis within the jet. He rigorously proved that there is essentially only one instability wave which arises, and that therefore an infinite number of other waves which are solutions to the homogeneous problem can be ignored. This investigation differs from that effected by Morgan in so far as a ring rather than a point source is used and furthermore that both subsonic and supersonic flows are contemplated.

The organization and method chosen here for analysis are as follows. In Chapter II, the problem is formulated and its solution in the Fourier transformed space is obtained in the form of a multiple integral whose integrand involves complicated Bessel and Hankel functions. Chapter III contains the derivation of an approximate version of the integral solution

for the transmitted field; this is based on the assumption that the jet source radii are sufficiently large so that the two leading terms from the appropriate asymptotic (large argument) series expansions of Bessel and Hankel functions can be used. It is shown that proper attention is required on the different forms of Bessel function expansions over the argument regions. As a limiting case of both radii becoming arbitrarily large but retaining a finite difference between them, the first term is shown to reproduce the exact solution to the simplest model previously described, i.e. the transmitted field across a plane vortex sheet due to a line source embedded in the flow medium. The second term corresponds to the first order curvature effects. In approximating with these expansion terms, contributions arising from internal reflections are isolated and neglected, leaving a representation for only the primary or directly transmitted field. Howe[13] (1970) suggests that instability becomes significant after a time which is long enough for sound to travel backwards and forwards several times between opposite faces of the jet, when the acoustic coupling between these faces becomes large. The present analysis essentially calculates the transmitted field due to that sound which is emitted before these internal reflection effects become important.

Singularities of the integrand are examined in Chapter IV prior to the inverse analysis. The branch points and the real pole which exists when $M > 2$ associated with neutral stability wave are identical to that found in the plane vortex sheet case. However, the instability pole is shown to be a function of wavenumber as well as frequency in contrast to the plane case where it is independent of the former. Furthermore, as the pole remains

complex for all Mach numbers, its transition to the neutral stability mode observed in the plane case does not take place. The coupling that exists between frequency and wavenumber in the integrand is responsible for this difference and indubitaly acts to complicate the inverse analysis. The condition of causality would be satisfied unambiguously if the double integral is carried out first with respect to frequency, but a procedure is not found to do this. Instead, in a fashion similar to Chao's application of Cagniard's technique, a change in the order of integration is facilitated by deforming the frequency integration contour consistent with causality. In the plane case, this then leads to the simple solution forms alluded to previously. The solution obtained here is expectedly less simplex. Due to the curvature effects, the solution now exhibits a radial decay factor of $1/\sqrt{r}$. In the evaluation for the specularly transmitted field, a branch point particular to the present problem is produced. As a result, in addition to the term that is similar to the corresponding field for the plane case, a second term arises from integration along the resulting branch cut. Evaluation of this branch cut integration is accomplished numerically by Gaussian interpolation. Related to neutral stability wave for $M > 2$ is a pole in the wavenumber space which is again distinctive to the curved vortex sheet problem as a consequence of its curvature being finite. This pole results in an additional term that is shown to decay exponentially away from the neutral stability wave and thus appears to effect a broadening of its singular wavefront.

The integral that remains unresolved is one in which the moving instability pole is directly involved. An analysis of this integral is

presented in Chapter V where the essential features of instability wave is made relevant. First, it is shown that in the limit of $kr_0 \to \infty$ where k is the wavenumber and r_0 is the jet radius, the pole reduces to the instability pole for the plane case as anticipated. The pole is observed to move when kr_0 is varied, but as kr_0 becomes small, its movement cannot be adequately described by the approximate form derived from the two-term asymptotic expansions. Even though several terms would be needed to approximate the profile generated by the moving pole, it is shown that only one additional term is sufficient in establishing the general trend. A clear picture emerges when movement of the pole is determined for small kr_0 as well by taking the leading terms in the convergent power series of the cylinder functions. From these considerations, the way in which the pole moves is approximated for all Mach numbers. Of particular interest is for $M > 2\sqrt{2}$ where neutral stability instead of instability is predicted in the plane case because the complex pole becomes real. Here the pole is real only in the $kr_0 \to \infty$ limit but remains complex for other values indicating the persistence of instability even for such high Mach numbers. As a consequence, $M = 2\sqrt{2}$ is not a clear cut transition point as predicted in the case of a plane vortex sheet that when $M < 2\sqrt{2}$ the system is unstable and when $M > 2\sqrt{2}$ the system is neutrally stable. In fact, instability waves may arise at all Mach numbers but further analysis shows that they are dependent on kr_0 and cease to exist for sufficiently small kr_0. In other words, instability waves will be caused by wavelengths large (high frequency) compared to the jet radius for all Mach numbers. The way in which this dependence takes effect is also shown to relate to the spatial extent of instability wave's presence, which is seen to con-

tract towards the vortex sheet with increasing wavelength. This prediction appears to be in agreement with the strong directional acoustic radiation observed in some jet noise experiments. In Chapter VI, some numerical results are presented and discussed.

The idealized problem of the curved vortex sheet enclosing a cylindrical column of jet presented in this thesis is of particular interest since it is a first approximation to the real jet. As a next step in the modelling, it is desirable to include a rigid attachment to the flow to simulate a jet nozzle. This will bring out any contribution to the noise generation process of edge scattering which may in fact be extremely important in the overall picture. Problems associated with edge scattering have mixed boundary values and are in general rather difficult to handle. Nevertheless, a significant literature on that subject exists, including contributions by Crighton[4] (1972), Crighton & Leppington[5] (1974), and more recently by Miura[25] for the plane case and by Munt[27] (1977) for the curved case, just to mention a few. It is also desirable to consider a finite shear layer instead of an infinitesimally thin vortex sheet since in all practicality it never occurs even near the jet nozzle exit because of boundary layer. Some investigators have ventured into plane shear layer models such as Graham & Graham[10] (1968), Jones[17] (1977), and Koutsoyannis[18] (1980) for example, but none has considered a curved shear layer.

II. FORMULATION OF THE PROBLEM

Consider the problem in which a cylindrical column of jet fluid moves axially through a similar stationary fluid medium, extending over the entire space. The two fluids are ideally separated by a vortex layer that is equivalent to a shear layer of zero thickness. The jet is taken with its axis along the z-axis of a cylindrical polar coordinate system (r, θ, z) and to have constant speed U and radius r_o. Within the jet, oriented along the z 0 plane, is placed a ring shaped mass source of radius r_s as shown in Figure II-1.

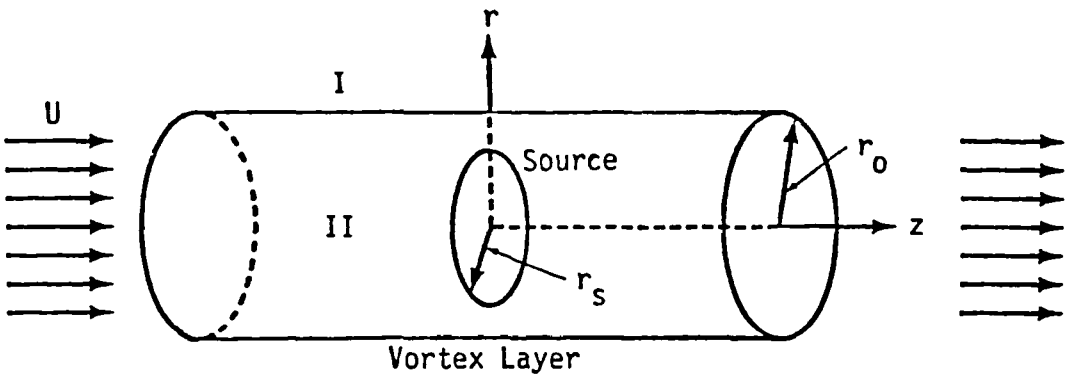

FIGURE II-1 Sketch of the Problem Geometry

Without affecting the underlying phenomena, both fluids are assumed to have the same speed of sound and density to keep the details simple. All nonlinear effects including those of viscosity and thermal conductivity will be ignored, which is expected to introduce some uncertainties, especially in the amplitude prediction of instability waves. Because of

the axisymmetric nature of the problem, all quantities are independent of Θ variation and the equations satisfied by the velocity potential $\phi\ (r, z, t)$ are then as follows:

in region I outside the jet

$$\frac{1}{a^2}\ \frac{\partial \phi_1}{\partial t^2} - \nabla^2 \phi_1 = 0 \qquad r > r_o \qquad \text{(II-1)}$$

in region II inside the jet

$$\frac{1}{a^2}\left(\frac{\partial}{\partial t} + U\frac{\partial}{\partial z}\right)^2 \phi_2 - \nabla^2 \phi_2 = \frac{Q\delta(z)\delta(r - r_s)\delta\ (t)}{2\pi r_s} \qquad r < r_o \qquad \text{(II-2)}$$

where

$$\nabla^2 = \frac{\partial^2}{\partial r^2} + \frac{1}{r}\frac{\partial}{\partial r} + \frac{\partial^2}{\partial z^2} \qquad \text{(II-3)}$$

a is the speed of sound and Q is the strength of the ring source which is impulsively activated, i.e. turned on and off at time t = 0. The plane vortex sheet geometry is a special case of the above when r_o and r_s become arbitrarily large. Then, by the fact that $Q = 2\pi r_s q$, where q is the source strength per unit length, Equations II-1 & 2 are replaced by:

$$\frac{1}{a^2}\ \frac{\partial^2 \phi_1}{\partial t^2} - \nabla^2 \phi_1 = 0 \qquad y > o \qquad \text{(II-1a)}$$

$$\frac{1}{a^2}\left(\frac{\partial}{\partial t} + U\frac{\partial}{\partial x}\right)^2 \phi_2 - \nabla^2 \phi_2 \qquad y < o \qquad \text{(II-2a)}$$

$$= q\,\delta(x)\,\delta(y + y_s)\,\delta(t)$$

where now

$$\nabla^2 = \frac{\partial^2}{\partial x^2} + \frac{\partial^2}{\partial y^2} \qquad \text{(II-3a)}$$

x being the axial coordinate of the rectangular coordinate system (x,y,z), the vortex sheet being located at $y = 0$, and the line source at $y = -y_s$, $x = 0$. This line source problem had been investigated by Chao[4] and his results will form a basis for comparison with the present problem.

There are two matching conditions at the common boundary $r = r_o$ of the two regions of irrotational motion. The dynamical condition that the pressure is continuous across the boundary gives

$$\frac{\partial \phi_1}{\partial t} = \frac{\partial \phi_2}{\partial t} + U \frac{\partial \phi_2}{\partial z} \qquad \text{(II-4)}$$

The kinematic condition for equal particle displacement η on both sides of the vortex layer gives

$$\frac{\partial \phi_1}{\partial r} = \frac{\partial \eta}{\partial t} \quad , \quad \frac{\partial \phi_2}{\partial r} = \frac{\partial \eta}{\partial t} + U \frac{\partial \eta}{\partial z} \qquad \text{(II-5)}$$

In addition, there are the following conditions that must be satisfied by the solution. The radiation condition requires that the field

be radiating outwards at infinity, the finiteness condition is required at the center of the jet that insures no blow up of the solution there, and finally the causality condition, which states that the field be unperturbed before time t = 0, will apply.

Define $\psi\ (r,k,\omega)$, the Fourier transform of $\phi\ (r,z,t)$ as:

$$\psi_j = \frac{1}{4\pi^2} \int_{\infty}^{\infty}\int_{\infty}^{\infty} \phi j\ e^{\,i(\omega t - kz)}\, dz\, dt \qquad \text{(II-6a)}$$

$$\phi_j = \int_{ck} \int_{c\omega} \psi j\ e^{-i\,(\omega t - kz)}\, d\omega\, dk \qquad \text{(II-6b)}$$

where j = 1, 2, and C_k and C_ω are integration contours in the wave number k-plane and the frequency ω-plane respectively which will satisfy the causality condition.

Then Eqs. II-1 & 2 reduce to

$$\left(\frac{d^2}{dr^2} + \frac{1}{r}\frac{d}{dr}\right)\psi_1 + \gamma_1^2 \psi_1 = 0 \qquad \text{(II-7)}$$

$$\left(\frac{d^2}{dr^2} + \frac{1}{r}\frac{d}{dr}\right)\psi_2 + \gamma_2^2 \psi_2 = -\frac{Q\,\delta(r-r_s)}{8\pi^3 r_s} \qquad \text{(II-8)}$$

where

$$\gamma_1^2 = \frac{\omega^2}{a^2} - k^2$$

$$\gamma_2^2 = \left(\frac{\omega}{a} - kM\right)^2 - k^2 \qquad \text{(II-9)}$$

$M = U/A$ is the Mach number of the flow.

The boundary conditions at $r = r_s$, Eqs. II-4 & 5 become:

$$\omega \psi_1 = (\omega - Uk) \psi_2 \qquad \text{(II-10)}$$

$$(\omega - Uk) \frac{d\psi_1}{dr} = \omega \frac{d\psi_2}{dr} \qquad \text{(II-11)}$$

Eqs. II-7 & 8 can be recognized as the zeroth order Bessel's equations and the solution to Eq. II-7 which is for region I is

$$\psi_1 = A_1 H_o^{(1)} (\gamma_1 r) + B_1 H_o^{(2)} (\gamma_1 r) \qquad \text{(II-12)}$$

where $H_o^{(1)}$ and $H_o^{(2)}$ are Hankel functions of the first and second kind respectively, and A_1, B_1 are constants to be determined. The γ's are generally complex and if the argument of γ_1 is restricted to non-negative values, i.e., $Im(\gamma_1) > 0$, then by the radiation condition, $B_1 = 0$ and ψ_1 reduces to

$$\psi_1 = A_1 H_o^{(1)} (\gamma_1 r) \qquad \text{(II-13)}$$

For region II, the solution to Eq. II-8 can be put down as:

$$\psi_2 = A_2 J_o (\gamma_2 r) + B_2 Y_o (\gamma_2 r) \qquad \text{(II-14)}$$

where J_o and Y_o are Bessel's functions of the first and second kind respectively, and as the equation has an inhomogeneous right hand side, A_2 and B_2 are functions of r determined by the variation of parameters. Thus,

$$A_2 = \frac{Q}{16\pi^2} Y_o (\gamma_2 r_s) H (r - r_s) + C_1$$

and

$$B_2 = - \frac{Q}{16\pi^2} J_o (\gamma_2 r_s) H (r - r_s) + C_2 \qquad \text{(II-15)}$$

where C_1 and C_2 are constants to be determined and H stands for Heaviside function.

It is to be noted that in the limiting case of $r_s \to 0$, $Y_o \to \infty$. However, with $H(r - r_s) = 1 - H(r_s - r)$, A_2 can be rewritten as

$$A_2 = - \frac{Q}{16\pi^2} Y_o (\gamma_2 r_s) H (r_s - r) + C_1' \qquad \text{(II-16)}$$

where now as $r_s \to 0$, $A_2 \to C_1'$.

By the finiteness condition, C_2 is necessarily zero since as $r \to 0$, $Y_o \to -\infty$. Therefore, Eq. II-14 becomes

$$\psi_2 = C_1' \, J_o (\gamma_2 r) - \frac{Q}{16\pi^2} \, S_H (r) \qquad \text{(II-17)}$$

where $S_H(r) = Y_o (\gamma_2 r_s) J_o (\gamma_2 r) H (r_s - r) + J_o (\gamma_2 r_s) Y_o(\gamma_2 r) H(r - r_s)$. Even though the condition $\mathrm{Im}(\gamma_2) > 0$ is not required, that branch is assumed for consistency with γ_1 and this choice also happens to yield a better form. The constants A_1 and C_1' can now be solved by applying boundary conditions Eqs. II - 10 & 11.

$$A_1 = \frac{Q \, \omega(\omega - UK) \, J_o (\gamma_2 r_s)}{8\pi^3 r_o S_J}$$

and

$$C_1' = \frac{Q \, J_o (\gamma_2 r_s) \, S_Y}{16\pi^2 S_J} \qquad \text{(II-18)}$$

where $S_J = \gamma_1 (\omega - UK)^2 H_1^{(1)} (\gamma_1 r_o) J_o (\gamma_2 r_o) - \gamma_2 \omega^2 H_o^{(1)} (\gamma_1 r_o) J_1 (\gamma_2 r_o)$

$S_Y = \gamma_1 (\omega - UK)^2 H_1^{(1)} (\gamma_1 r_o) Y_o (\gamma_2 r_o) - \gamma_2 \omega^2 H_o^{(1)} (\gamma_1 r_o) Y_1 (\gamma_2 r_o)$

Finally, the transformed solutions are obtained as:

$$\psi_1 = \frac{Q \, \omega(\omega - UK) \, J_o \, (\gamma_2 r_s) \, H_o^{(1)} (\gamma_1 r)}{8\pi^3 r_o \, S_J} \qquad \text{(II-19)}$$

and

$$\psi_2 = \frac{Q}{16\pi^2}\left[\frac{J_o(\gamma_2 r_s)\, J_o(\gamma_2 r)\, S_\gamma}{S_J} - S_H(r)\right] \qquad \text{(II-20)}$$

The purpose of this work is to derive for the transmitted field exterior of the jet alone, and therefore only Eq. II-19 will be dealt with for its inverse. This, in reality, is clearly of more practical value and interest than the corresponding reflected field internal to the jet. However, one may seek to find it as well by inverting Eq. II-20 in a manner similar to that which will be described in the following text, although more difficulties are expected, as ψ_2 appears substantially more complex than ψ_1. The integral in question is given by Eq. II-6b and substituting Eq. II-19 into it gives:

$$\phi_1 = \frac{Q}{8\pi^3 r_o}\int_{-\infty}^{\infty}\int_{-\infty+i\varepsilon}^{\infty+i\varepsilon} \frac{\omega(\omega-UK)\, J_o(\gamma_2 r_s) H_o^{(1)}(\gamma_1 r)}{S_J} e^{-i(\omega t-kz)}\, d\omega dk \qquad \text{(II-21)}$$

A brief discussion on the selection of integration contours is appropriate here. Note that integration with respect to time is to be carried out prior to space. This is to ascertain that the causality condition can be dealt with rigorously and unambiguously. If space integration was to be performed first, then the contour C_k does not have a clear cut choice and one may obtain a solution which is non-causal. The way in which causality is satisfied is by selecting an ε large enough such that any and all

singularities associated with the integrand will lie below the contour. This requires that none of the zeros of S_J be at infinity, an assumption which will be shown to hold in a later section. It is then apparent that the field is quiet before time t = 0 by invoking Jordan's Lemma. Since the causality condition is duly fulfilled in the time domain and there isn't a comparative condition in the space domain, C_K assumes the usual intergration contour along the real axis.

The proposed method of attack is in the spirit of so-called Cagniard's method which was in wide application on seismic wave propagation problems until recent times. The method may be summarized in simple terms as a sequence of a change of integration variable, a contour deformation, and an exchange in the order of integration. Friedland and Pierce[9] were first to apply this method on any problem involving wave propagation in fluid mediums. Its success depends largely on the particular contour chosen for deformation, as examplified by Chao[3].

First, make the change of variable. Let

$$\xi = \frac{\omega}{ka} \tag{II-22}$$

which is the complex phase speed. This differs from the original Cagniard's method in which k/ω or the wave slowness is the new variable. Eq. II-21 becomes

$$\phi_1 = \frac{aQ}{8\pi^3 r_o} \int_{-\infty}^{\infty} \int_{C(k)} \frac{\xi(\xi-M) J_o(k\Gamma_2 r_s)\, H_o^{(1)}(k\Gamma_1 r)}{S_J'} e^{-ik(\xi at - z)}\, d\xi\, dk \qquad \text{(II-23)}$$

where

$$S_J' = \Gamma_1(\xi-M)^2 H_1^{(1)}(k\Gamma_1 r_o) J_o(k\Gamma_2 r_o) - \Gamma_2 \xi^2 H_o^{(1)}(k\Gamma_1 r_o) J_1(k\Gamma_2 r_o) \qquad \text{(II-24)}$$

and

$$k\Gamma_1 = k\,(\xi^2 - 1)^{\frac{1}{2}} = \gamma_1$$

$$k\Gamma_2 = k\left[(\xi-M)^2 - 1\right]^{\frac{1}{2}} = \gamma_2 \qquad \text{(II-25)}$$

The contour $C_\xi = C(k)$ is now a function of k in accordance with Eq. II-22 and is shown below. It consists of two horizontal paths such that all the singularities lie below C_+ when $k > 0$ and above C_- when $k < 0$. The causality condition is observed by again applying Jordan's Lemma.

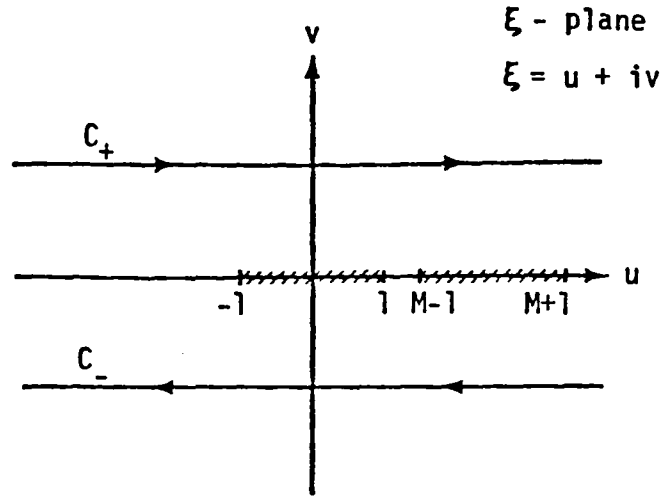

Figure II-2 Integration Contour C(k) and Branch Cuts for Γ_1, Γ_2

Γ_1 and Γ_2 defined by Eq. II-25 have four branch points at

$$\xi = \pm 1 \quad \text{and} \quad \xi = M \pm 1$$

To satisfy the commitment made previously which restricts $\text{Im}(\gamma_1) > 0$ and $\text{Im}(\gamma_2) > 0$, the imaginary parts of Γ_1 and Γ_2 must have the same sign as k while integrating along C(k) in the ξ-plane. Accordingly, branch cuts are placed as illustrated in Fig. II-2. This restricts each of the arguments of $\xi \pm 1$ and $\xi \pm 1 - M$ between the range of $-\pi$ and π while the range of argument for both Γ_1 and Γ_2 will fall within 0 and π above or $-\pi$ and 0 below the real axis for all points, thus automatically satisfying the requirement on the Γ's. Due to the complex nature of Eq.

II-23, an exact expression for ϕ_1 is not possible and some approximations will have to be made next.

III. THE APPROXIMATE SOLUTION

a. ASYMPTOMATIC EXPANSION OF BESSEL FUNCTIONS

Carrying out the exact inverse transform as presented by Eq. II-23 has not been possible because of the complicated Bessel and Hankel functions in the integrand. These cylinder functions are now approximated. First, observe their arguments to contain r_o, the jet radius, r_s, the source radius, and r, the radial distance out from the jet. These are physical parameters which can and will be assumed to be large for the present problem. Then, provided $k\Gamma_1$ and $k\Gamma_2$ remain finite, the asymptotic (large argument) series expansions of the cylinder functions can be used. Γ_1 and Γ_2 can never be zero since all their zeros must lie within the strip bounded by the integration contours $C_{\pm}$. But the integral in k clearly will pass through zero and the arguments will become vanishingly small near that point. However, it will be shown that contribution from small k can be ignored except in dealing with instability. The expansions for Hankel functions are:

$$H_o^{(1)}(z) = \sqrt{\frac{2}{\pi z}}\left[1 - \frac{i}{8z}\right] e^{i\left(z - \frac{\pi}{4}\right)}$$

$$H_1^{(1)}(z) = \sqrt{\frac{2}{\pi z}}\left[1 + \frac{i3}{8z}\right] e^{i\left(z - \frac{3\pi}{4}\right)} \qquad -\pi < \arg z < 2\pi \qquad \text{(III-1)}$$

But the expansions for Bessel functions take on different forms.

$$J_0(z) = \frac{1}{2}\sqrt{\frac{2}{\pi z}}\left\{\left[1 + \frac{i}{8z}\right] e^{-i(z - \frac{\pi}{4})} \pm \left[1 - \frac{i}{8z}\right] e^{i(z - \frac{\pi}{4})}\right\}$$

$$J_1(z) = \frac{1}{2}\sqrt{\frac{2}{\pi z}}\left\{\left[1 - \frac{i3}{8z}\right] e^{-i(z - \frac{3\pi}{4})} \pm \left[1 + \frac{i3}{8z}\right] e^{i(z-\frac{3\pi}{4})}\right\} \quad \text{(III-2)}$$

where plus is for $-\pi < \arg z < \pi$ and minus for $0 < \arg z < 2\pi$.

While asymptotic expansions of functions with complex arguments may vary in different regions, they usually do not take on different forms in an overlapping region as indicated by Eq. III-2. That the expansions for J_0 and J_1 differ by the small term in the range of argument between 0 and π is recognized as Stokes' phenomenon, so called because it was first discovered by Stokes[30] in 1857. It has been confirmed in the present study that a correct analysis must account for this subtle difference. This situation does not arise if only one term in the expansion series is used as Tam[29] did in his analysis. But the solution then simplifies to that for the plane case because curvature effects enter through higher order terms. The two forms of expansions for $J(z)$ are each applied in the following manner. Recall in Chapter II the branch cuts of Γ_1 and Γ_2 are defined so that their arguments fall within $-\pi$ and π. This means for $k > 0$,

$$-\pi < \arg(k\Gamma_j) < \pi$$

but for $k < 0$,

$$0 > \arg(k\Gamma_j) < 2\pi, \quad j = 1, 2$$

By approximately combining Eq. III-1 with Eq. III-2, the following approximation is obtained.

$$\left.\begin{aligned} J_o\,(kr_s\Gamma_2)\,H_o^{(1)}(kr\Gamma_1) &= \frac{1}{\pi k\sqrt{r\,r_s\Gamma_1\Gamma_2}}\left[D_1 e^{ik(r\Gamma_1 - r_s\Gamma_2)} \mp E_1 e^{ik(r\Gamma_1 + r_s\Gamma_2)}\right] \\ J_o\,(kr_o\Gamma_2)\,H_1^{(1)}(kr_o\Gamma_1) &= \frac{1}{\pi kr_o\sqrt{\Gamma_1\Gamma_2}}\left[D_2 e^{ikr_o(\Gamma_1-\Gamma_2)} \mp E_2 e^{ikr_o(\Gamma_1+\Gamma_2)}\right] \\ J_1\,(kr_o\Gamma_2)\,H_o^{(1)}(kr_o\Gamma_1) &= \frac{1}{\pi kr_o\sqrt{r_1\,r_2}}\left[D_3 e^{ikr_o(\Gamma_1-\Gamma_2)} \mp E_3 e^{ikr_o(\Gamma_1+\Gamma_2)}\right] \end{aligned}\right\} \quad \text{(III-3)}$$

where plus sign is for $k < 0$ and negative sign for $k > 0$.

In the above,

$$\begin{aligned} D_1 &= 1 + \frac{i}{8k}\left(\frac{1}{r_s\Gamma_2} - \frac{1}{r\Gamma_1}\right) \\ D_2 &= \frac{1}{8k\,r_o}\left(\frac{1}{\Gamma_2} + \frac{3}{\Gamma_1}\right) - i \\ D_3 &= \frac{1}{8kr_o}\left(\frac{3}{\Gamma_2} + \frac{1}{\Gamma_1}\right) + i \\ E_1 &= \frac{1}{8k}\left(\frac{1}{r_s\Gamma_2} + \frac{1}{r\Gamma_1}\right) + i \\ E_2 &= 1 - \frac{i}{8kr_o}\left(\frac{1}{\Gamma_2} - \frac{3}{\Gamma_1}\right) \\ E_3 &= 1 + \frac{i}{8kr_o}\left(\frac{3}{\Gamma_2} - \frac{1}{\Gamma_1}\right) \end{aligned} \quad \text{(III-4)}$$

Now, to show that contributions from small k can be ignored, leading terms from the power series expansions of the cylinder functions are substituted into the integrand of Eq. II-23.

$$- \frac{\xi(\xi - M) \quad \ln\left(\frac{k r \Gamma_1}{2}\right)}{\frac{1}{k r_o \Gamma_1}\left[\Gamma_1(\xi - M)^2 + \Gamma_2 \xi^2 \quad \frac{(k r_o \Gamma_1)^2}{2} \quad \ln\left(\frac{k r_o \Gamma_1}{2}\right)\right]} \tag{III-5}$$

In the limit of $k \to 0$, the above quantity can be seen to vanish except at the zeros of the denominator. When treating with instability, its effect on the integral will be studied. Here, Eq. II-23 is replaced by the approximate form using Eqs. III-3 and 4.

$$\phi_1 = \frac{aQ}{8\pi^3\sqrt{r_s r}} \left\{ \int_{-\infty}^{0} \int_{c^-} \frac{\xi(\xi - M)\, D_1 \left[1 + \frac{E_1}{D_1} e^{i2kr_s\Gamma_2} \right] e^{ikf}}{\sigma_1 \left[1 - \frac{\sigma_2}{\sigma_1} e^{i2k\, r_o \Gamma_2} \right]} \, d\xi \, dk \right.$$

$$\left. + \int_{0}^{\infty} \int_{c^+} \frac{\xi(\xi - M) D_1 \left[1 - \frac{E_1}{D_1} e^{\, i2kr_s\Gamma_2} \right] e^{ikf}}{\sigma_1 \left[1 + \frac{\sigma_2}{\sigma_1} e^{i2kr_o\Gamma_2} \right]} \right\} d\xi \, dk \tag{III-6}$$

where

$$f = z + \Gamma_1 (r - r_o) + \Gamma_2 (r_o - r_s)\, \xi \text{ at} \tag{III-7}$$

$$\sigma_1 = \frac{1}{8kr_o\Gamma_1\Gamma_2} (\Gamma_1^2 - \Gamma_2^2)(1 - 3\Gamma_1\Gamma_2) - i(\Gamma_1 + \Gamma_2)(1 + \Gamma_1\Gamma_2)$$

$$\sigma_2 = \frac{i}{8kr_o\Gamma_1\Gamma_2} (\Gamma_1^2 - \Gamma_2^2)(1 + 3\Gamma_1\Gamma_2) - (\Gamma_1 - \Gamma_2)(1 - \Gamma_1\Gamma_2) \quad \text{(III-8)}$$

This expression represents the transmitted field from a large ring-shaped source positioned within a cylindrical jet of large radius r_o with the source plane normal to the jet axis. Hence, the radial field distance r is at least as large as r_o. In the special case of r_o and r_s becoming arbitrarily large but retaining a finite difference between them, Eq. III-6 reduces to

$$\phi_1 = \frac{iaq}{4\pi^2} \int_{-\infty}^{\infty} \int_{c(k)} \frac{\xi(\xi - M) e^{ik\left[z + \Gamma_1 y + \Gamma_2 y_s - \xi at\right]}}{(\Gamma_1 + \Gamma_2)(1 + \Gamma_1\Gamma_2)} \, d\xi \, dk \quad \text{(III-9)}$$

which is not unexpectedly the exact solution to the line source problem as stated by Eqs. II-1a through 3a. Hence, it may be concluded that the small k or high frequency effects may be lost when a real jet is approximated by a plane vortex sheet.

b. FURTHER APPROXIMATIONS

The approximate expression of Eq. III-6 for the transmitted field ϕ_1 is still too complex for evaluation and further approximations are necessary. An examination of the integrand shows its denominator to con

tain a term exponentially small due to the fact that $\mathrm{Im}(k\Gamma_2) > 0$, and this permits the following series expansions:

$$\left[1 \mp \frac{\sigma_2}{\sigma_1} e^{i2kr_o\Gamma_2}\right]^{-1} = 1 \pm \frac{\sigma_2}{\sigma_1} e^{i2kr_o\Gamma_2} + \left(\frac{\sigma_2}{\sigma_1}\right)^2 e^{i4kr_o\Gamma_2} \pm \ldots. \qquad \text{(III-10)}$$

Rewrite Eq. III-6 as

$$\phi_1 = \frac{aQ}{8\pi^3\sqrt{r_s r}} \left\{ \int_{-\infty}^{o}\int_{c^-} \frac{\xi(\xi-M)D_1}{\sigma_1}\left[1+\frac{E_1}{D_1} e^{i2kr_s\Gamma_2} + \frac{\sigma_2}{\sigma_1} e^{i2kr_o\Gamma_2} + \ldots.\right] e^{ikf}\, d\xi\, dk + \int_{o}^{\infty}\int_{c^+} \frac{\xi\,(\xi-M)D_1}{\sigma_1}\left[1 - \frac{E_1}{D_1} e^{i2kr_s\Gamma_2} - \frac{\sigma_2}{\sigma_1} e^{i2kr_o\Gamma_2} - \ldots\right] e^{ikf}\, d\xi dk \right\} \qquad \text{(III-11)}$$

Thus, the integrands in Eq. II-23 have been transformed to infinite series following two successive approximations. The integrals are assumed to be uniformly convergent so that the order of integration and summation can be interchanged. Eq. III-11 then represents the transmitted solution as a sum of infinite number of integrals. By attaching physical significance to contribution from each integral, it will now be demonstrated that only a finite number of terms are needed to generate a fairly descriptive picture of the transmitted field. First, it is simple to observe the exact solution to the line source problem as given by Eq. III-9 is again reducible from Eq. III-11, requiring however only its first term. Second, a wealth

of information can be gleaned through the examination of exponential factors in these integral solutions. For instance, this factor in Eq. III-9 carries with it the sense of a wave front and subsequent motion initiating from $x = 0$, $y = -y_s$, which are points on the line source. This reasoning will be substantiated in a later section for the factors found in each term of Eq. III-11, which have a parallel functionality. The first of these is f as defined by Eq. III-8a and it is identical to the corresponding factor in Eq. III-9 just described. Fig. III-1a illustrates the fact that f carries the information on wave front as it relates to signals coming from the source point closest to the observer field position. The factors in the subsequent terms all contain f and an expression based on $k\ r_2$, and it is not difficult to find an interpretation for each of them. Thus, the second term relates to signals coming from the source point farthest to the field position as depicted by Fig. III-1b. Since the signals will be continuous following the wavefront, combination of the first two terms of Eq. III-11 is seen as descriptive of the transmitted field due to the primary source-vortex layer interaction, beginning with the wave front coming from A and ending with the contribution from B. The primary interaction is clearly without any reflected contributions, which as expected can be found in the succeeding terms. The field resulting from a single reflection is contained in the third and fourth terms as indicated by their respective exponential factor (fourth term is not shown in Eq. III-11 but basically it is the product of second and third terms). As illustrated in Figs. III-1c and 1d, it begins from A and ends at B with a single reflection at the interface. This simple argument can be applied on subsequent terms to show that they represent multiple reflections of increasing

order. Howe[13] suggests that after several reflections, the acoustic coupling between opposite faces of the jet may become large. It

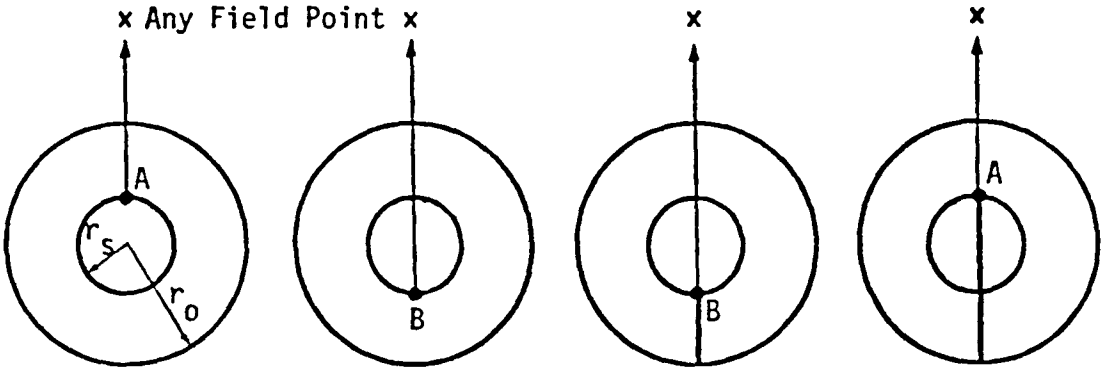

Figure III-1 Physical Significance of Terms in Eq. III-11

will be assumed here that for small time the contributions arising from these internal reflections are negligible to the total transmitted field. With these considerations, just the first two pair of terms in Eq. III-11 will be evaluated to focus attention on the added role played by the curvature effects in the transmission mechanism.

c. NON-DIMENSIONAL FORM

First, rewrite Eq. III-11 as follows,

$$\phi_1 = \phi_f + \phi_g$$

$$= \frac{aQ}{8\pi^3\sqrt{r_s r}}\left\{\left[\int_{-\infty}^{0}\int_{c^-}^{+} + \int_{0}^{\infty}\int_{c^+}^{+}\right] \frac{\xi(\xi-M)D_1}{\sigma_1}\, e^{ikf}\, d\xi\, dk \right.$$

$$\left. + \left[\int_{-\infty}^{0}\int_{c^-}^{-} - \int_{0}^{\infty}\int_{c^+}^{+}\right] \frac{\xi(\xi-M)E_1}{\sigma_1}\, e^{ikg}\, d\xi\, dk\right\} \qquad \text{(III-12)}$$

where

$$g = z + \Gamma_1 (r - r_o) + \Gamma_2 (r_o + r_s) - \xi at$$

Notice the similarity as well as the difference between ϕ_f and ϕ_g. They will be treated separately from here on.

$$\phi_f = \frac{aQ}{8\pi^3\sqrt{r_s r}}\left[\int_{-\infty}^{0}\int_{c^-} + \int_{0}^{\infty}\int_{c^+}\right]\frac{i\xi(\xi-M)\left[1 + \lambda_-/kr_o\right] e^{ikf}}{\Lambda_1 + \dfrac{\Lambda_2}{\Gamma_1\Gamma_2\, kr_o}}\, d\xi\, dk \qquad \text{(III-13)}$$

where

$$\Lambda_1 = (\Gamma_1 + \Gamma_2)\,(1 + \Gamma_1\,\Gamma_2) \qquad \text{(III-13a)}$$

$$\Lambda_1 = i\,(\Gamma_1^{\,2} - \Gamma_2^{\,2})(1 - 3\,\Gamma_1\,\Gamma_2)/8$$
$$\lambda_- = \frac{iro}{8}\left(\frac{1}{\Gamma_2\, r_s} - \frac{1}{\Gamma_1\, r}\right) \qquad \text{(III-13b)}$$

A check on Eq. III-13 reveals the imaginary part to vanish as anticipated and hence it can be put in the following equivalent form, with Re to mean the real part of the integrals.

$$\phi_f = \frac{aQ}{4\pi^3\sqrt{r_s r}}\ \mathrm{Re}\int_{0}^{\infty}\int_{c^+}\frac{i\xi(\xi-M)\left[1 + \dfrac{\lambda_-}{kr_o}\right]e^{\,ikf}}{\Lambda_1 + \dfrac{\Lambda_2}{\Gamma_1\Gamma_2\, kr_o}}\, d\xi\, dk \qquad \text{(III-14)}$$

After some algebraic manipulations, this equation is non-dimensionalized as follows:

$$\Phi_F = \frac{1}{4\pi^3\sqrt{R_S R}} \mathrm{Re} \int_o \int_{c^+}^{\infty} i\xi(\xi-M) \left\{ \frac{K\left[1 - \frac{\Lambda_1 L_-}{\Lambda_2}\right]}{\Lambda_1\left[K + \frac{\Lambda_2}{\Gamma_1\Gamma_2\Lambda_1}\right]} + \frac{L_-}{\Lambda_2} \right\} e^{iKF}\, d\xi\, dK \qquad \text{(III-15)}$$

with non-dimensional quantities:

$$\left.\begin{aligned} R_S &= \frac{r_s}{r_o}\ , \quad R = \frac{r}{r_o}\ , \quad K = kr_o\ , \quad Z = \frac{z}{r_o} \\ F &= Z + \Gamma_1 (R - 1) + \Gamma_2 (1 - R_S) - \xi\tau \end{aligned}\right\} \qquad \text{(III-15a)}$$

$$L_- = \frac{i}{8}\left(\frac{\Gamma_1}{R_S} - \frac{\Gamma_2}{R}\right)\ , \quad \tau = \frac{at}{r_o}\ , \quad \Phi_F = \frac{\phi_f\, r_o^2}{aQ}$$

ϕ_g is similarly put in its non-dimensional form:

$$\Phi_G = \frac{1}{4\pi^3\sqrt{R_S R}} \mathrm{Re} \int_o \int_{c^+}^{\infty} \xi(\xi-M) \left\{ \frac{K\left[1 + \frac{\Lambda_1 L_+}{\Lambda_2}\right]}{\Lambda_1\left[K + \frac{\Lambda_2}{\Gamma_1\Gamma_2\Lambda_1}\right]} - \frac{L_+}{\Lambda_2} \right\} e^{iKG}\, d\xi dK \qquad \text{(III-16)}$$

Here,

$$L_+ = \frac{i}{8}\left(\frac{\Gamma_1}{R_S} + \frac{\Gamma_2}{R}\right)\ , \quad \Phi_G = \frac{\phi_g\, r_o^2}{aQ} \qquad \text{(III-16a)}$$

$$G = Z + \Gamma_1 (R - 1) + \Gamma_2 (1 + R_S) - \xi\tau$$

Φ_F and Φ_G do not differ greatly in their appearance but retracing from previous discussions on the significance of each term, it is to be kept in mind that while the former contains information on the wave front, the latter should be free of it since there can only be a single wave front. Whether or not this is indeed the case will become apparent in the final evaluation of the solutions.

IV. INVERSE ANALYSIS

a. THE CONDITION OF CAUSALITY

In two previous chapters, an integral solution of the transmitted field which approximates for large values of radial lengths and which excludes any contributions arising from internal reflections is derived. This inversion integral with its non-dimensional form as given by Eqs. III-15 & 16 is evaluated in the present chapter to the simplest analytic representation possible. To begin with, an examination of the integrand is made (see Appendix A) to identify all the singularities. The branch points and the real pole which exists when $M > 2$ associated with neutral stability wave are identical to that found in the plane vortex sheet case. The instability pole is complicated by being a function of wavenumber as well as frequency in contrast to the plane case and detailed examination will be presented later in its appropriate place.

Recall the integration paths for ξ and K are originally as follows. K runs from 0 to ∞ while ξ moves along the path C_+ such that all singularities are restricted to lie below it. Then, the condition of causality can be checked by invoking Jordan's Lemma as illustrated in Figure IV-2.

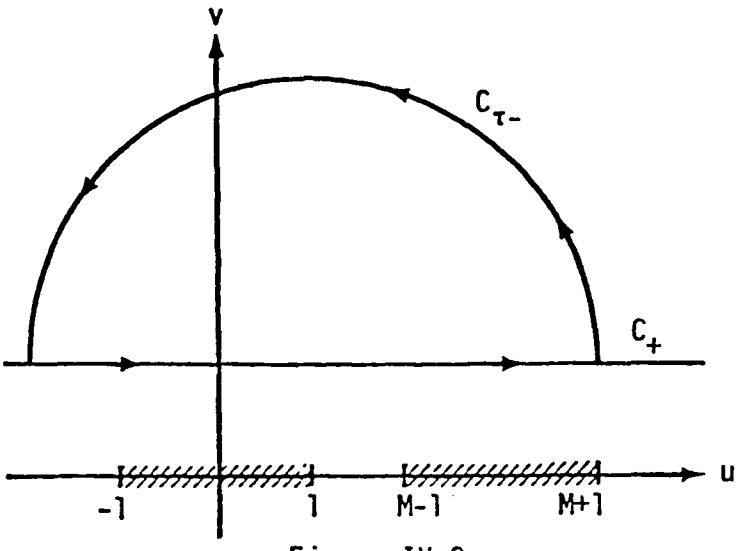

Figure IV-2

Since there is no singularities within the closed contour of C+ and the deformed path $C_{\tau-}$, the integrals vanish by Cauchy's Integral Theorem. That is,

$$\left.\begin{aligned} R - R_s > \tau, \quad \Phi_F = 0 \\ R + R_s > \tau, \quad \Phi_F = 0 \end{aligned}\right\} \quad \text{(IV-3)}$$

The first implies that before time τ equals $R - R_s$, which is the minimum time for the waves to reach the field point R, Φ_F remains zero to satisfy the physics that before the secondary sources on the interface are excited, there cannot be any response from the transmitted field. Before elaborating on the second condition given in Eq. IV-3, it is expedient to reflect on the differences between Φ_F and Φ_G that are easily discernible in Eqs. III-15 & 16. The development of Chapter III pointed to the fact that their sum characterizes only the directly transmitted field, having disregarded all successive terms arising from one or more reflections at

the interface. A question comes up as to why the characterization goes in pairs, whose answer may very well rest with the curvature variations. For if the field point of interest is at P, as illustrated in Fig. IV-3, the top half of the circular interface is seen to have the curvature, say, in a positive sense. Top half of the ring source similarly has its curvature in the same sense, but that of the lower half clearly has the opposite sense. This makes it plausible for an interpretation of Φ_F and Φ_G in the manner described below. Φ_F is representative of the transmitted field arising from top half of the source as depicted in Fig. IV-3b, and the first condition of Eq. IV-3 which implies the initiation of the wave front from point A nearest point P, applies as it gives the minimum time necessary for the waves to make contact with the field point. Obviously, transmission cannot occur prior to this time. On the other hand, Φ_G represents the field originating from lower half of the source as is apparent from Fig. IV-3c, and the second condition of Eq. IV-4 which cannot have anything to do with the wave front, applies as again it furnishes the minimum time before transmission from any point on the lower half source is possible.

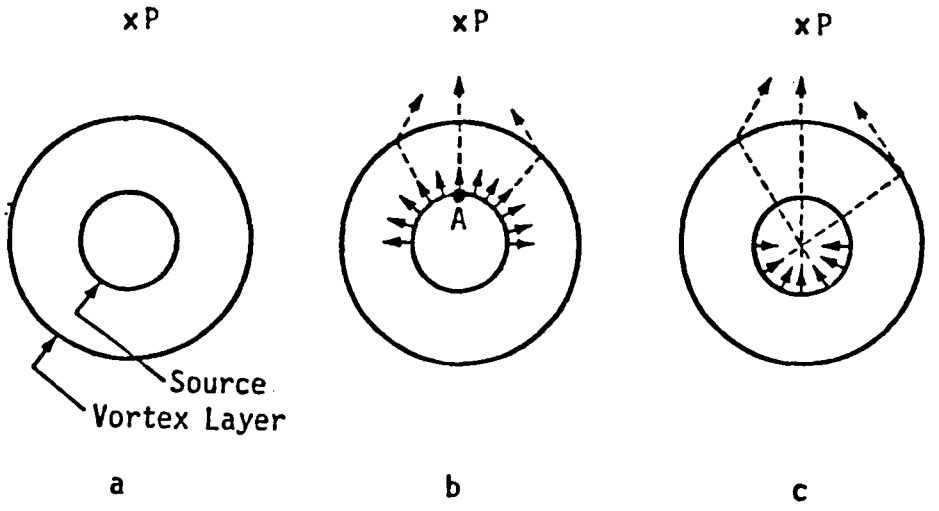

Figure IV-3

It can be concluded from the previous discussion that the integral solutions represented by Eqs. III-15 & 16 exhibit the causality conditions properly and this clears the way for the inverse analysis. For the inequalities of Eq. IV-3 to hold in the opposite sense, i.e. $<$ instead of $>$, Jordan's Lemma requires taking the lower semi-circle on Fig. IV-2 which now together with C+ forms a region containing all the singularities as well as the branch cuts. Basically, the inverse analysis entails the evaluation of residues coming from the singularities and integrating around the branch cuts. While residues are relatively simple to evaluate, branch cut integrations for complicated integrand such as the ones encountered presently are not likely to be easy nor manageable to yield a final expression useful for applications. This is the reason why a particular technique is demanded for the analysis.

b. ZERO IMAGINARY CONTOURS

Cagniard's technique will be employed in similar fashion as Chao applied it to his plane vortex sheet problems. The success to this method lies in finding a path for contour deformation such that integration along the branch cuts need not be concerned with and an exchange in the order of integration can be made consistent with the causality condition. In other words, the idea is to find a way to integrate with respect to K first instead of ξ because that is substantially less cumbersome to carry out than the other way around. An examination of Eqs. III-15 & 16 shows that if a contour on which Im(F) or Im(G) is greater than zero can be found, then the power raised to the exponent in either integral will have a

negative real quantity for all K, and along such a path, the order of integration can be altered without any violation. So the functions F and G will be studied next. Recall

$$F = Z + \Gamma_1 (R - 1) + \Gamma_2 (1 - R_S) - \xi\tau$$

$$G = Z + \Gamma_1 (R - 1) + \Gamma_2 (1 - R_S) - \xi\tau \qquad \text{(IV-4)}$$

First, it is observed that they are purely real along the real axis not covered by the branch cuts of Γ_1 and Γ_2. A parametric equation which defines the curves of Im(F) = 0 or Im(G) = 0 not on the real axis can be determined. Chao showed in his plane vortex sheet problem that these curves are oval-shaped. Here the same is anticipated as the functions are quite similar, but the curves which shall be designated C_{FO} and C_{GO} are numerically searched instead. A computer program can be set up with relative ease and generate a whole array of them by varying the parameters X, R, R_s, and τ. Some examples are shown in Fig. IV-4 with just the top half as they are symmetrical about the real axis. Several observations can be made regarding these curves. Whether or not they split into two depends primarily on the Mach number. For M < 2 when the branch cuts overlap, a single curve is maintained, whereas for M > 2 after the branch cuts become separated, two similar curves will evolve around the cuts when the time τ is at least greater than that shown in the inequality of Eq. IV-3. When time is small, the oval-shaped curve is very large for all Mach numbers. As time grows larger, the curve starts to move in and becomes

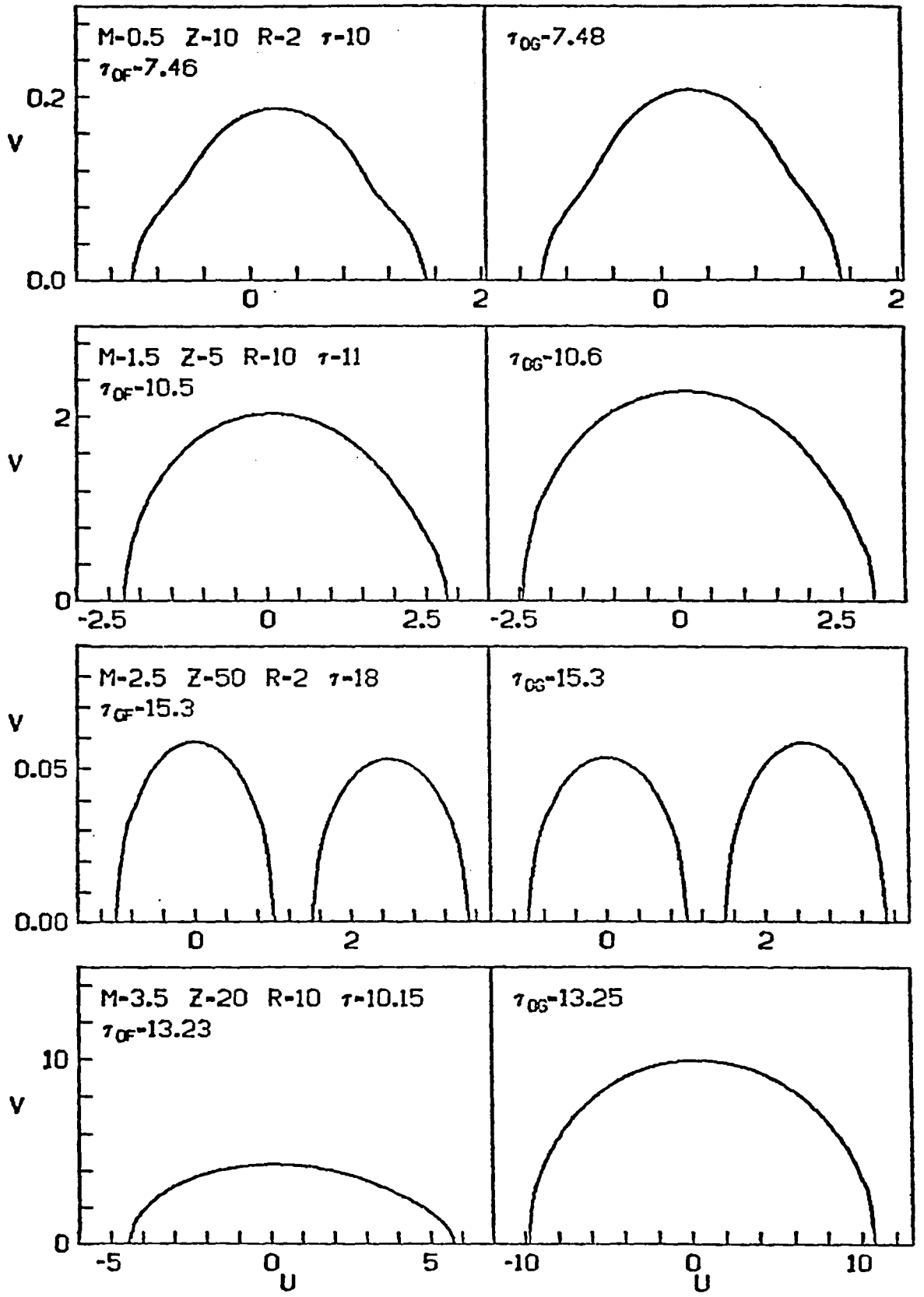

FIGURE IV-4 EXAMPLES ØF ImF-0(L.) AND ImG-0(R.) FØR R_S-0.1

smaller until when τ gets infinitely large, the curve(s) will just barely wrap around the branch cuts. Finally, the curves usually bias to one side or the other depending on the values of R and R_s as they resemble weights to Γ_1 and Γ_2 respectively. All the background information just secured on C_{FO} and C_{GO} will help in the analysis later.

Now that the question of where and how the imaginary parts of F and G vanish has been thoroughly resolved, it is possible to establish the contours along which the individual imaginary parts are always greater than zero. These shall be designated by C_{F+} and C_{G+} respectively and a sketch is shown in Fig. IV-5.

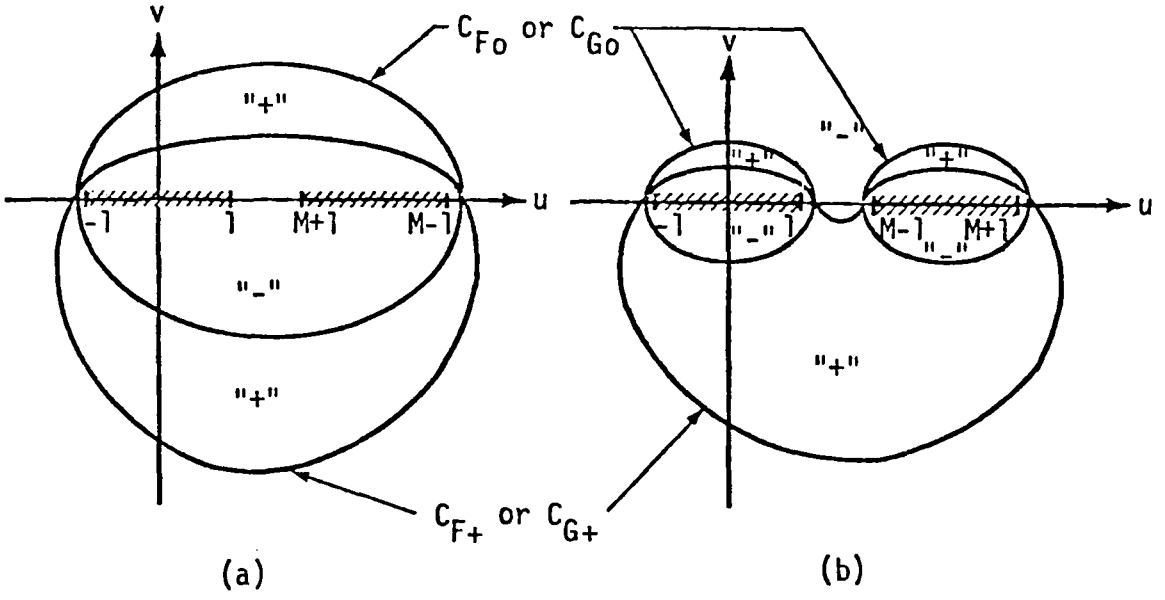

Figure IV-5 Sketch of Contours C_{F+}, C_{G+}

The plus and the minus symbols in double prime quotes are indicative of the signs of F or G in the various regions. The jumps across contours where the imaginary parts vanish are distinctly clear. C_{F+}, or identically C_{G+}, for that matter, wades through the positive imaginary regions in the manner shown. Fig. IV-5a illustrates the case when $M < 2$ or $M > 2$ but t small. In such a case, the contour is inside of C_{F0} above the real axis and outside of C_{F0} below. When $M > 2$ and there are two of the zero imaginary curves as illustrated by Fig. IV-5b, then the contour takes a little detour into the lower half spaces between the branch cuts such that the local portion of the real axis outside of C_{F0} is exterior of C_{F+} as well. A point which is rather self-evident will be made here. Note that whereas the contour C_{F0} or C_{G0} is uniquely determined for a given set of parametric values, there is no clear-cut choice on C_{F+} or C_{G+}. This is simply due to the fact that regions of positive imaginary part spread over a large area. The added flexibility thus acquired in the selection of a contour might be interpreted on first thought to give rise to some technical difficulties in performing the actual contour deformation. However, taking a closer look, one would expect the final solution to be independent of the particular contour selected, because there cannot possibly be more than one solution for a problem so well defined as the present. This supposition will in fact be shown to be true.

From here on, the analysis will be described for Φ_F only, with the understanding that results for Φ_G could be similarly obtained. It is easy to see that while some singularities will be enclosed by C_{F+}, others will be left out depending on the particular contour chosen. The final results

however will be the same regardless of the choice made. Actually, the question of where the poles are located with respect to C_{FO} is of greater importance and is examined next. As the imaginary part of F is zero along C_{FO}, it is natural to look at the sign of F to see whether a point is in or out of the closed contour. First, consider ξ_1 and ξ_2 which are given in Eq. A-2. Substitute them into F defined by Eq. IV-4 and sort out the real and imaginary parts.

$$F = Z + \tfrac{1}{2}\left[\sqrt{M^2+1} - 1\right](R + R_S - 2) - \frac{\tau M}{2}$$
$$\pm \left[(M^2+1)^{\frac{1}{2}} - \left(\frac{M^2}{4} + 1\right)\right]^{\frac{1}{2}}\left[\frac{(R - R_S)}{M}\left(\sqrt{M^2+1}+1\right) - \tau\right]$$
$$= \alpha \pm i\,\beta \qquad \text{(IV-5)}$$

In agreement with Fig. IV-5, $\xi_{1,2}$ will be inside of C_{FO} if $\beta > 0$ and outside if $\beta < 0$. Using the Heaviside step function, let

$$H_1 = H\left[\tau - \frac{(R - R_S)}{M}\left(\sqrt{M^2+1} + 1\right)\right] \qquad \text{(IV-5a)}$$

ξ_3, ξ_4 and ξ_5 as defined in Eq. A-2 are on the real axis along which the imaginary part of F vanishes. Therefore, some other check is needed to determine where they are in relation to C_{FO}. First of all, these poles will be enclosed by C_{FO} as long as it is a single curve. When they split into two, then a condition exists for the poles to fall outside of C_{FO}. Since its derivation is similar to that found in Appendix 1 of Chao[3],

only the condition itself will be presented here. The poles $\xi_{3,4,5}$ will be outside of C_{FO} if the inequality represented by the following is satisfied.

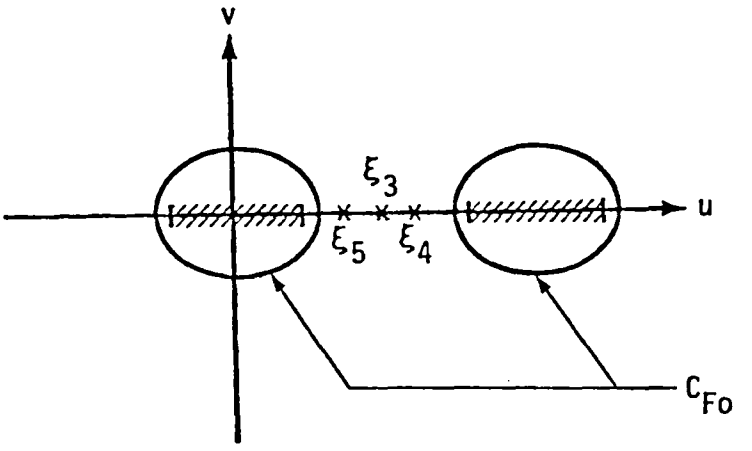

Figure IV-6

$$\tau > \frac{\xi_m(R-1)}{\Gamma_1(\xi_m)} + \frac{(\xi_m - M)\,(1 - R_s)}{\Gamma_2\,(\xi_m)} \qquad m = 3, 4, 5 \qquad \text{(IV-6)}$$

ξ_6, which is the pole of $K + \Lambda_2 / (\Gamma_1\ \Gamma_2\ \Lambda_1)$, will be examined later for its movement as a function of K and how that will relate to C_{FO}.

c. EVALUATION OF INTEGRALS

To begin with, break up Φ_F given by Eq. III-15 into three parts as follows:

$$\Phi_A = \int_0^\infty \int_{C^+} \frac{i\xi(\xi-M)}{\Lambda_1} \frac{K}{K + \frac{\Lambda_2}{\Gamma_1\Gamma_2\Lambda_1}} e^{iKF}\, d\xi\, dK \qquad \text{(IV-8)}$$

$$\Phi_B = -\int_0^\infty \int_{C^+} \frac{i\xi(\xi-M)L_-}{\Lambda_2} \frac{K}{K + \frac{\Lambda_2}{\Gamma_1\Gamma_2\Lambda_1}} e^{iKF}\, d\xi\, dK \qquad \text{(IV-9)}$$

$$\Phi_C = \int_0^\infty \int_{C^+} \frac{i\xi(\xi-M)L_-}{\Lambda_2} e^{iKF}\, d\xi\, dK \qquad \text{(IV-10)}$$

Φ_B and Φ_C can be combined but they are evaluated separately for mathematical simplicity. As discussed at some length earlier, the main idea in the inverse analysis is to deform from C_+ to C_{F+} as illustrated in Fig. IV-7. By Cauchy's Integral Theorem, integration along C_+ is now equivalent to the sum of integrations along C_{F+}, $C_{\tau+}$ as $\rho_{\tau+} \to \infty$ and C_j's which gives the residues of all the poles exterior to C_{F+}. Because the integrands decay as good or better than $1/\xi^2$ for ξ becoming very large, the contour makes no contribution by Jordan's Lemma and thus Eqs. IV-8 to 10 following the contour deformation becomes (with the poles indexed in accordance with Appendix A):

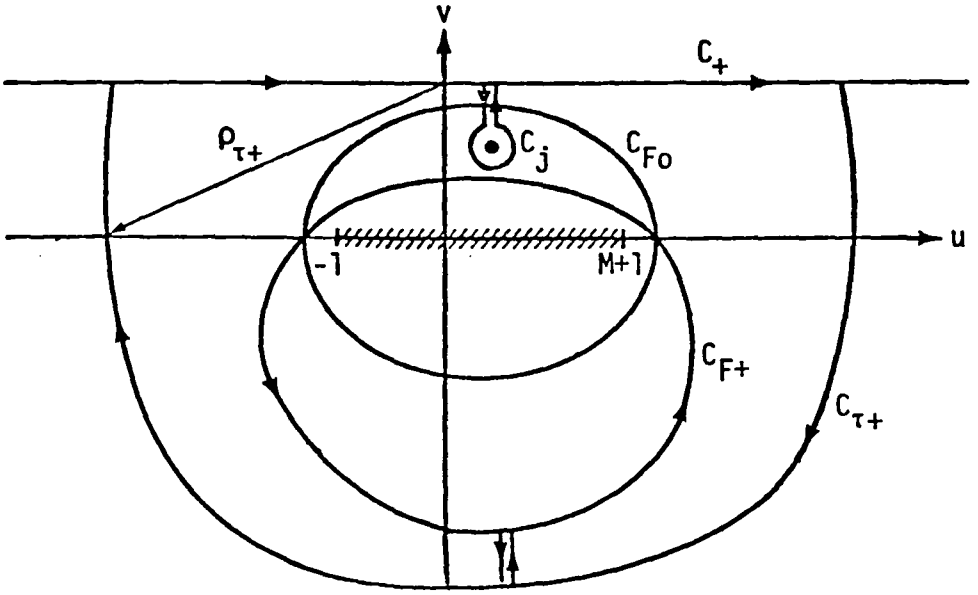

Figure IV-7 Integration Contours

$$\Phi_A = \Phi_{A1} + \Phi_{A2} = \oint_{C_{F+}} \frac{i\xi(\xi-M)}{\Lambda_1} \int_0^\infty \frac{K}{K + \frac{\Lambda_2}{\Gamma_1\Gamma_2\Lambda_1}} e^{iKF}\, dK\, d\xi$$

$$+ \int_0^\infty \sum_{j=1}^{6} \oint_{C_j} \frac{i\xi(\xi-M)}{\Lambda_1} \frac{K}{K + \frac{\Lambda_2}{\Gamma_1\Gamma_2\Lambda_1}} e^{iKF}\, d\xi\, dK \qquad \text{(IV-11)}$$

$$\Phi_B = \Phi_{B1} + \Phi_{B2} = -\oint_{C_{F+}} \frac{i\xi(\xi-M)L_-}{\Lambda_2} \int_0^\infty \frac{K}{K + \frac{\Lambda_2}{\Gamma_1\Gamma_2\Lambda_1}} e^{iKF}\, dK\, d\xi$$

$$- \int_0^\infty \sum_j \oint_{C_j} \frac{i\xi(\xi-M)L_-}{\Lambda_2} \frac{K}{K + \frac{\Lambda_2}{\Gamma_1\Gamma_2\Lambda_1}} e^{iKF}\, d\xi\, dK,\ j = 3,6 \qquad \text{(IV-12)}$$

$$\Phi_C = \Phi_{C1} + \Phi_{C2} = \oint_{C_{F+}} \frac{i\xi(\xi-M)L_-}{\Lambda_2} \int_0^\infty e^{iKF}\, dK\, d\xi$$

$$+ \int_0^\infty \oint_{C_3} \frac{i\xi(\xi-M)L_-}{\Lambda_2} e^{iKF}\, d\xi\, dK \qquad \text{(IV-13)}$$

In the representations above, an exchange of order of integration has been effected along C_{F+} where the real part of iKF is positive. For the present, all poles have been assumed to fall outside of C_{F+} even though the final outcome will not depend on where the poles lie in relation to C_{F+}.

First, let

$$I_K = \int_o^\infty \frac{K}{K + \frac{\Lambda_2}{\Gamma_1 \Gamma_2 \Lambda_1}} e^{iKF} \, dK \qquad \text{(IV-14)}$$

and evaluate this integral which occurs in Φ_{A1} and Φ_{B1}. By a simple translation and a rotation of the K-coordinate, it is possible to transform I_K into a form involving exponential integral as follows:

$$I_K = \frac{i}{F} - K_\xi \, e^{iK_\xi F} \, E_i \, (- i \, K_\xi \, F) \qquad \text{(IV-15)}$$

where $K_\xi = - \Lambda_2 / (\Gamma_1 \Gamma_2 \Lambda_1)$ is the moving pole in the K-plane discussed in Appendix A and $E_i \, (-iK_\xi F)$ represents the exponential integral

$$E_i \, (z) = \int_{-\infty}^{z} \frac{e^t}{t} \, d_t$$

Thus,

$$\Phi_{A1} = \Phi_{A11} + \Phi_{A12} = -\oint_{C_{F+}} \frac{\xi(\xi-M)}{\Lambda_1 F}\, d\xi - \oint_{C_{F+}} \frac{i\xi(\xi-M)}{\Lambda_1} K_\xi e^{iK_\xi F} E_i(-iK_\xi F)\, d\xi \qquad \text{(IV-16)}$$

$$\Phi_{B1} = B11 + B12 = \oint_{C_{F+}} \frac{\xi(\xi-M)L_-}{\Lambda_2 F}\, d\xi + \oint_{C_{F+}} \frac{i\xi(\xi-M)L_-}{\Lambda_2} K_\xi e^{iK_\xi F} E_i(-iK_\xi F)\, d\xi \qquad \text{(IV-17)}$$

$$\Phi_{C1} = \oint_{C_{F+}} \frac{\xi(\xi-M)L_-}{\Lambda_2 F}\, d\xi$$

Notice that Φ_{B11} and Φ_{C1} are the same integrals but opposite in sign to drop out from the above. Now, the integrand of Φ_{A11} behaves as

$$\frac{\xi(\xi-M)}{\Lambda_1 F} \rightarrow \frac{1}{\xi^2}, \quad |\xi| \rightarrow \infty$$

making it possible to deform from C_{F+} to C_∞ as shown in Fig. IV-8.

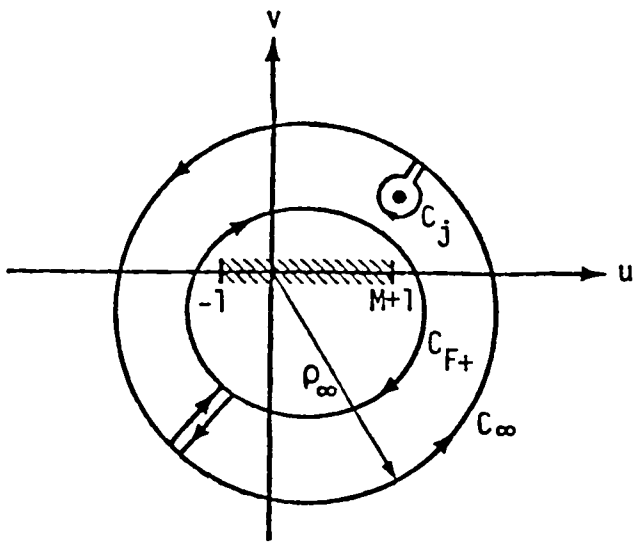

Fig. IV-8 Contour Deformation of Φ_{A11}

Integration over C_∞ does not contribute as can be seen from the above by taking ρ_∞ infinitely large. Thus,

$$\Phi_{All} = \sum_{j=1}^{5} \oint_{C_j} \frac{\xi(\xi-M)}{\Lambda_1 F} d\xi + \int_{C_o} \frac{\xi(\xi-M)}{\Lambda_1 F} d\xi \qquad \text{(IV-18)}$$

where C_0 is evaluated if and when the zero of F lies exterior of C_{F+}. C_j's prevail by the previous assumption that the enclosed poles are all outside of C_{F+}. By the residue theorem, Eq. IV-18 is evaluated to give

$$\Phi_{All} = -2\pi i \left\{ \sum_{j=1}^{5} \frac{Q_{\Lambda_1}(\xi)}{\frac{d\Lambda_1}{d\xi}} \Bigg|_{\xi=\xi_j} + \frac{Q_F(\xi)}{\frac{dF}{d\xi}} \Bigg|_{\xi=\xi_o} \right\} \qquad \text{(IV-19)}$$

where

$$Q_{\Lambda_1}(\xi_j) = \frac{\xi_j(\xi_j-M)}{F(\xi_j)} \qquad \text{and} \qquad Q_F(\xi_o) = \frac{\xi_o(\xi_o-M)}{\Lambda_1(\xi_o)}$$

The zero of F is denoted by ξ_0 and deserves some discussion for its physical significance. Consider first the fact that those points where F vanishes are also the intersection points for Re(F) and Im(F) where they both vanish. Earlier, it was shown (Fig. IV-4) that curves of Im(F) = 0 which are denoted by C_{F0} are oval-shaped. In Fig. IV-9, the curves of Re(F) = 0 are illustrated along with the corresponding curves C_{F0}. These curves in general must and can be determined numerically without much difficulties. Basically, the real part of F is shown to vanish along a curve that approaches a straight line perpendicular to the real axis when

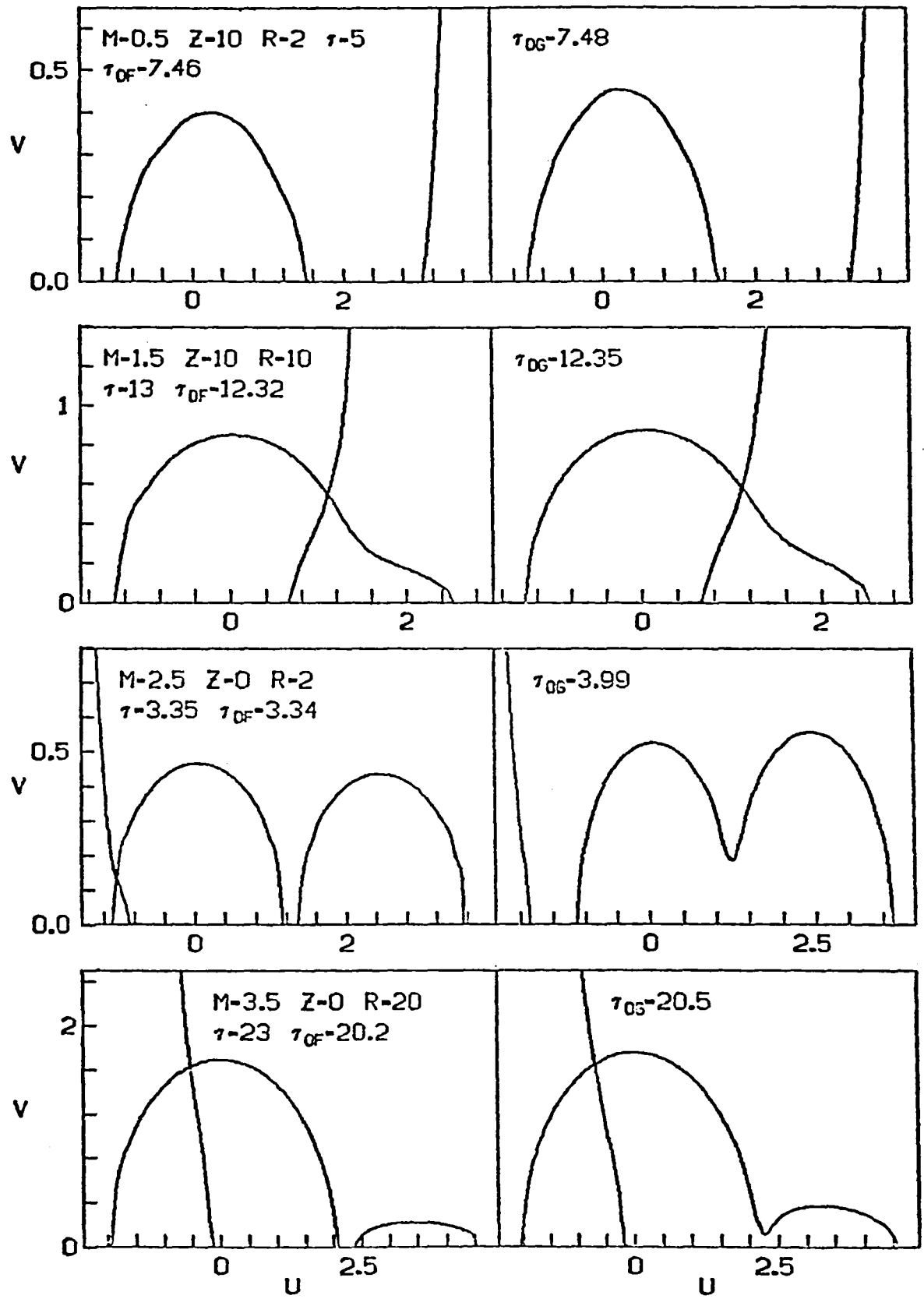

FIGURE IV-9 EXAMPLES ØF ImF-0, ReF-0(L.) AND ImG-0, ReG-0(R.) FØR R_S-0.1

far away from C_{F0}. Only the upper half is shown in both Figs. IV-4 and 9 because the curves are symmetric about the real axis. Furthermore, C_{F+} is such that it always encloses the lower half of C_{F0} together with the branch cuts and hence the need to include them in the analysis is circumvented as a consequence of the contour deformation.

The position of ξ_0 is found to be a function of time. For small time, it is on the real axis exterior of C_{F0} which when substituted into Eq. IV-19 gives rise to a purely imaginary quantity. This clearly does not contribute to the real transmitted field represented by Φ_F of Eq. III-15. ξ_0 moves toward C_{F0} with growing time (Fig. IV-10a) and reaches the point where C_{F0} meets the real axis (Fig. IV-10b). Beyond this time, ξ_0 becomes complex by moving onto and oscillating back and forth on C_{F0} (Fig. IV-10c) for all times. This is true with one exception that occurs for $M > 2$ when C_{F0} splits into two parts as exemplified in Figure IV-9. For these cases, ξ_0 may fall onto the real axis between the two parts so that even for time greater than τ_{0F}, it can become real again. Whereas ξ_0 does not contribute for time $\tau < \tau_{0F}$ because it gives rise to a purely imaginary quantity, it always yields a real quantity to Eq. IV-19 for $\tau > \tau_{0F}$ and therefore contributes to the transmitted sound field. Recall the condition of causality given by Eq. IV-3 which states that $\Phi_F = 0$ for $\tau < R - R_S$, the minimum time of sound propagation from source to vortex layer. Through numerical calculations, τ_{0F} is found to be the minimum time of wave arrival at a field point of interest and τ_{0F} $R - R_S$ is obvious. Thus, ξ_0 provides just the geometric acoustics contributions. In fact, it has been verified that all the remaining contributions, which arise from sound-vortex sheet interations, arrive at later times than τ_{0F}.

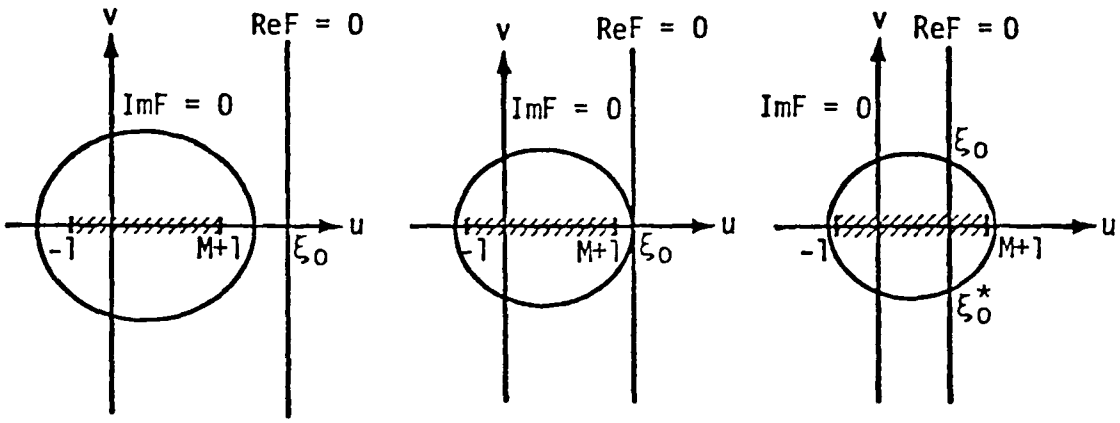

Figure IV-10 ξ_0 Motion Analogy of Wave Propagation

Next, focus attention on Φ_{A2} which can be rewritten from Eq. IV-11 as

$$\Phi_{A2} = \sum_{j=1}^{6} \Phi_{A2j}, \qquad \Phi_{A2j} = \int_0^{\infty} \oint_{C_j} \frac{i\xi(\xi-M)}{\Lambda_1} \frac{K}{K + \frac{\Lambda_2}{\Gamma_1\Gamma_2\Lambda_1}} e^{iKF}\, d\xi\, dK$$

When j = 1 and ξ_1 is inside of C_{FO} so that Im(F) > 0 on C_1, an exchange in the order of integration is possible. Then, by using Eqs. IV-14 & 15 for I_K, Φ_{A21} reduces to

$$\Phi_{A21} = 2\pi i \left. \frac{Q_{\Lambda_1}(\xi)}{\frac{d\Lambda_1}{d\xi}} \right|_{\xi=\xi_1} - \left. \Phi_{A2cj} \right|_{j=1} \qquad \text{(IV-20)}$$

where for general purposes

$$\Phi_{A2cj} = \oint_{cj} \frac{i\xi(\xi-M)}{\Lambda_1} K_\xi e^{iK_\xi F} E_i(-iK_\xi F) \, d\xi \qquad \text{(IV-20a)}$$

For the case of $j = 2$, ξ_2 has to be inside of C_{F+} when its complex conjugate ξ_1 lies within C_{FO}. Thus, $\Phi_{A22} = 0$. When $j = 1$ but ξ_1 is outside of C_{FO} so that $\mathrm{Im}(F) < 0$ on C_1, Φ_{A21} can be evaluated in the following manner.

$$\begin{aligned}\Phi_{A21} &= \oint_{c_j} \frac{i\xi(\xi-M)}{\Lambda_1}\left[\int_{-\infty}^{\infty} - \int_{-\infty}^{o}\right] \frac{K}{K + \dfrac{\Lambda_2}{\Gamma_1\Gamma_2\Lambda_1}} e^{iKF} \, dK \, d\xi \\ &= 2\pi i \left.\frac{Q_{\Lambda_1}(\xi)}{\dfrac{d\Lambda_1}{d\xi}}\right|_{\xi=\xi_1} - \Phi_{A2C1} + \left.\Phi_{A2K_j}\right|_{j=1} .H_1 \end{aligned} \qquad \text{(IV-21)}$$

where again for general purpose

$$\Phi_{A2Kj} = \int_{-\infty}^{\infty} \oint_{c_j} \frac{i\xi(\xi-M)}{\Lambda_1} \frac{K}{K + \dfrac{\Lambda_2}{\Gamma_1\Gamma_2\Lambda_1}} e^{iKF} \, d\xi \, dK \qquad \text{(IV-21a)}$$

Eq. IV-21 alone is sufficient to represent Φ_{A21} for both cases since the Heaviside function H_1, which is defined by Eq. IV-5a, is zero when ξ_1 lies outside of C_{FO} and Eq. IV-20 is recovered. When ξ_1 is outside of C_{FO}, so is ξ_2 and it may lie on the outside of C_{F+}. Then,

$$\Phi_{A22} = 2\pi i \left.\frac{Q_{\Lambda_1}(\xi)}{\frac{d\Lambda_1}{d\xi}}\right|_{\xi=\xi_2} - \Phi_{A2C2} \qquad \text{(IV-22)}$$

ξ_4 and ξ_5 are points on the real axis and exterior of C_{F+} so that the imaginary part of F is greater than zero on the portion of C_4 and C_5 below the real axis and less than zero above. Thus,

$$\Phi_{A2m} = 2\pi i \left.\frac{Q_{\Lambda_1}(\xi)}{\frac{d\Lambda_1}{d\xi}}\right|_{\xi=\xi_m} - \Phi_{A2Cm} + \Phi_{A2Km}, \quad m = 4, 5 \qquad \text{(IV-23)}$$

In Φ_{A2Km}, the integral along C_m is for the upper half only. When j = 3, the situation is similar to j = 4 or 5 because ξ_3 is also a point on the real axis exterior of C_{F+}.

$$\Phi_{A23} = 2\pi i \left.\frac{Q_{\Lambda_1}(\xi)}{\frac{d\Lambda_1}{d\xi}}\right|_{\xi=\xi_3} - \Phi_{A2C3} + \Phi_{A2K3} \qquad \text{(IV-24)}$$

In summary,

$$\Phi_{A2} = \sum_{j=1}^{5} \left\{ 2\pi i \left.\frac{Q_{\Lambda_1}(\xi)}{\frac{d\Lambda_1}{d\xi}}\right|_{\xi=\xi_j} - \Phi_{A2Cj} + \Phi_{A2Kj} \right\} + \Phi_{A26} \qquad \text{(IV-25)}$$

Evaluation of Φ_{A26} will be saved for a later section as it requires special treatment. Note the absence in Eq. IV-25 of any additional factors to indicate when and where each term is present. For example, Φ_1 is present only when $M < 2\sqrt{2}$ and where it is exterior of C_{F+} so that the corresponding terms would vanish if these conditions are not met. The same in a consistent manner is implied on Eq. IV-19 but the factors are not tagged on in the meantime for simplicity. By duplicating the procedure of Φ_{A2}, the following results are obtained.

$$\Phi_{B2} = -2\pi i \left.\frac{Q_{\Lambda_2}(\xi)}{\frac{d\Lambda_2}{d\xi}}\right|_{\xi=\xi_3} + \Phi_{B2C} - \Phi_{B2K} + \Phi_{B2K3} - \Phi_{B26} \qquad \text{(IV-26)}$$

$$\Phi_{C2} = 2\pi i \left.\frac{Q_{\Lambda_2}(\xi)}{\frac{d\Lambda_2}{d\xi}}\right|_{\xi=\xi_3} + \xi_{C2K} \qquad \text{(IV-27)}$$

where

$$Q_{\Lambda_2}(\xi_3) = \left.\frac{\xi(\xi-M)L_-}{F}\right|_{\xi=\xi_3}$$

$$\Phi_{B2K} = \Phi_{C2K} = \int_{\infty}^{\infty} \oint_{C_3} \frac{i\xi(\xi-M)L_-}{\Lambda_2} e^{iKF}\, d\xi\, dK$$

$$\Phi_{B2K3} = \int_{\infty}^{\infty} \oint_{C_3} \frac{i\xi(\xi-M)L_- e^{iKF}}{K\,\Gamma_1\Gamma_2\Lambda_1 + \Lambda_2}\, d\xi\, dK$$

$$\Phi_{B2C} = \oint_{C_3} \frac{i\xi(\xi-M)L_-}{\Lambda_2} K_\xi e^{iK\xi F} E_i(-iK_\xi F)\, d\xi$$

Again, Φ_{B26} will be evaluated later along with Φ_{A26}. Next, Φ_{A2K3} and Φ_{B2K3} are simplified further by directly substituting $\xi_3 = M/2$ into these integrals and working out the double integration.

$$\Phi_{A2K3} = 2\pi^2 \left\{ \left. \frac{\xi(\xi-M)}{\frac{d\Lambda_1}{d\xi}} \right|_{\xi=\xi_3} \delta\left[F(\xi_3)\right] + \left. \frac{Q_A(\xi)}{\frac{d\Lambda_1}{d\xi}} \right|_{\xi=\xi_3} \cdot H_{KF} \right\} \qquad \text{(IV-28)}$$

$$\Phi_{B2K3} = 2\pi^2 \left. \frac{Q_B(\xi)}{\frac{d\Lambda_1}{d\xi}} \right|_{\xi=\xi_3} \cdot H_{KF} \qquad \text{(IV-28a)}$$

where

$$Q_A(\xi_3) = \xi_3(\xi_3-M)\, K_3\, e^{-K_3 F(\xi_3)}, \quad Q_B(\xi_3) = \left. \frac{Q_A(\xi_3)}{K_3} \frac{iL_-}{\Gamma_1\Gamma_2} \right|_{\xi=\xi_3} \qquad \text{(IV-28b)}$$

$$K_\xi = -\frac{3M \pm 8}{2\sqrt{M^2-4}\,(8-M^2)}$$

$$H_{KF} = H\left[F(\xi_3)\right] H\left[M-2\right] H\left[2\sqrt{2}-M\right] - H\left[-F(\xi_3)\right] H\left[M-2\sqrt{2}\right]$$

It will now be shown that $\Phi_{A2Kj's}$, where $j = 1, 2, 4, 5$ all vanish in reference to earlier remarks. Take Φ_{A2K1} for illustration and the rest will follow in likeness.

$$\Phi_{A2K1} = \int_{-\infty}^{\infty} \oint_{C_1} \frac{i\xi(\xi-M)\,K}{\Lambda_1\left(K + \frac{\Lambda_2}{\Gamma_1\Gamma_2\Lambda_1}\right)} e^{iKF}\, d\xi\, dK$$

$$= \int_{-\infty}^{\infty} \oint_{C_1} \frac{i\xi(\xi-M)}{\Lambda_1} e^{iKF}\, d\xi dK - \int_{-\infty}^{\infty} \oint_{C_1} \frac{i\xi(\xi-M)\Lambda_2\, e^{iKF}}{\Lambda_1(\Gamma_1\Gamma_2\Lambda_1\, K + \Lambda_2)}\, d\xi\, dK$$

Then, it is quite clear that the residue contribution from the two parts are equal but opposite in sign to bring about a zero net contribution.

Integrals dealt with up to the present have not involved elaborate treatment and most have been reduced to analytic simplicity, with the remainder purposely left incomplete for the moment. Next, attention will be placed on Φ_{A12} and Φ_{B12} which are expressed in Eqs. IV-16 & 17. First, recall the exponential integral is likewise expressible in terms of the incomplete Gamma function, i.e. $E_i(z) = -\Gamma(0, -z)$. $\Gamma(\alpha, z)$ is an entire function of α, but in general, except when α is an integer, it is a many-valued function of z with a branch point at $z = 0$[7]. Since $\alpha = 0$ here, $E_i(-iK_\xi F)$ is analytic in the ξ-plane. However, at ξ_0, which is the zero of F, the argument vanishes and this causes the exponential integral to diverge. Thus, ξ_0 is a singular point. Expressed in series,

$$E_i(-iK_\xi F) = \gamma + \ln(iK_\xi F) + \sum_{n=1}^{\infty} \frac{(-iK_\xi F)^n}{n!\, n} \qquad \text{(IV-29)}$$

where γ is Euler's constant. Clearly, in the limit as $\xi \to \xi_0$, so that $F \to 0$, E_i presents there a logarithmic singularity which is defined as a branch point. For each ξ_0 when it is complex, there is also its complex conjugate ξ_0^*. But since this point will always be enclosed by C_{F+}, only ξ_0 needs to be concerned with. Now, as $|\xi| \to \infty$, $iK_\xi F \to 1/\xi$.

Certainly, $E_i(0)$ diverges, but note $-iK_\xi FE_i\ (-iK_\xi F)$ which for large behaves as

$$\frac{1}{\xi}\int_{1/\xi}^{\infty}\frac{e^{-t}}{t}\,dt$$

By L'Hospital's rule

$$\lim_{\xi\to\infty}\ \frac{\int_{1/\xi}^{\infty}\frac{e^{-t}}{t}\,dt}{\xi} = \lim_{\xi\to\infty}\ \frac{1}{\xi^2}\ \frac{e^{-t}}{t}\Bigg|_{t=\infty} \to 0$$

Furthermore,

$$\lim_{\xi\to\infty}\ e^{iK_\xi F} \to \lim_{\xi\to\infty}\ e^{1/\xi} \to 1$$

and in Φ_{A12} and Φ_{B12}, respectively,

$$\frac{\xi(\xi-M)}{\Lambda_1 F} \to \frac{1}{\xi^2}\ ,\quad \frac{\xi(\xi-M)L_-}{\Lambda_2 F} \to \frac{1}{\xi}$$

Therefore, the integrands of Φ_{A12} and Φ_{B12} are shown to behave as $1/\xi^3$ or better for ξ becoming very large. This makes it possible to deform the integration contour in a manner identical to that illustrated by Fig. IV-8 used in the evaluation of Φ_{A11}. Without the branch point, contibutions arise only from those poles exterior of C_{F+}, as in the case before. Here, with the branch point at ξ_0, additional contribution will result from integration over the branch cut that must be made to account for the multi-valuedness. Thus,

$$\Phi_{A12} = \Phi_{A12s} + \Phi_{A12b}$$

$$= -\sum_{j=1}^{5} \oint_{C_j} \frac{i\xi(\xi-M)}{\Lambda_1} K_\xi e^{iK_\xi F} E_i(-iK_\xi F)\, d\xi$$

$$- \int_{C_b} \frac{i\xi(\xi-M)}{\Lambda_1} K_\xi e^{iK_\xi F} E_i(-iK_\xi F)\, d\xi \qquad \text{(IV-30)}$$

where C_b is the contour around the branch cut which is to be discussed next. The character of ξ_0 was examined in detail and portrayed by Fig. IV-10. Essentially, before time equals τ_{0F}, which is the minimum time for the waves to arrive at a given field point, ξ_0 stays on the real axis. After τ_{0F}, ξ_0 moves onto C_{F0} to become complex. There is no unique way of making the branch cut but definitely it should be made in the most uncomplicating manner. For instance, it is highly desirable that the cut be straight and bypass C_{F0} and C_{F+}. So, the cut can be made in the subsequent forms. Before $\tau = \tau_{0F}$, depending on which side the point ξ_0 may be positioned, it is made along the real axis away from C_{F0} as depicted in Fig. IV-11. This simplifies the integration in that it is performed with respect to u alone. Substitute the series expression Eq. IV-29 for the exponential integral into Eq. IV-30 and clearly, only the ln term will contribute as the other two terms are single valued on C_b.

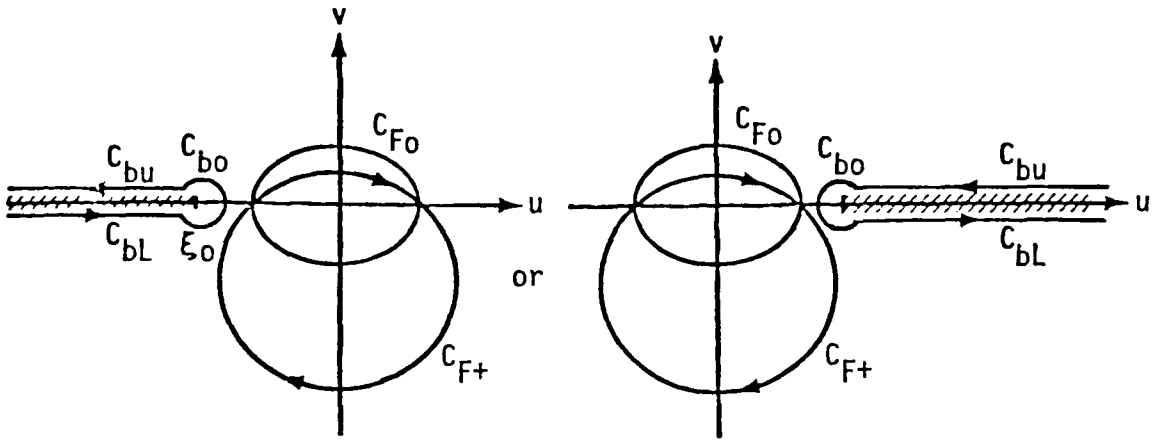

$$C_b = C_{bo} + C_{bu} + C_{bL}$$

Figure IV-11 Branch Cut Before τ_{OF}

With the branch point not contributing over the vanishing circle C_{bo}, Φ_{A12b} becomes

$$\Phi_{A12b} = - \int_{C_{bu}+C_{bL}} \frac{i\xi(\xi-M)}{\Lambda_1} K_\xi e^{iK_\xi F} \ln (iK_\xi F)\, d\xi$$

Let (IV-31)

$$S_F = \frac{i\xi(\xi-M)}{\Lambda_1} K_\xi e^{iK_\xi F}$$

which is real along C_{bu} and C_{bL}. But,

$$\ln (iK_\xi F) = \ln (\zeta e^{i\theta}) = \ln \zeta + i\theta$$

where $\zeta = |iK_\xi F|$ is the same but θ is discontinuous on the two paths. For $\xi_o < 0$, $\theta = \pi$ on C_{bu} and $\theta = -\pi$ on C_{bL}, and for $\xi_o > 0$, $\theta = 0$ on C_{bu} and $\theta = 2\pi$ on C_{bL}. This quite simply leads to:

$$\left.\begin{aligned} \Phi_{A12b} &= i\,2\,\pi \int_{-\infty}^{\xi_o} S_F(u)\,du \qquad \xi_o < o \\ &= i\,2\,\pi \int_{-\infty}^{\xi_o} S_F(u)\,du \qquad \xi_o > o \end{aligned}\right\} \qquad \text{(IV-32)}$$

Since the above is a purely imaginary quantity, it will not add on to the overall transmitted field. However, later in dealing with Φ_G, the same integral would yield a real quantity which will be shown to have a significance relating to the causality condition.

The expression for Φ_{A12b} obtained above is for τ less than τ_{OF} when ξ_o is real. Now, turn attention to τ greater than τ_{OF}. Once more, the branch cut can be made straight and away from C_{FO} and C_{F+} as depicted in Fig. IV-12 for the two possible cases of (1) ξ_0 being complex and (2) ξ_0 being real but in between two C_{FO}'s.

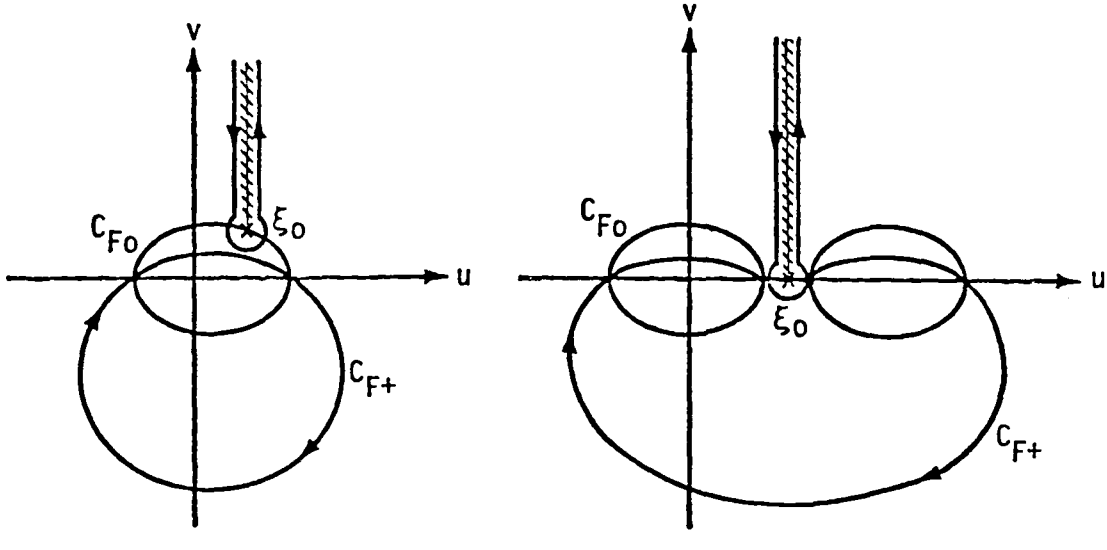

Figure IV-12 Branch Cut After τ_{OF}

The simplification of Φ_{A12b} directly follows by employing again the procedure taken for $\tau < \tau_{OF}$.

$$\Phi_{A12b} = -i2\pi \int_{v_o}^{\infty} S_F\,(u_o + iv)\,dv \qquad \text{(IV-32a)}$$

where $\xi_o = u_o + iv_o$. By the same development,

$$\Phi_{B12} = \Phi_{B12s} + \Phi_{B12b} \qquad \text{(IV-33)}$$

where for $\tau < \tau_{OF}$

$$\left.\begin{aligned} \Phi_{B12b} &= -i\,2\pi \int_{\infty}^{\xi_o} T_F\,(u)\,du \qquad \xi_o < o \\ &= -i\,2\pi \int_{\infty}^{\xi_o} T_F\,(u)\,du \qquad \xi_o > o \end{aligned}\right\} \qquad \text{(IV-34)}$$

for $\tau > \tau_{OF}$

$$\Phi_{A12b} = i\,2\pi \int_{v_o}^{\infty} T_F(u_o + iv)\,dv \qquad \text{(IV-34a)}$$

with

$$T_F\,(\,\xi\,) = \frac{i\xi(\xi-M)L_-}{\Lambda_2}\,K_\xi\,e^{iK_\xi F} \qquad \text{(IV-34b)}$$

and

$$\Phi_{B12S} = \sum_{j=1}^{5} \oint_{C_j} \frac{i\xi(\xi-M)L_-}{\Lambda_2} K_\xi e^{iK_\xi F} E_i(-iK_\xi F)\, d\xi \qquad \text{(IV-35)}$$

Note however that when $j \neq 3$, $-iK_\xi F \to \infty$. Express the exponential integral by its asymptotic expansion for large arguments,

$$E_i(-iK_\xi F) = -\frac{e^{-iK_\xi F}}{iK_\xi F}\left[1 - \frac{1}{iK_\xi F} + \frac{2}{(iK_\xi F)^2} + \ldots.\right]$$

and substitution into Eq. IV-35 leads to, for $j = 3$,

$$\oint_{C_j} \frac{i\xi(\xi-M)L_-}{\Lambda_2}\left[1 - \frac{1}{iK_\xi F} + \frac{2}{(iK\xi F)^2} + \ldots..\right] d\xi$$

The above shows that those points are no longer poles and hence reduce to zero. Thus Eq. IV-35 is replaced by

$$\Phi_{B12s} = \oint_{C_3} \frac{i\xi(\xi-M)L_-}{\Lambda_2} K_\xi\, e^{iK_\xi F}\, E_i(-iK_\xi F)\, d\xi \qquad \text{(IV-35a)}$$

This completes the analysis of Φ_F with the exception of Φ_{A26} and Φ_{B26} which will be dealt with in the section on instability as they can be directly linked together. For the time being, an intermediate summary shall be made by collecting all the terms which have just been evaluated. The reason for having kept some terms in their incompleted forms becomes immediately clear as a multitude of cancellation takes place. So, write

$$\Phi_F = \frac{1}{4\pi^3\sqrt{R_S R}} \text{Re}\left[-2\pi i \left.\frac{Q_F(\xi)}{\frac{dF}{d\xi}}\right|_{\xi=\xi_o} + \Phi_{A2K3} + \Phi_{B2K3} + \Phi_{A126} + \Phi_{A26} - \Phi_{B26}\right] \qquad \text{(IV-36)}$$

Interpretation of these results will be reserved for a subsequent section but a brief description is in place here for clarity of the above equation. The first term (Eqs. IV-4 & 19) requires a simple analytic evaluation which is only complicated slightly in the determination of ξ_o. The second and third terms defined by Eqs. IV-28 & 28a contain details on the resonance waves as indicated by the delta function operating on $F(\xi_3)$ which is fairly simple to calculate. The definition of Φ_{A12b} and Φ_{B12b} from Eq. IV-31 to Eq. IV-34b depends on the time τ and their evaluation require numerical integrations that may lead to some technical difficulties. Finally, the last two terms whose definitions can be found in Eqs. IV-11 & 12 will be tackled later as mentioned.

To complete the analysis, Eq. IV-16 for Φ_G will be evaluated next. Since the course taken is identical to that for Φ_F, the intermediary steps leading to the final solution will not be described. However, while there are similarities between Φ_F and Φ_G to high extent, there are also subtle but distinct differences and these are pointed out in careful examination. First, write down the results as follows:

$$\Phi_G = \frac{1}{4\pi^3\sqrt{R_S R}} \text{Re}\left[-2\pi \left.\frac{Q_G(\xi)}{\frac{dG}{d\xi}}\right|_{\xi=\xi_o} + \Phi_{D2K3} + \Phi_{E2K3} + \Phi_{D12b} + \Phi_{E12b} + \Phi_{D26} + \Phi_{E26}\right] \qquad \text{(IV-37)}$$

where the expression for G is found in Eq. IV-4 and

$$Q_G(\xi_o) = Q_F(\xi_o) = \frac{\xi_o(\xi_o - M)}{\Lambda_1(\xi_o)} \qquad \text{(IV-37a)}$$

$$\Phi_{D2K3} = -2\pi^2 i \left\{ \left. \frac{\xi(\xi-M)}{\frac{d\Lambda_1}{d\xi}} \right|_{\xi=\xi_3} \delta\left[G(\xi_3)\right] + \left. \frac{Q_D(\xi)}{\frac{d\Lambda_1}{d\xi}} \right|_{\xi=\xi_3} \cdot H_{KG} \right\} \qquad \text{(IV-37b)}$$

$$\Phi_{E2K3} = -2\pi^2 \, i \left. \frac{Q_E(\xi)}{\frac{d\Lambda_1}{d\xi}} \right|_{\xi=\xi_3} \cdot H_{KG} \qquad \text{(IV-37c)}$$

$$Q_D(\xi_3) = \xi_3(\xi_3 - M)\, K_3 e^{-K_3 G(\xi_3)} \;, \quad Q_E(\xi_3) = \left. \frac{Q_D(\xi_3)}{K_3} \frac{iL_+}{\Gamma_1 \Gamma_2} \right|_{\xi=\xi_3}$$

with L_+ defined way back in Eq. III-16a and K_3 in Eq. IV-28b.

$$H_{KG} = H\left[G(\xi_3)\right] H\left[M-2\right] H\left[2\sqrt{2-M}\right] - H\left[-G(\xi_3)\right] H\left[M - 2\sqrt{2}\right]$$

Before the wave arrives $\tau < \tau_{OG}$, where now ξ_o is the zero of G.

$$\left.\begin{aligned} \Phi_{D12b} &= -2\pi \int_{u_o}^{\infty} S_G(u)\, du \qquad \xi_o > o \\ &= -2\pi \int_{u_o}^{-\infty} S_G(u)\, du \qquad \xi_o < o \\ \\ \phi_{E12b} &= -2\pi \int_{u_o}^{\infty} T_G(u)\, du \qquad \xi_o > o \\ &= -2\pi \int_{u_o}^{\infty} T_G(u)\, du \qquad \xi_o < o \end{aligned}\right\} \qquad \text{(IV-37d)}$$

and after the wave arrives $\tau > \tau_{OG}$

$$\left.\begin{aligned} \Phi_{D12b} &= -2\pi \int_{v_o}^{\infty} S_G\,(u_o + iv)\,dv \\ \Phi_{E12b} &= -2\pi \int_{v_o}^{\infty} T_G\,(u_o + iv)\,dv \end{aligned}\right\} \qquad \text{(IV-37e)}$$

with

$$S_G(\xi) = \frac{i\xi(\xi-M)}{\Lambda_1} K_\xi e^{iK_\xi G}$$

$$T_G(\xi) = \frac{i\xi(\xi-M)L+}{\Lambda_2} K_\xi e^{iK_\xi G}$$

Lastly,

$$\left.\begin{aligned} \Phi_{D26} &= \int_o^{\infty} \oint_{C_6} \frac{\xi(\xi-M)}{\Lambda_1} \frac{K}{K + \frac{\Lambda_2}{\Gamma_1\Gamma_2\Lambda_1}} e^{iKG}\,d\xi\,dK \\ \Phi_{E26} &= \int_o^{\infty} \oint_{C_6} \frac{\xi(\xi-M)L+}{\Lambda_2} \frac{K}{K + \frac{\Lambda_2}{\Gamma_1\Gamma_2\Lambda_1}} e^{iKG}\,d\xi dK \end{aligned}\right\} \qquad \text{(IV-37f)}$$

It is immediately recognizable that there is a certain oddity about the first item in that this quantity can be non-zero before time equals τ_{OG} which is the minimum time for signals from the lower half of the ring source to arrive at a given field position. This appears to be in violation of the causality condition established in Eq. IV-3, but a closer examination points to the resolution of this contradiction at once. It might be kept in mind that the causality condition simply requires Φ_G to be zero before τ_{OG} and not each term which makes up its expression. So, if the terms can be shown to sum up to zero, then the causality condition is

quite obviously satisfied. To do this, first examine the terms that make up Φ_F where this problem is not encountered. The reason is there, in Eq. IV-36, the first term vanishes before τ equals τ_{OF} and furthermore, the terms Φ_{A12b} and Φ_{B12b} make zero contribution as they are purely imaginary quantity. Now, returning to Φ_G, it can be seen that while the first term is real before τ_{OG}, Φ_{D12b} and Φ_{E12b} which correspond to Φ_{A12b} and Φ_{B12b} also make purely real contribution. The fact that Φ_G had been shown to satisfy the causality condition at the outset and then having properly carried out the integration all the way provides for a sufficient ground to assume that these terms have the self-cancellation quality. However, this point cannot be easily substantiated as direct proof is not possible. It will be necessary to perform the numerical integration on Φ_{D12b} and Φ_{E12b} and then to compare with the quantity of the first term. Next, observe that Φ_{D2K3} and Φ_{E2K3} are purely imaginary in contrast with the parallel terms in Φ_F which are real and as mentioned can be related to resonance waves. Here, they simply do not contribute probably due to the influence of curvature effects. Lastly, it will just be remarked that Φ_{D26} and Φ_{E26} are again referred to as instability integrals and together with their counterparts in Φ_F will be treated in the next section.

V. THE INSTABILITY ANALYSIS

This chapter is devoted to the examination of those terms identified as instability integrals in the last section. First, restate them:

$$\Phi_{A26} = \int_0^\infty \oint_{C_6} \frac{i\xi(\xi-M)}{\Lambda_1} \frac{K}{K+\frac{\Lambda_2}{\Gamma_1\Gamma_2\Lambda_1}} e^{iKF}\, d\xi\, dK$$

$$\Phi_{B26} = \int_0^\infty \oint_{C_6} \frac{i\xi(\xi-M)L_-}{\Lambda_2} \frac{K}{K+\frac{\Lambda_2}{\Gamma_1\Gamma_2\Lambda_1}} e^{iKF}\, d\xi\, dK$$

Φ_{D26} is similar to Φ_{A26} except in the absence of i and the function F being replaced by G. Taking away i and replacing L_- and F by L_+ and G respectively in Φ_{A26} transforms it to the expression for Φ_{E26}. What these integrals have in common is the fact that they all diverge. It can and will in fact be shown that this occurs only in a limited region in space and time as expected. Recall that C_6 is a small circle of vanishing radius about the moving pole of $1/(K+\Lambda_2/\Gamma_1\Gamma_2\Lambda_1)$. Clearly, C_6 is a function of K and by continuously varying K, the movement of the pole will follow a certain path C. This path C is merely an approximation to the actual path C_S which is traced from the original eigenequation S_J defined in Eq. II-24. In fact, C_S may not be the only path of S_J. However, any other possible paths of S_J will not be be considered as they play no role in the stability analysis, which is the real concern here. That any path other than C_S can be disregarded has been shown by Morgan[26] and Munt[27]. The most central issue here is, how well does C approximate C_S? Getting the answer to this question is not a trivial matter as C_S remains an

unknown because of its complexity which was the reason for making approximations in the first place. So the alternative is to obtain not the exact but a fairly accurate picture by taking more terms in the asymptotic expansions. But before going on with that idea, examine first the curve C which can be constructed rather simply. Fig. V-1 shows a number of curves for various Mach numbers. Observe that in the limit of K tending to infinity, every curve independent of the Mach number moves toward the corresponding point of $1 + \Gamma_1 \Gamma_2 = 0$. This comes as no surprise since K equals infinite is the short wavelength limit where the plane vortex sheet analysis is valid and the zeros of $1 + \Gamma_1 \Gamma_2$ give rise to instability waves in that analysis. In the other extreme of K tending to 0, observe the curve moves toward and overshoots M slightly for the case of M = 0.5. This path is surely acceptable since the original path of integration C_+ can be placed above the curve in accordance with its requirement. But the figures show that for all the other Mach numbers, their corresponding curves C seem to move out toward infinity. If this was true, then C_+ would have been crossed in violation of the causality condition. However, considering the present problem to be well set up, there is no reason to believe that such incompatibility can take place and the paths are highly suspicious of being far from representing the true paths C_S. The fact that C appears to fail in describing C_S for small K is not entirely unexpected since the asymptotic expansions for large K were carried only to the second term. Now, one more term will be appended as suggested beforehand. Thus, the expansions for Hankel functions are:

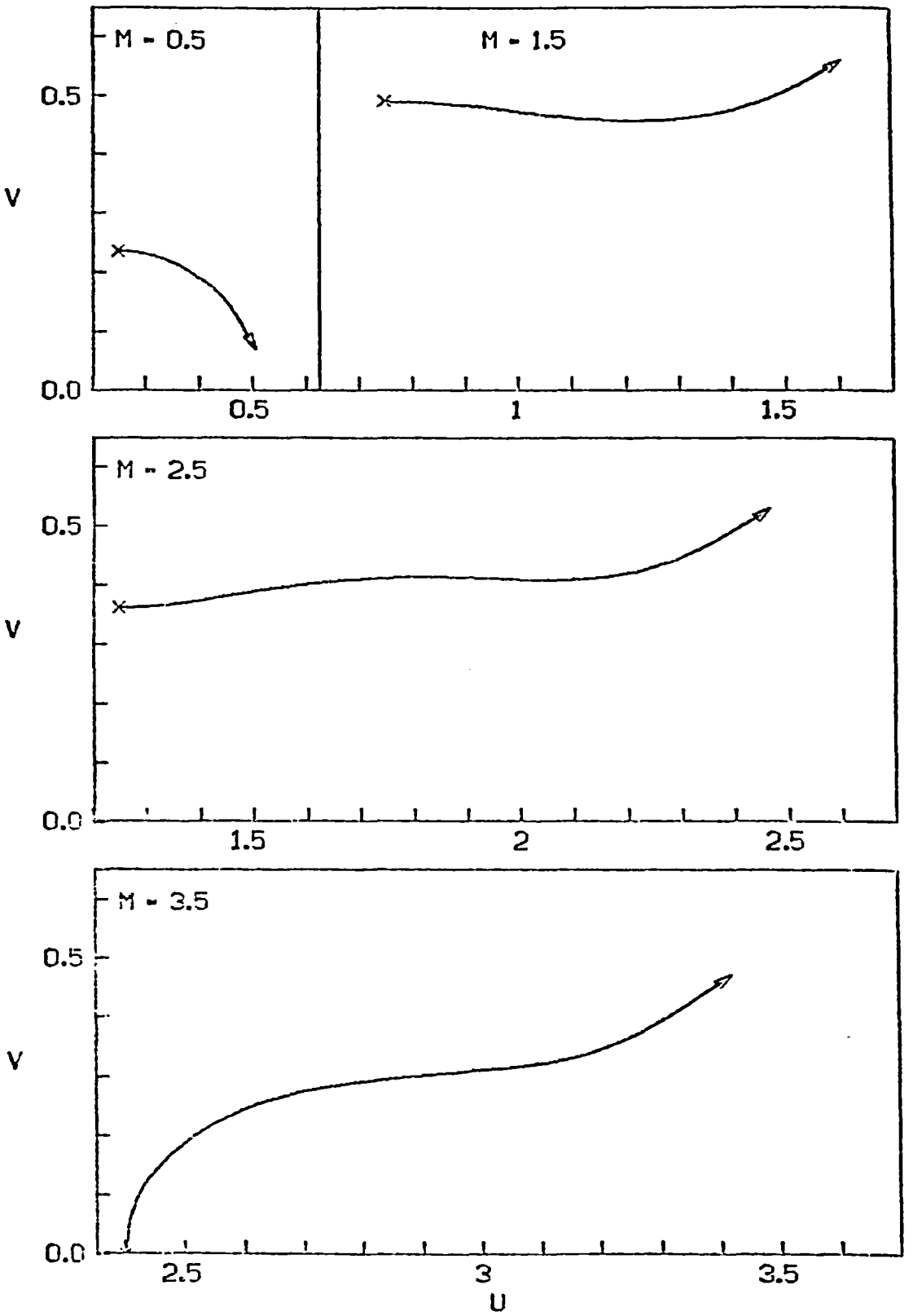

FIGURE V-1 MØVING PØLE PRØFILES FRØM TWØ-TERM EXPANSIØNS

$$H_0^{(1)}(z) = \sqrt{\frac{2}{\pi z}}\left[1 - \frac{i}{8z} - \frac{9}{128z^2}\right] e^{i(z - \frac{\pi}{4})}$$

$$H_1^{(1)}(z) = \sqrt{\frac{2}{\pi z}}\left[1 + \frac{i3}{8z} + \frac{15}{128z^2}\right] e^{i(z - \frac{3\pi}{4})}$$

with their arguments in between $-\pi$ and 2π. The expressions for Bessel functions are:

$$J_0(z) = \frac{1}{2}\sqrt{\frac{2}{\pi z}}\left\{\left[1 - \frac{i}{8z} - \frac{9}{128z^2}\right] e^{i(z-\frac{\pi}{4})} + \left[1 + \frac{i}{8z} - \frac{9}{128z^2}\right] e^{-i(z-\frac{\pi}{4})}\right\}$$

$$J_1(z) = \frac{1}{2}\sqrt{\frac{2}{\pi z}}\left\{\left[1 + \frac{i3}{8z} + \frac{15}{128z^2}\right] e^{i(z-\frac{3\pi}{4})} + \left[1 - \frac{i3}{8z} + \frac{15}{128z^2}\right] e^{-i(z-\frac{3\pi}{4})}\right\}$$

where these expansions are valid in the region $-\pi$ to π. The expansions for the region of 0 to 2π deviate from the above in the manner consistent with the differences between Eqs. III-2 of the two-term expansions. Then, in reference to Eqs. III-4 & 5, the following definitions are derived.

$$D_1 = 1 + \frac{i}{8k}\left(\frac{1}{\Gamma_2 r_s} - \frac{1}{\Gamma_1 r}\right) + \frac{1}{64k^2}\left(\frac{1}{\Gamma_1\Gamma_2 r_s r} - \frac{9}{2\Gamma_1^2 r^2} - \frac{9}{2\Gamma_1^2 r_s^2}\right)$$

$$D_2 = -i + \frac{1}{8kr_o}\left(\frac{1}{\Gamma_2} + \frac{3}{\Gamma_1}\right) + \frac{i}{64k^2 r_o^2}\left(\frac{3}{\Gamma_1\Gamma_2} - \frac{15}{2\Gamma_1^2} + \frac{9}{2\Gamma_2^2}\right)$$

$$D_3 = i + \frac{1}{8kr_o}\left(\frac{3}{\Gamma_2} + \frac{1}{\Gamma_1}\right) - \frac{i}{64k^2 r_o^2}\left(\frac{3}{\Gamma_1\Gamma_2} + \frac{9}{2\Gamma_1^2} - \frac{15}{2\Gamma_2^2}\right)$$

$$E_1 = i + \frac{1}{8k}\left(\frac{1}{\Gamma_2 r_s} + \frac{1}{\Gamma_1 r}\right) - \frac{i}{64k^2}\left(\frac{1}{\Gamma_1\Gamma_2 r_s r} + \frac{9}{2\Gamma_1^2 r^2} + \frac{9}{2\Gamma_2^2 r_s^2}\right)$$

$$E_2 = 1 - \frac{1}{8kr_o}\left(\frac{1}{\Gamma_2} - \frac{3}{\Gamma_1}\right) + \frac{1}{64k^2r_o^2}\left(\frac{3}{\Gamma_1\Gamma_2} + \frac{15}{2\Gamma_1^2} - \frac{9}{2\Gamma_2^2}\right)$$

$$E_3 = 1 + \frac{i}{8kr_o}\left(\frac{3}{\Gamma_2} - \frac{1}{\Gamma_1}\right) + \frac{1}{64k^2r_o^2}\left(\frac{3}{\Gamma_1\Gamma_2} - \frac{9}{2\Gamma_1^2} + \frac{15}{2\Gamma_2^2}\right)$$

Following some algebraic manipulations, σ_1 and σ_2 in Eq. III-8 now become

$$\sigma_1 = -i(\Gamma_1+\Gamma_2)(1+\Gamma_1\Gamma_2) + \frac{1}{8kr_o\Gamma_1\Gamma_2}(\Gamma_1+\Gamma_2)(\Gamma_1-\Gamma_2)(1-3\Gamma_1\Gamma_2)$$
$$+ \frac{i3}{128(kr_o\Gamma_1\Gamma_2)^2}(\Gamma_1+\Gamma_2)(\Gamma_1-\Gamma_2)^2(3-5\Gamma_1\Gamma_2)$$

$$\sigma_2 = -(\Gamma_1-\Gamma_2)(1-\Gamma_1\Gamma_2) + \frac{i}{8kr_o\Gamma_1\Gamma_2}(\Gamma_1-\Gamma_2)(\Gamma_1+\Gamma_2)(1+3\Gamma_1\Gamma_2)$$
$$+ \frac{3}{128(kr_o\Gamma_1\Gamma_2)^2}(\Gamma_1+\Gamma_2)^2(3+5\Gamma_1\Gamma_2)\quad(\Gamma_1-\Gamma_2)$$

Without getting into the mathematical details, it can simply be stated that the above will transform the expression for the moving pole in the denominators of Eqs. III-15 & 16 to the form

$$K^2 + \frac{\Lambda_2}{\Gamma_1\Gamma_2\Lambda_1}K + \frac{\Lambda_3}{(\Gamma_1\Gamma_2)^2\Lambda_1}$$

where Λ_1 and Λ_2 are defined as before in Eq. III-13a and 13b, and

$$\Lambda_3 = -\frac{3}{128}(\Gamma_1+\Gamma_2)(\Gamma_1-\Gamma_2)^2(3-5\Gamma_1\Gamma_2)$$

Obviously, the quadratic equation will allow for two branch of curves traced by its zero as a function of K. In order to select the appropriate branch, first rewrite the above for its zero as

$$K + \frac{i(\Gamma_1 - \Gamma_2)(1-3\,\Gamma_1\Gamma_2)}{16\Gamma_1\Gamma_2\,(1+\Gamma_1\Gamma_2)}\left\{1 \pm \left[1 - \frac{6(3-5\Gamma_1\Gamma_2)(1+\Gamma_1\Gamma_2)}{(1-3\,\Gamma_1\Gamma_2)^2}\right]^{\frac{1}{2}}\right\} = 0 \quad \text{(V-1)}$$

Then, it is at once clear that the plus branch is to be taken since near the zeros of $(1+\Gamma_1\Gamma_2)$, this expression reduces to

$$K + \frac{i(\Gamma_1 - \Gamma_2)(1 - 3\Gamma_1\Gamma_2)}{8\Gamma_1\Gamma_2\,(1+\Gamma_1\Gamma_2)} = 0$$

which is dealt with when two-term expansions are used. Now, a new set of curves C are obtained numerically and sketched in Fig. V-2 based on the positive branch of Eq. V-1 and the same curves in Fig. V-1 have been superposed for the sake of comparison. For M = 0.5, the two curves are very nearly the same and approach the point $\xi = M = 0.5$ overshooting in the former and undershooting presently. For higher Mach numbers, the two curves are decidedly different except near the $K = \infty$ limit where falling back to the points of the zeros of $1+\Gamma_1\Gamma_2$ is expected. In the case of M = 1.5, the curve appears to head toward the point $\xi = M$ but then undershoots it drastically. For both M = 2.5 and 3.5, the curves again visibly diverge but not before the move towards their respective point of $\xi = M$ has become more than evident. Once more, the reason for diverging in the direction of infinity is inescapably due to the smallness of K on that portion of the curves. It might be concluded then that the three-term expansion still falls short of yielding a representative picture of C_S, thus requiring additional terms. On the other hand, there is no question about the notable improvement of the three-term curves over the two-term ones in snowing more sense of direction. Unmistakably visible is the fact that all curves now seem to move toward the point $\xi = M$, leading to the

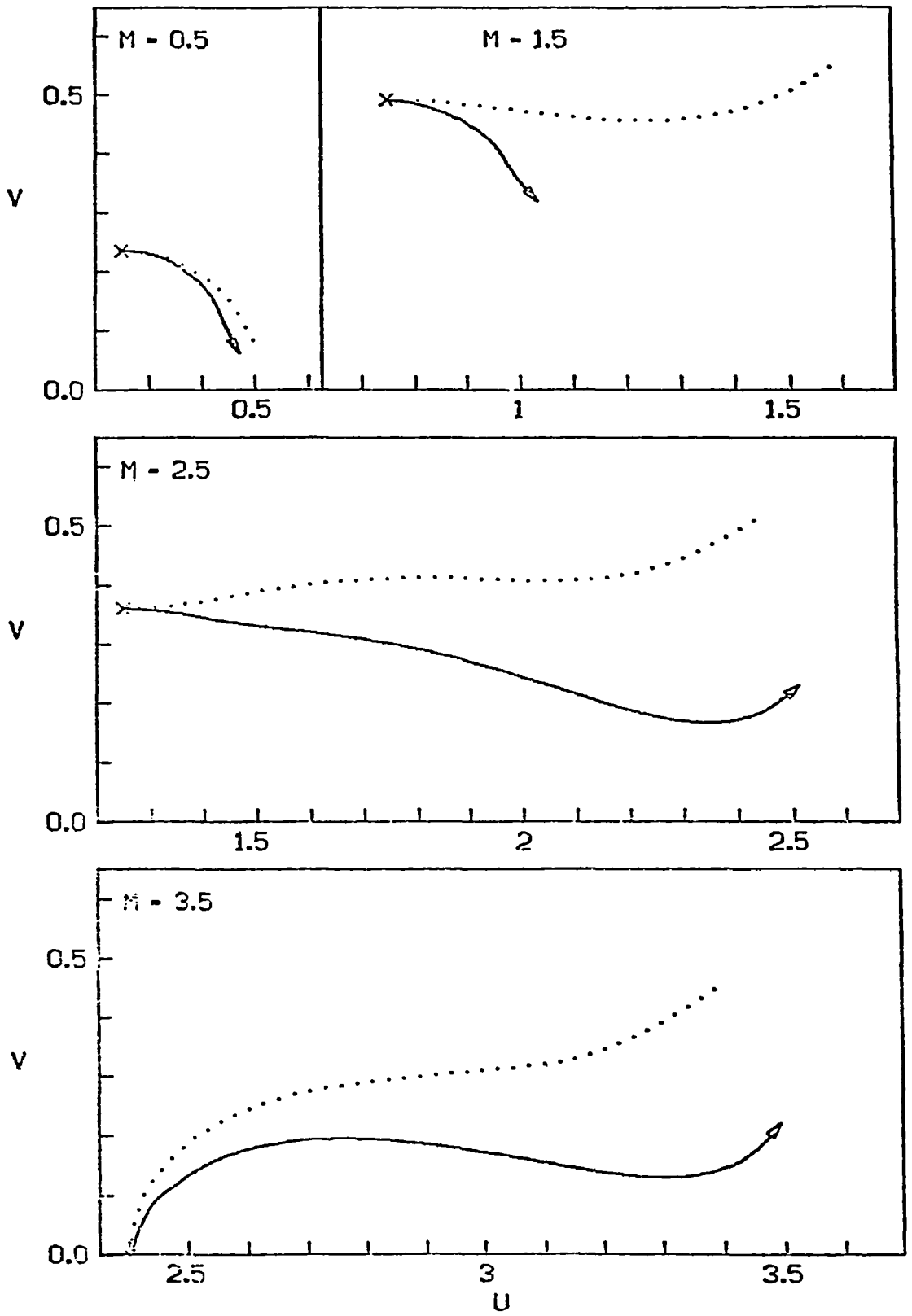

FIGURE V-2 MØVING PØLE PROFILES FRØM THREE-TERM EXPANSIØNS

speculation that C_S is a smooth curve whose end points are at the zeros of $1 + \Gamma_1 \Gamma_2$ in the large K limit and at $\xi = M$ in the small K limit. Therefore, it would suffice to prove that the curve can indeed be traced to $\xi = M$ in the limit of $K \to 0$. This approach is preferred over manipulating on extra terms in the asymptotic expansions which can be rather cumbersome. For small K, it is necessary to exapnd S'_J in ascending series and here to the second terms as follows:

$$J_0(z) = 1 - \frac{z^2}{4} + \ldots$$

$$J_1(z) = \frac{z}{2} - \frac{z^3}{16} + \ldots$$

$$H_0^{(1)}(z) = \left(1 - \frac{z^2}{4}\right) + i\,\frac{2}{\pi}\left\{\ln\left(\frac{z}{2}\right) - \frac{z^2}{4}\left[\ln\left(\frac{z}{2}\right) + \gamma - 1\right]\right\} + \ldots.$$

$$H_1^{(1)}(z) = \left(\frac{z}{2} - \frac{z^3}{16}\right) - i\,\frac{2}{\pi}\left\{\frac{1}{z} - \frac{z}{2}\left[\ln\left(\frac{z}{2}\right) - \frac{1}{2} + \gamma\right]\right\} + \ldots$$

where γ is the Euler's constant. Substituting these into the expression for S'_J in Eq. II-24 and collecting only the leading terms deliver the following equation for the zeros.

$$\Gamma_1 (\xi - M)^2 + \Gamma_2 \xi^2 \frac{(K\Gamma_1)^2}{2} \ln\left(\frac{K\Gamma_1}{2}\right) = 0 \qquad \text{(V-2)}$$

Clearly, when K = 0 the above reduces to a zero at $\xi = M$ and on first inspection it appears to be a zero of order two. But noting $(\xi - M)$ is as well a part of the numerator in Eq. II-23 makes $\xi = M$ just a simple pole,

thus in consistency with the poles for all values of K. This completes the proof on where C_S begins its path at the K = 0 end. Now Eq. V-2 can be used to show, as illustrated in Fig. V-3, how it approximates C_S for small K. Note the curves from Figs. V-1 & 2 have been superposed so that the combination of all three sets of curves can help to shed light on the general nature of C_S. Here, those curves resulting from two-term expansions are labeled C_1, C_2 for three-term, and C_3 for small K. For M = 0.5, C_3 is sandwiched in between C_1 and C_2 in the most conspicuous manner that C_S can be safely assumed to lie within that narrow strip, beginning at ξ = M and ending at $\xi = \xi_1$, the corresponding zero of $1+ \Gamma_1 \Gamma_2$ which is displayed in Eq. IV-2. For M = 1.5, there is no doubt in seeing C_3 to approach the other end point at $\xi = \xi_1$, so a dashed line has been extended from C_3 to complete a curve most likely to portray C_S. For either M = 2.5 and 3.5, C_3 seems to head a little off course but still appears to proceed toward the other end, so a dashed line is drawn in each case to simulate the likely profile of C_S.

It is established that the path C traced by the two-term expansions does not come close to approximating C_S, especially in the small K limit. The situation is remedied by taking one extra term and at the same time approaching from the small K end by using ascending series expansions. The results have been shown to furnish sufficient grounds for drawing up a conclusive picture of C_S's profile. As remarked in the beginning of this section, C_S has not been found exactly due to the complex nature of S'_J, but the approximate picture obtained is all that is necessary in showing the moving pole to be bounded. So in working with Φ_{A26} etc., the pole will be

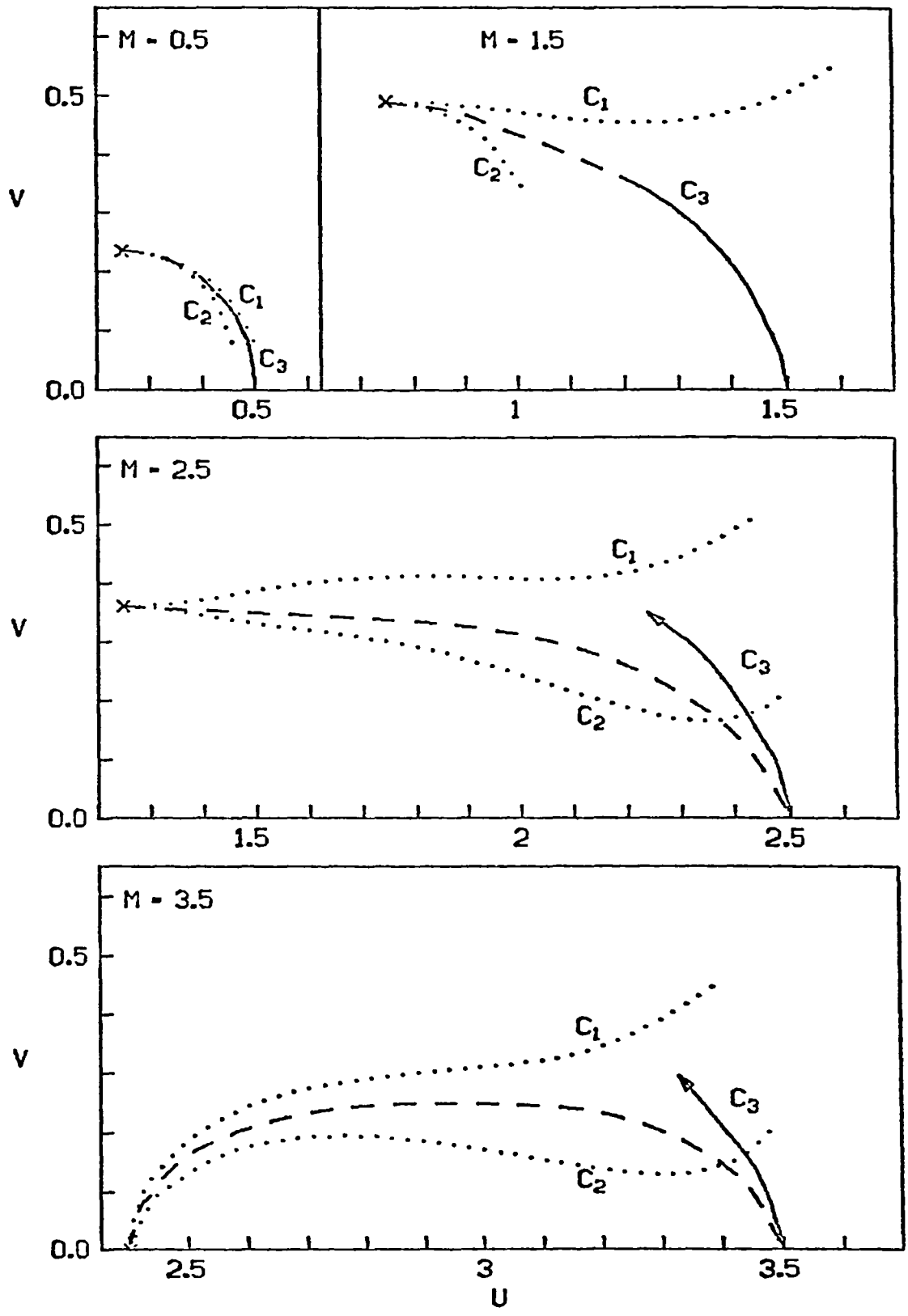

FIGURE V-3 MØVING PØLE PRØFILES FRØM SERIES EXPANSIØNS

taken to move along in that fashion. With this knowledge, the instability waves can be examined for the spatial extent in which they propagate. The moving pole illustrates specifically the presence of a singularity for every value of K, where the one corresponding to $K = \infty$ is precisely the singularity found in the line source problem that gives rise to instability waves. The integrals under consideration, i.e. Φ_{A26} etc., can therefore be regarded as made up of infinitely many integrals, with each given rise to instability waves at a distinct K. The idea then is to get a picture of how the region of propagation varies with K. First, express the integrals in a representative form.

$$\frac{i}{4\pi^2}\int_{-\infty}^{\infty}\oint_{C_6}\frac{Q_I(\xi)}{\xi-\xi_6}\,e^{iKF}\,d\xi\,dK \qquad \text{(V-3)}$$

with ξ_6 continuously varying for all K such that for the integral corresponding to $K \to \infty$, $\xi_6 = \xi_1$ or ξ_4. ξ_2 and ξ_5 are no longer included since ξ_2 is always in the lower half while ξ_5 moves into the lower half as soon as $K \neq \infty$ and it was shown in the last section that any poles below the real axis can be enclosed within C_{F+} to nullify their contributions. Inversion of the above can be shown to lead to $Q_I(\xi_6) \cdot \delta[F(\xi_6)] \cdot Q_I(\xi_6)$ represents the magnitude which is generally expected to be large. For $M < 2\sqrt{2}$, it is supplemented by H_1, (see Eq. IV-5a) the Heaviside factor containing the information on when ξ_1 is exterior of C_{F+} which is directly related to space and time. Observe the delta function has a complex argument. Using the notation of Eq. IV-5, that is for $F(\xi_6) = \alpha + i\beta$ it can be shown that

$$\delta(\alpha + i\beta) = \sum_{n=0}^{\infty} \frac{(i\beta)^n}{n!} \delta^{(n)}(\alpha)$$

Thus, the instability waves propagate along $\sigma = 0$ in the region $\beta < 0$. The spatial extent can be determined by eliminating time between the two to find it boundary. Recall first

$$F = Z + \Gamma_1 (R - 1) + \Gamma_2 (1 - R_S) - \tau\xi$$

For $K = \infty$, $\xi = \xi_1 = M/2 + i\eta$ and

$$\alpha = Z + \frac{1}{2}\left[\sqrt{M^2 + 1} - 1\right](R + R_S - 2) - \frac{\tau M}{2}$$

$$\beta = \eta\left[\frac{1}{M}\left(\sqrt{M^2 + 1} + 1\right)(R - R_S) - \tau\right]$$

from which the boundary line for the instability waves becomes

$$Z = \frac{1}{2}\left[\sqrt{M^2 + 1} + 1\right](R - R_S) - \frac{1}{2}\left[\sqrt{M^2+1} - 1\right](R+R_S-2) \quad \text{(V-4)}$$

Since $dZ/dR = 1$, it is clear that the line makes a 45^o angle with the axial direction. For $K \neq \infty$, the boundary equation becomes, with $\xi_6(K) = u + iv$,

$$Z = \frac{u}{v} I_m\left[\Gamma_1(R - 1) + \Gamma_2(1-R_S)\right] - Re\left[\Gamma_1(R-1) + \Gamma_2(1 - R_S)\right] \quad \text{(V-5)}$$

and

$$\frac{dz}{dR} = \frac{u}{v} \; I_m \Gamma_1 - Re\Gamma_1$$

This means the boundary no longer makes a 45^0 angle but still is a straight line. The expressions of ξ_6 for $K \neq \infty$ are not known explicitly and must be resorted to approximations provided by Fig. V-3. By tracing from $K = \infty$ along the possible profiles for C_S, the values of ξ_6 can be roughly estimated to be used in Eq. V-5. For illustrative purpose, the boundary lines thus obtained are shown in Fig. V-4a for the case $M = 0.5$ since C_S is believed to be most accurately predicted there. The boundary lines for the instability waves from both Φ_F coming first and Φ_G second are included. It is clear from these figures that the boundary line for $K = \infty$ is always the outermost while the other lines, for K moving away from ∞, all fall to the right with lesser angles. The instability waves propagate in these regions where $\beta(K) < 0$ as singular wave forms defined by $\alpha(K) = 0$, which are straight lines more or less perpendicular to the boundary lines as shown. At this point, it might be recalled that as K becomes smaller, the corresponding point on C_S approaches the point $\xi = M$. What this means is that because $\xi = M$ is always enclosed by C_{F0}, somewhere along the way as K becomes small, say at some critical value $K = K_C$, ξ_6 will cease to be outside of C_{F0}, which is equivalent to being enclosed by C_{F+} as shown in the last section, and hence for $K < K_C$, instability waves may no longer appear. This relationship is illustrated by Fig. V-5. It must be recognized that the present analysis is only an approximation, and just as the explicit expression for ξ_6 as a function of K remains undetermined,

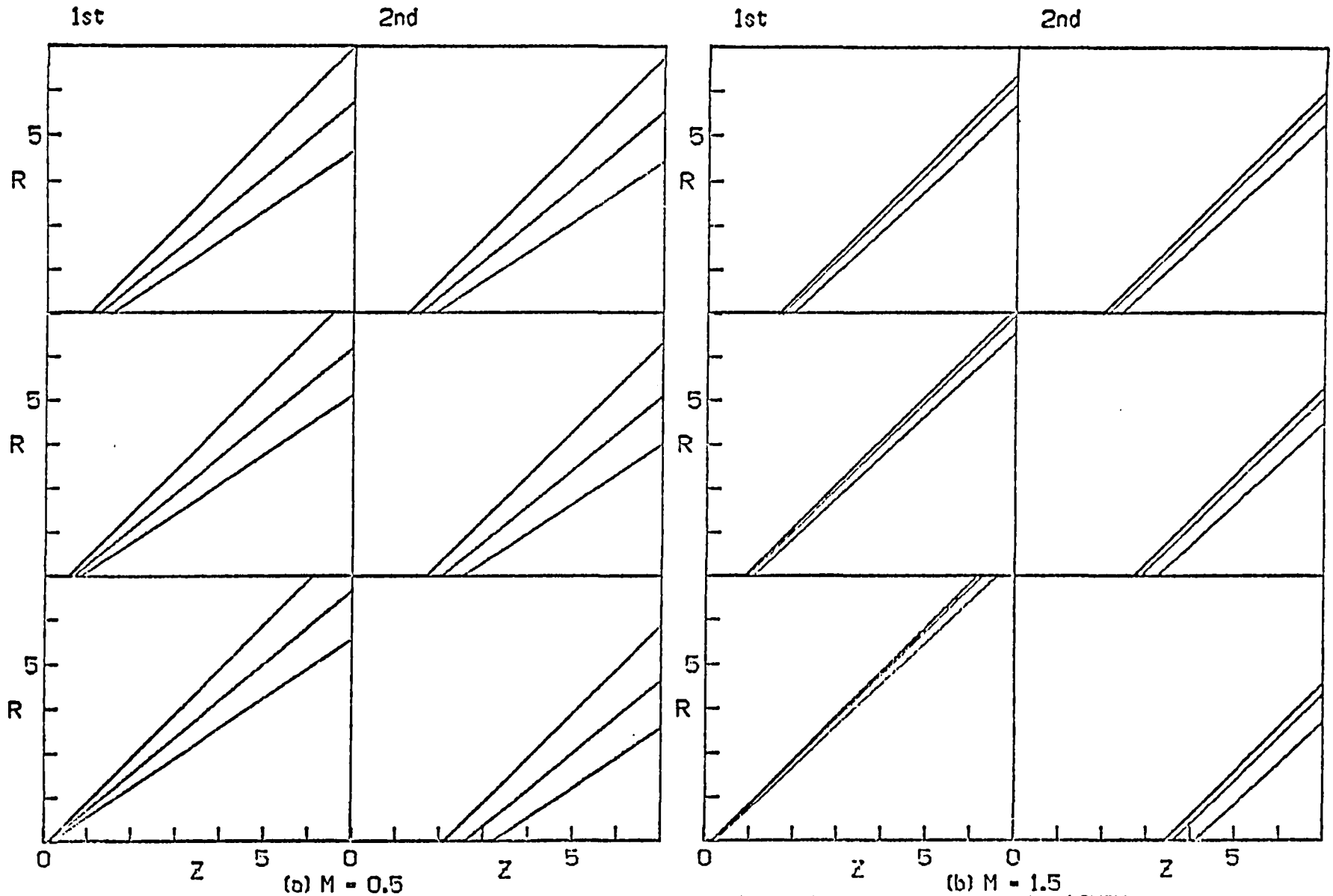

FIGURE V-4 WAVENUMBER DEPENDENCE OF INSTABILITY WAVE BOUNDARY LINES
TOP R_S=0.1, MIDDLE R_S=0.5, BOTTOM R_S=0.9

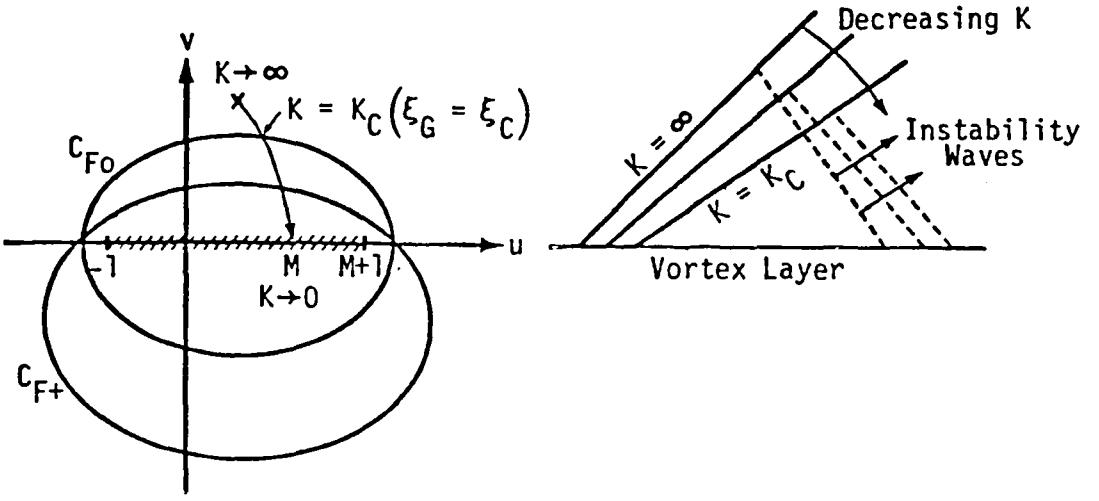

Figure V-5 The moving instability pole and its connection to the region of propagation

the value of K_C and consequently that of ξ_C are approximation, and just as the explicit expression for ξ_6 as a function of K remains undetermined, the value of K_C and consequently that of ξ_C are unknown quantities. Therefore, the precise location of the boundary line for $K = K_C$ cannot be established. But quantitatively, K_C is of the order of 1 and since $K = kR_o$, K_C is of the order of the jet radius. The possibility remains for that line to come in contact with the vortex layer. Then the instability waves may be characterized as having their presence in a limited region which is a function of wavelengths such that for short waves, the boundary makes a 45^o angle with the vortex layer and as wavelengths become large, the boundary moves to the right and draws near the discontinuous surface until finally, at some critical wavelengths, the boundary comes to fall on the vortex layer to end the instability propagation for any longer waves. This characterization is merely an assumption and it is actually more defensible to simply state that the instability waves have wavelengths on

the shorter end. Even though the profile of C_S for M = 1.5 is less perceptible from Fig. V-3, an attempt has been made at obtaining the corresponding boundary lines and these are shown in Fig. V-4b. In contrast to the lines for M = 0.5, these are tighter together and the angular variation is nearly absent. Similar pictures are expected for higher Mach numbers so the previous contention that the boundary line for $K = K_C$ may fall on the vortex layer is less probable.

The preceding discussion has centered on the case of M < 2 2. Basically, the curvature effects are responsible for the predicted functional dependence of the spatial extent of instability waves on the wavelengths. Next, consider what happens for M > 2 2. In the plane vortex sheet model, the instability waves will cease to exist as the complex poles become real to characterize the neutral stability waves. However, an examination of Fig. V-3, for the case of M = 3.5, reveals the vortex layer model to yield a different picture. The profile of C_S clearly shows that the pole is truly on the real axis only when $K = \infty$ and as K is varied from large to small, it moves into the complex domain. Since in reality, $K = \infty$ corresponding to zero wavelength is just a limit, the overall picture calls for the continued presence of instability waves at the higher Mach numbers. The representative Eq. V-3 can be used once again to ascertain the spatial extent. Here, however, when $K = \infty$, the inverse is accompanied by H_4 defined in Eq. IV-7. Eliminating time between this expression and $F(\xi_6) = 0$, which is now real, yields the boundary line equation as follows.

$$Z = \frac{R - 1}{\sqrt{\xi_4^2 - 1}} - \frac{M_5 - 1}{\sqrt{\xi_5^2 - 1}} (1 - R_S)$$

where ξ_4 and ξ_5 are given in Eq. IV-2. dZ/dR is less than unity so that the angle which this line makes with the horizontal is less than 45^o. When $K \neq \infty$, ξ_6 becomes complex and the boundary lines can be determined identical to the $M < 2\sqrt{2}$ case. These lines as expressed by Eq. V-5 are again expected to fall to the right and closer to the vortex layer until at some critical wavelength, the pole moves inside of C_{FO} to end the instability wave presence.

In summary, it has been shown the instability integrals will give rise to instability waves for all Mach numbers but that they are wavelength dependent and cease to exist for wavelengths large compared to the jet radius. Furthermore, the region of propagation is similarly affected in that it becomes less extensive for longer wavelengths.

VI. RESULTS AND DISCUSSIONS

To validate and interpret the results obtained in the previous chapters, a computer program based on the analytical solution was developed and numerous cases have been investigated. These numerical results are now presented and discussed in this chapter.

First, the organization and method chosen for analysis are summarized. In Chapter II, the problem is formulated and its solution in the Fourier transformed space is obtained in the form of a multiple integral whose integrand involves complicated Bessel and Hankel functions. Chapter III contains the derivation of an approximate version of the integral solution for the transmitted field; this is based on the assumption that the jet and source radii are sufficiently large so that the two leading terms from the appropriate asymptotic (large argument) series expansions of Bessel and Hankel functions can be used. In approximating with these expansion terms, contributions arising from internal reflections are isolated and neglected. Singularities of the integrand are examined in Chapter IV prior to the inverse analysis which is carried out in the spirit of Cagniard's technique of contour deformation.

The results are now put together and presented below.

$$\Phi = \Phi_F + \Phi_G$$

$$= \frac{1}{4\pi^3\sqrt{R_S R}} \text{Re} \left\{ \Phi_{SF} + \Phi_{A2K3} + \Phi_{B2K3} + \Phi_{A12} + \Phi_{B12} + \Phi_{A26} - \Phi_{B26} \right\}$$

$$+ \frac{1}{4\pi^3\sqrt{R_S R}} \text{Re} \left\{ \Phi_{SG} + \Phi_{D12} + \Phi_{E12} + \Phi_{D26} + \Phi_{E26} \right\}$$

where Φ_F and Φ_G represent the fields from upper and lower half of the source respectively. Each is subdivided into component parts as specularly transmitted, instability, and neutral stability waves. The instability waves (Φ_{A26}, Φ_{B26} and Φ_{E26}) requiring a separate analysis are discussed in detail in Chapter IV. And while both halves of the source may give rise to instability, the neutral stability waves are caused only by the upper half. They are, like the instability waves, confined to a limited wedge-like region whose boundary is described by the elimination of time between $F(\xi_3) = 0$ and $\tau - \frac{M(R - R_S)}{\sqrt{M^2-4}} = 0$. A field that would modify the specularly transmitted field in the region of its propagation appears to follow these neutral stability waves, as represented by Φ_{A2K3} and Φ_{B2K3} defined in Eqs. IV-28.

The remaining terms in Eq. VI-1 form the specularly transmitted field. If the solution were approximated by just the one-term asymptotic expansion of Bessel functions, Φ_{SG} would have been absent because its prediction is a consequence of accounting for the finite curvature which is lacking in the simpler approximation. Since upper and lower halves of the ring source have their curvatures opposite in sense, it is not surprising to find Φ_{SF} and Φ_{SG} somewhat different in characteristics as pointed out previously. In fact, every term in Φ_F is different from the corresponding one in Φ_G, although the mathematical differences would not be meaningful unless they can be interpreted and explained from the physical point of view. Φ_{SF} and Φ_{SG} given in Eqs. IV-19 & 37 are fundamentally unequal in the order of arrival at a given field point. Arising from the upper half closer to the point, Φ_{SF} clearly arrives ahead of Φ_{SG}. This means that

Φ_{SF} should have the identity of a wavefront while Φ_{SG}, which comes in succession, should not because the total field Φ cannot possess but a single wavefront. As mentioned formerly, the only way to substantiate the above is by working out numerical evaluations and some examples will be presented a little later.

Next, attention will be focused on the last remaining terms of Φ_{A12}, Φ_{B12}, Φ_{D12} and Φ_{E12} defined in Eqs. IV-32 to 34b and Eqs. IV-27d and 37e. These integrals cannot be simplified analytically any further as shown in Section IV and again must resort to numerical evaluations. A significant point to look for is the way in which they will modify Φ_{SF} and Φ_{SG} to form the total specularly transmitted field. There is no uncertainty in $_F$ to satisfy the causality condition as both Φ_{SF} and Φ_{A12} and Φ_{B12} are zero before the time of arrival. But the same is not obvious for Φ_G, the field coming continuously after the wavefront. It is expected that Φ_{SG} and Φ_{D12} & Φ_{E12} sum to a zero value for the satisfaction of its causality since the two parts are non-zero separately. The numerical evaluations, which will be discussed now, indeed show this to be the case.

The calculations of Φ_{SF} and Φ_{SG} are fairly straight forward because of their analytic simplicity. For a given set of field and time data, it is just a matter of finding the zeros of F and G for substitution into the expressions. The minimum time of travel or the time of expected wavefront arrival for Φ is manifest in Φ_F. This time is directly related to F in that it corresponds to the time when Re(F) first intersects Im(F) at one point of C_{FO} on the real axis. One can find this time by trial and error numerically but to do so is both costly and unnecessary. For the

specularly transmitted field is something that is theoretically predictable from the approach of geometric acoustics. Surely the complex nature of the present problem is sufficient to discourage any such attempt but at least one information can be readily extracted without much difficulty. And that is precisely the minimum travel time. First, the minimum time for the signal to reach the surface of the jet is given by

$$\tau_{1F} = 1 - R_S$$

In this time, the source is imaged downstream to the point

$$Z_{1F} = \tau_{1F} M$$

And the minimum time to reach the field point (Z,R) strictly evaluated by geometric acoustics is then given by

For $Z < Z_{1F}$

$$\tau_{0F} = \tau_{1F} + \sqrt{(z - z_{1F})^2 + (R - 1)^2} \qquad M > 1 \qquad \text{(VI-2a)}$$

$$= \tau_{2F} + \sqrt{E_\tau^2 + (R - 1)^2} \qquad M < 1 \qquad \text{(VI-2b)}$$

where

$$E_\tau = z - M\tau_{2F} \pm (\tau^2_{2F} - \tau^2_{1F})^{\frac{1}{2}}$$

and $\pm$ is for $Z \lesseqgtr Z_{1F}$. For $Z > Z_F$, τ_{OF} is the same as Eq. VI-2b for both M less and greater than 1. In the above, $\tau_{2F} \geq \tau_{1F}$ and should yield a minimum in τ_{OF}. Therefore, $d\tau_{OF}/d\tau_{2F} = 0$ or

$$\sqrt{\left[E_\tau^2 + (R-1)^2\right](\tau_{2F}^2 - \tau_{1F}^2)} - E_\tau\left[M(\tau_{2F}^2 - \tau_{1F}^2)^{\frac{1}{2}} \mp \tau_{2F}\right] = 0$$

τ_{OF} is the minimum time of travel for Φ_F as well as Φ so that a wavefront is expected then. On the other hand, τ_{OG} is just the minimum travel time for Φ_G and it is different from τ_{OF} only in the expression for τ_{1G} which is now $(1+R_S)$ instead of $(1-R_S)$. In the examples to follow, τ_{OF} and τ_{OG} are calculated by the above expressions.

Numerical integrations of Φ_{A12} ect. are more difficult to perform. Considering the semi-infinite interval of integration, an initial attempt by Laguerre intergration proved unsuccessful because the integrands do not decay in a simple exponential fashion. More often than not, the path of integration would pass relatively close to a singularity causing the integrands to fluctuate. Therefore, the task is completed by Gaussian integration instead at the cost of considerably increased computation time. This involves subdividing the semi-infinite span into small intervals and integrating with Gaussian weights from the starting point. Each subinterval is integrated until the desired accuracy is attained. Then, the same is performed onward until two intervals in sequence do not differ in value greater than a specified amount. If the maximum number of Gaussian points used do not lead to a satisfactory result for any subinterval, then it is subdivided even further repetitively until necessary. Since the integrands decay smoothly and rapidly for large arguments, that

is, when the path leaves the region of singularities, convergence to three place accuracy usually occurs well before the argument reaches the order of 50000. Convergence is slower when τ is large because the integrated values are much reduced. The results presented will be divided into two regions. They are designated as the quiet and the noisy regions depending on the absence or the presence of instability waves. In the quiet region, integration always converges. But in the noisy region, convergence is difficult to obtain once entering the actual regions where instability waves propagate. This is because the branch cut integration now passes through the moving pole contour which influences the integrand to oscillate with large amplitudes. In reality, even if convergence is achieved, the transmited field thus calculated still does not include the contribution arising from instability waves. In order to predict the amplitudes for the instability waves, non-linear effects such as due to viscosity must be retained in the conservation equations. The present analysis based on the linear theory can only give a qualitative picture of where and when instability waves propagate and how large a region in space and time they occupy. Thus in the results to be presented, the instability regions will be indicated simply by blanks in that portion of the curves.

From the solution for the velocity potential, two field variables of more interest can be derived, namely the acoustic pressure and the vortex layer displacement. In the linearlized Euler equation, pressure is related to velocity potential by its time derivative which can be evaluated in analytic simplicity as shown in Appendix B. The derivation of vortex layer displacement found in Appendix C is more involved in that it requires

the same inverse analysis applied to velocity potential. Numerical calculations for all three field variables are performed by the computer program listed in Appendix D.

First, analyze what the solution predicts in the quiet region. Figs. VI-1 through 6 are plots of velocity potential Φ vs time τ for various field points, Mach numbers, and source radii. There are three curves in each plot. The dotted ones are Φ_F, the dashed ones Φ_G, and the solid ones Φ which is the sum of the other two. Several general features are immediately evident from these figures, some of which are rather significant. First of all, Φ_F admits a wavefront at the time of its arrival as expected. This is represented by an acute rise from zero at that instant and then followed by a sharp fall before a smooth decay takes place. Next, observe the behavior of Φ_G at its arrival which comes slightly behind Φ_F. Numerically, the sum of Φ_{SG} and Φ_{D12} & Φ_{E12} is shown to add up to zero within the desired accuracy. Thus, the causality condition is satisfied in the fact that Φ_G rises from zero. The total specularly transmitted field hence possesses just a single wavefront. These figures demonstrate the fundamental differences between Φ_F and Φ_G. To describe the sound field for the same data points, now look at the pressure vs time plots, which are presented in Figs. VI-7 through 12. The first five of these are for small ring radius, $R_S = 0.1$, so that the source is nearly centered on the jet axis. Fig. VI-7 is for a point downstream of the source fairly close to the jet. There isn't much difference except in the amplitude between it and Fig. VI-8 which is at the same downstream point but farther away from the jet. The reduced amplitudes and the smoother decays mean lower sound

pressure. If now the point is moved further downstream while keeping the same radial distance as in Fig. VI-9, a significant change in the curves are clearly observed for supersonic cases. Here the amplitudes are much increased and exceed the corresponding cases in Figs. VI-7 & 8 which are both for points closer to the jet. It is clear from this that more sound is refracted in the downstream direction. What this means is that with increasing jet speed, more sound is refracted downstream. This is even more evident from Fig. VI-11 which is for a point straight out from the jet, or more upstream than the other cases. While its distance from the jet is no greater than the point in Fig. VI-7, the amplitudes are much reduced indicating that very little sound is transmitted upstream, especially in the supersonic cases. Between Figs. VI-8 & 9, one can detect the effect, but otherwise the amplitudes are pretty much dependent on distance between the jet and the field point. The cases discussed thus far are more or less representative of the near field characteristics. If the point in Fig. VI-9 is moved outwards in the radial direction, but fixed axially as in Fig. VI-10, then it is out in the far field. A comparison reveals some interesting features. In addition to the amplitude loss due to radial decay, there is the apparent stretching in the time decay history so that it takes longer period for the quieter sound to fade away. The far field radiation also seems to affect the transmission characteristics for supersonic jets. The curve for M = 1.5 in this case is no longer distinguishable from that for the subsonic speed, and for M = 2.5, the curve appears to start losing its supersonic identity. Finally, the effect of source radius can somewhat be examined in Fig. VI-12 which is for the same field point as in Fig. VI-7. As the radius increases, the transmitted

field takes on a different look from previous cases. The relative lower amplitudes reflect the influence of the square root quantity on source radius in the denominator of the solution. The character of the pressure disturbance is also affected due to the fact that as source radius becomes larger, more time separates the signals from various parts of the source.

Next, examine the disturbed fields in the noisy region closer to the jet axis. In this region, vortex layer displacements as well as velocity potential and pressure can be examined. As mentioned earlier, instability regions are the blanked portion of the perturbation curves. But as the exact time of passage in the $K = \infty$ limit can be calculated, that time is indicated by a short vertical line in each case. In Fig. VI-13, the field point is relative downstream making a 30^{0} angle with the jet. Velocity potential is plotted on the top and pressure on the bottom for two Mach numbers. As expected, more sound is refracted into this region. While the disturbances decay rather smoothly in the quiet region, here they actually become increasingly unstable until the passage of instability waves is observed. After its passage, however, the disturbances die out quickly so that the noise covers just a short time period. This is especially true in the supersonic case where the impulsive nature of the source is very evident. Fig. VI-14 is a plot for vortex layer displacement vs time at two field points. On the upper left corner, the point is directly in line with the source relative upstream. For subsonic flows, represented by $M = 0.5$, the displacement is small and smoothly decays. For supersonic flows, as disturbances cannot propagate upstream, the vortex layer remains undisplaced for all times. The other three curves are for a point somewhat

downstream. In all cases, the vortex layer becomes excessively displaced and finally ends up with instabilities. But after its passage, vortex layer returns to quiet very soon. For M = 2.5, besides the instability disturbances, there is also the resonance disturbance which gives rise to the resonance modified field. This is indicated by the increased displacement following the passage of instability waves. This field which follows the resonance wave is shown to die out quickly. It may be concluded that the solution not only predicts a region of instability but also a region of resonance. Finally, Fig. VI-15 shows the time lapse downstream direction. It can be seen that for small time a disturbance begins to develop. This includes a wavefront followed by the instability and a smooth decay. Then as time increases, the disturbances move downstream with increasing amplitudes behind the wavefront. This large displacement is always quieted very quickly after the passage of instability disturbances, which is in agreement with the previous two figures.

In conclusion, an approximate solution to the problem of transmission of sound across a cylindrical vortex layer has been obtained. The results are considerably different from the plane vortex sheet case because of the added role played by the curvature of the jet. In comparison with the plane case, the specularly transmitted waves are more complex and requires some numerical integration. Resonance waves are identically predicted for $M > 2$, but there is also a wave field whose modified effect appears to extend the region of resonance just as the instability waves cover a region in space and time. The instability waves are predicted to exist for all Mach numbers but vanish for wavelengths large compared to the jet radius.

And the region of propagation is similarly wavelength dependent. The prediction that large wavelengths are unimportant in the transmitted field is in agreement with some experimental observations.

Legend to Figures VI-1 to 15

..... Φ_F

- - - - - Φ_G

——— $\Phi = \Phi_F + \Phi_G$

Non-dimensional quantities are defined as follows:

$$\Phi = \frac{\phi r_o^2}{aQ}, \quad Z = \frac{z}{r_o}, \quad R = \frac{r}{r_o}$$

$$R_S = \frac{r_s}{r_o}, \quad \tau = \frac{at}{r_o}, \quad M = \frac{u}{a}$$

$$P = \frac{r_o^3 p}{\rho a^2 Q}, \quad \eta = \frac{\eta r_o^2}{Q}$$

where (L = Length, T = Time, M = Mass)

ϕ - velocity potential of the transmitted field (L^2T^{-1})

r_o - jet radius (L)

a - speed of sound (LT^{-1})

Q - source strength (L^3)

z - distance along the jet (L)

r - radial distance (L)

r_s - ring source radius (L)

t - time (T)

u - jet speed (LT^{-1})

p - acoustic pressure ($ML^{-1}T^{-2}$)

ρ - fluid density (ML^{-3})

η - vortex layer displacement (L)

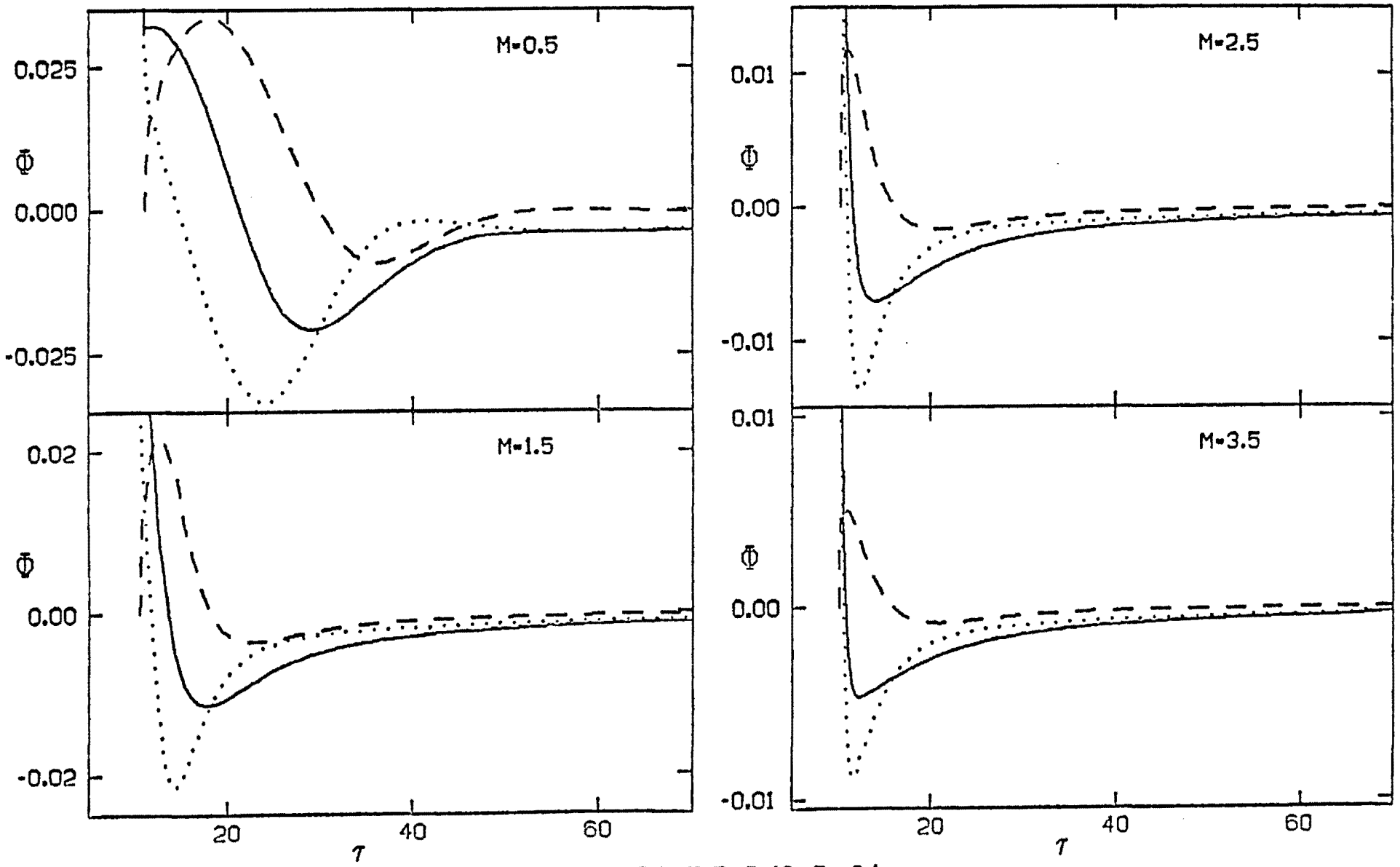

FIGURE VI-1 Z=5 R=10 R_S=0.1

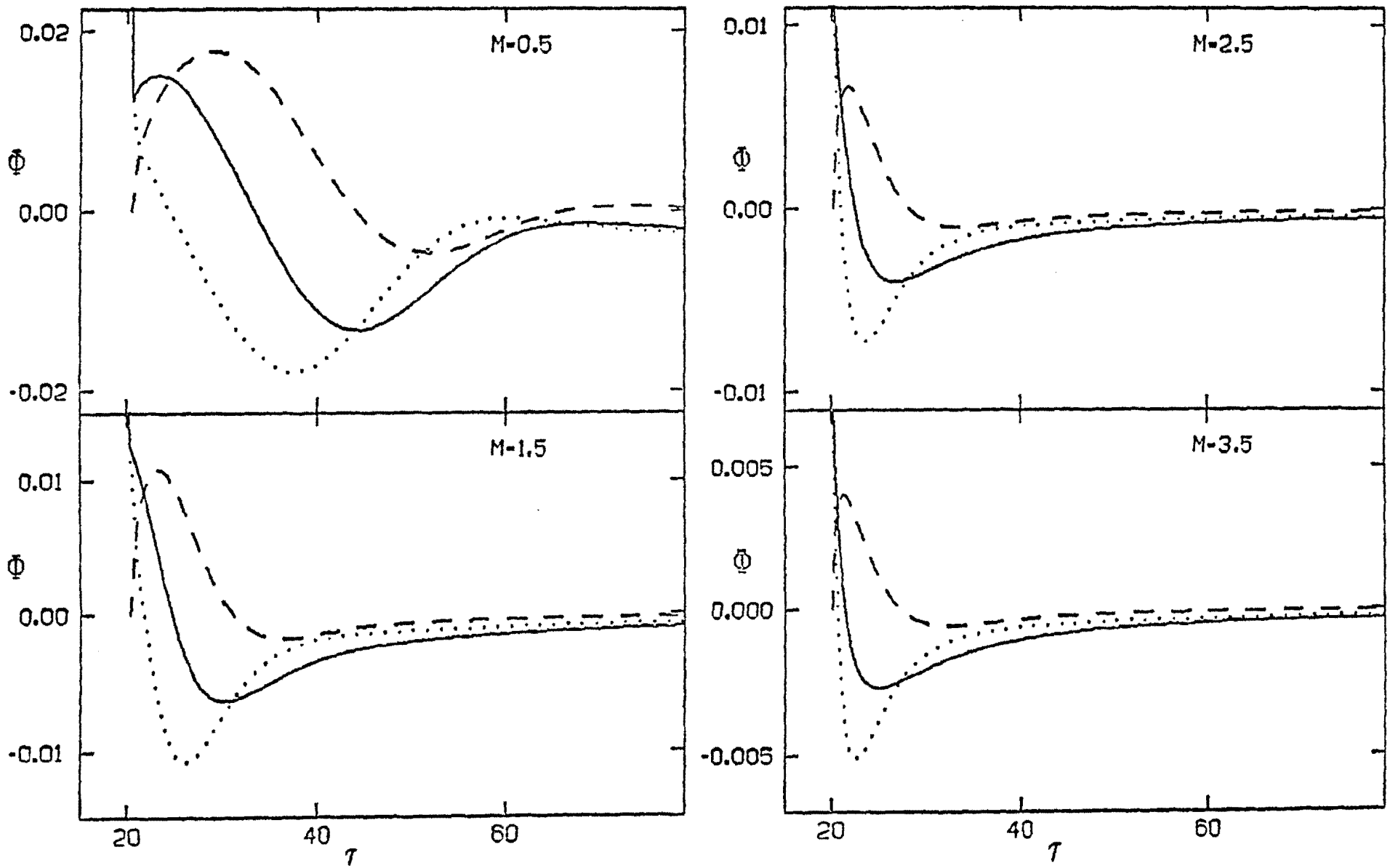

FIGURE VI-2 Z=5 R=20 R_s=0.1

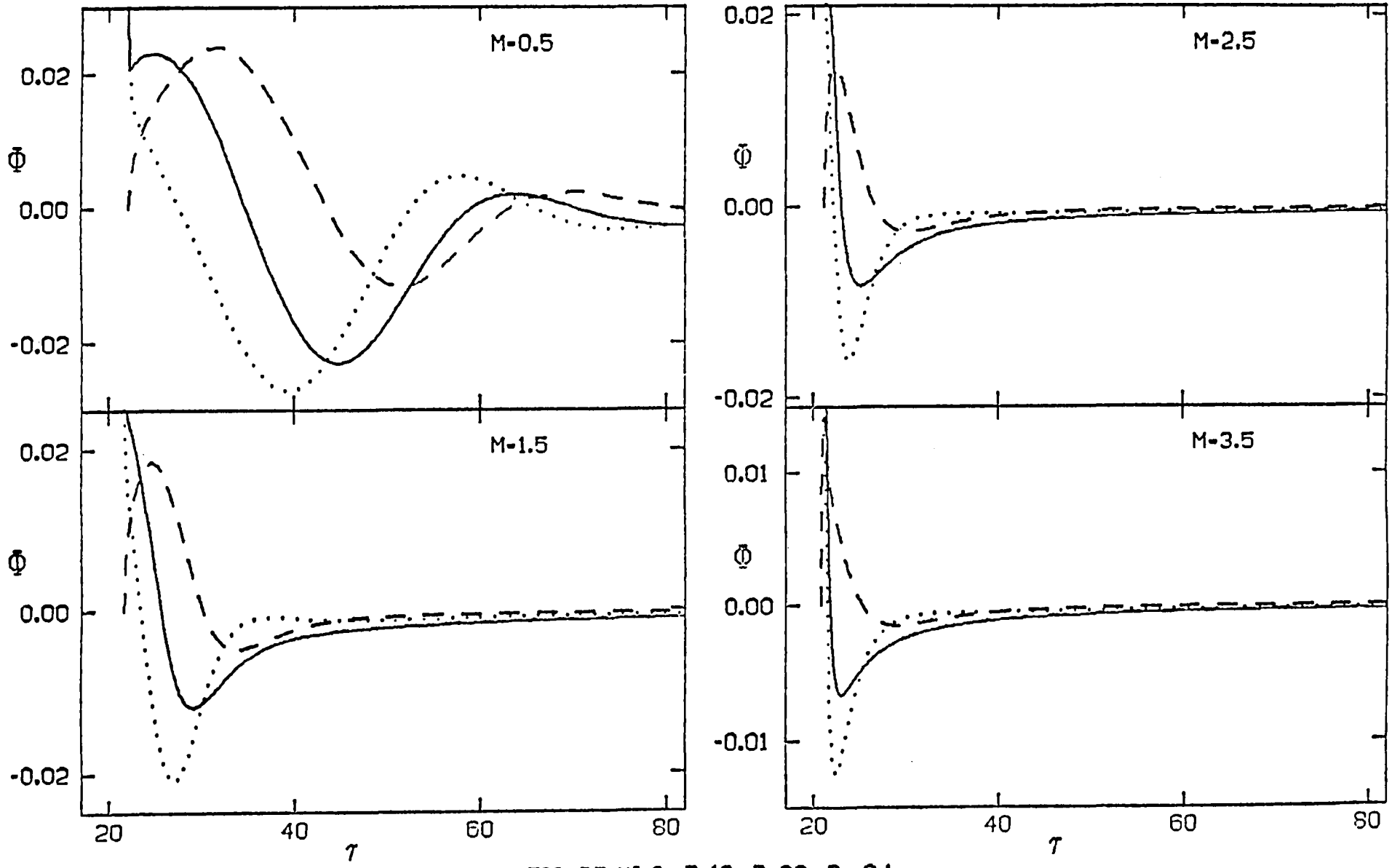

FIGURE VI-3 Z=10 R=20 R_S=0.1

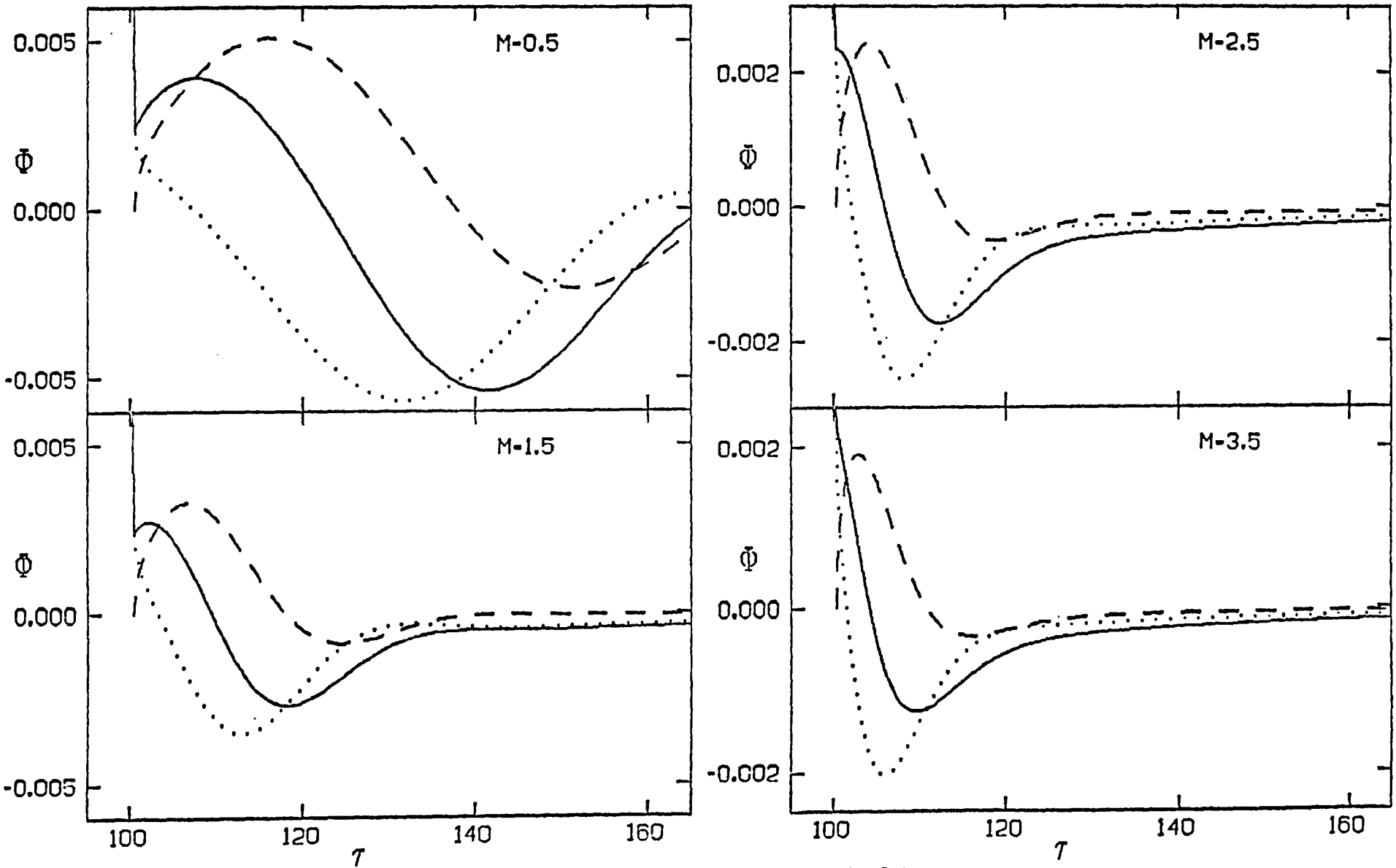

FIGURE VI-4 Z-10 R-100 R_S-0.1

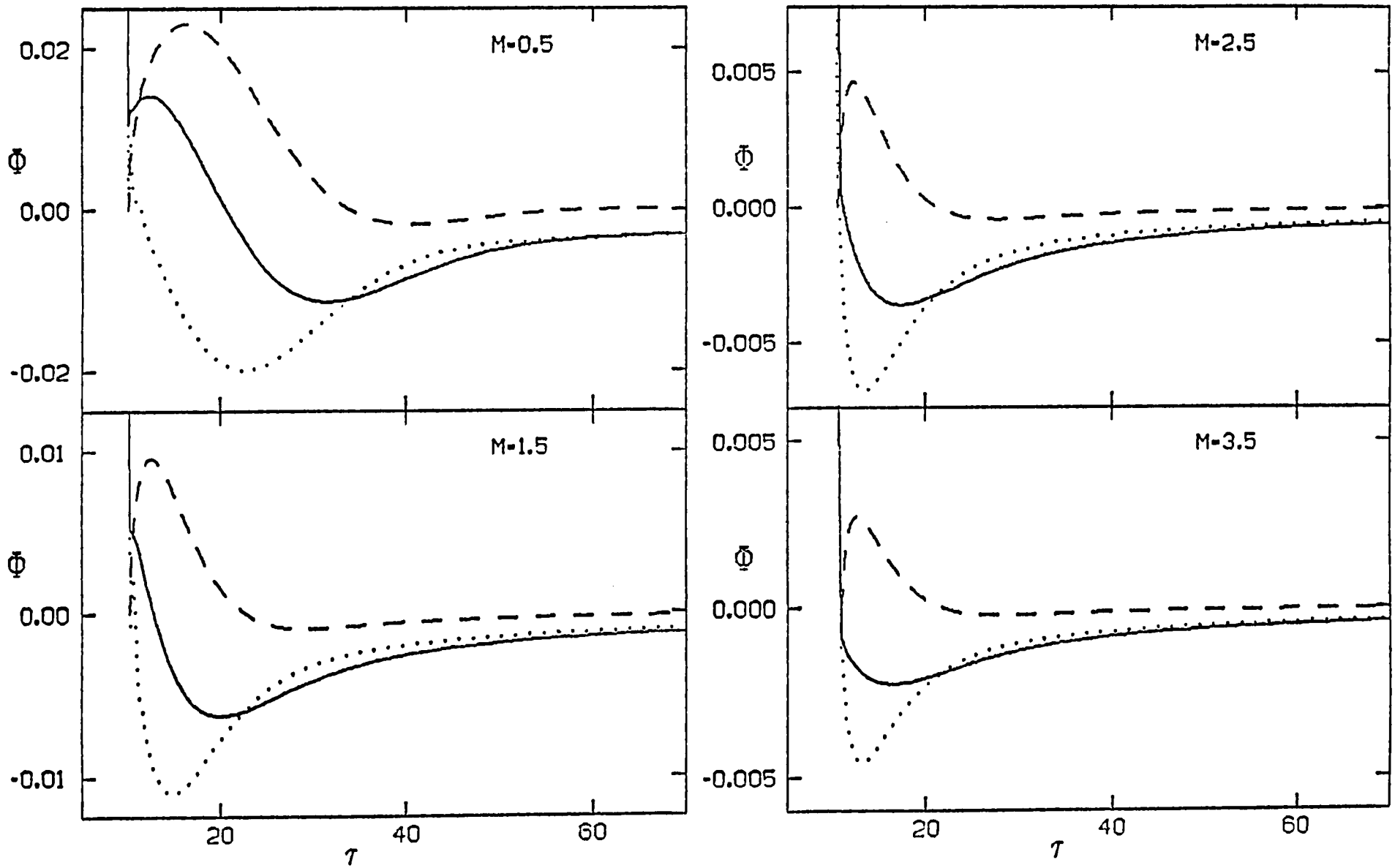

FIGURE VI-5 Z-0 R-10 R_S-0.1

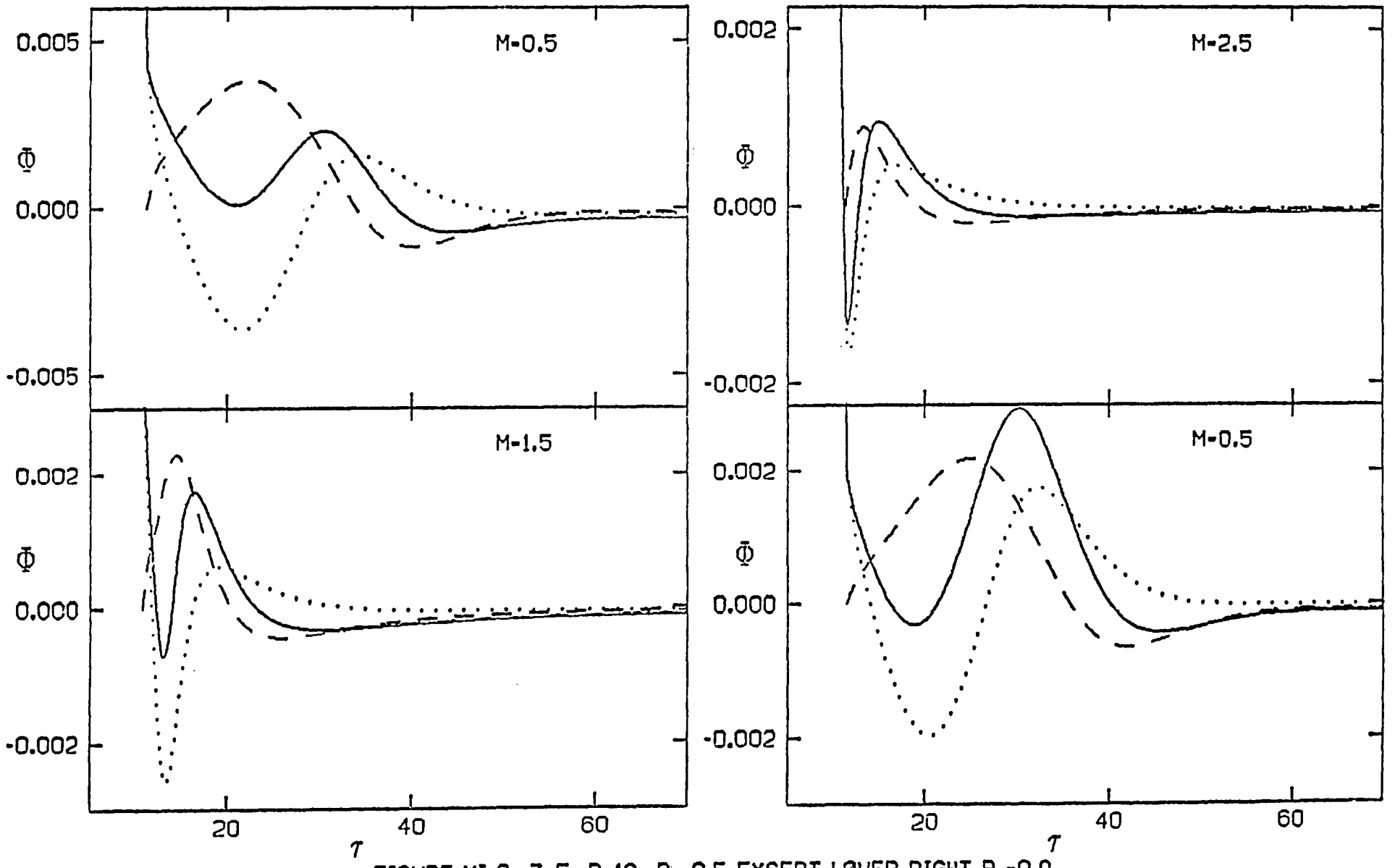

FIGURE VI-6 Z-5 R-10 R_s-0.5 EXCEPT LØWER RIGHT R_s-0.9

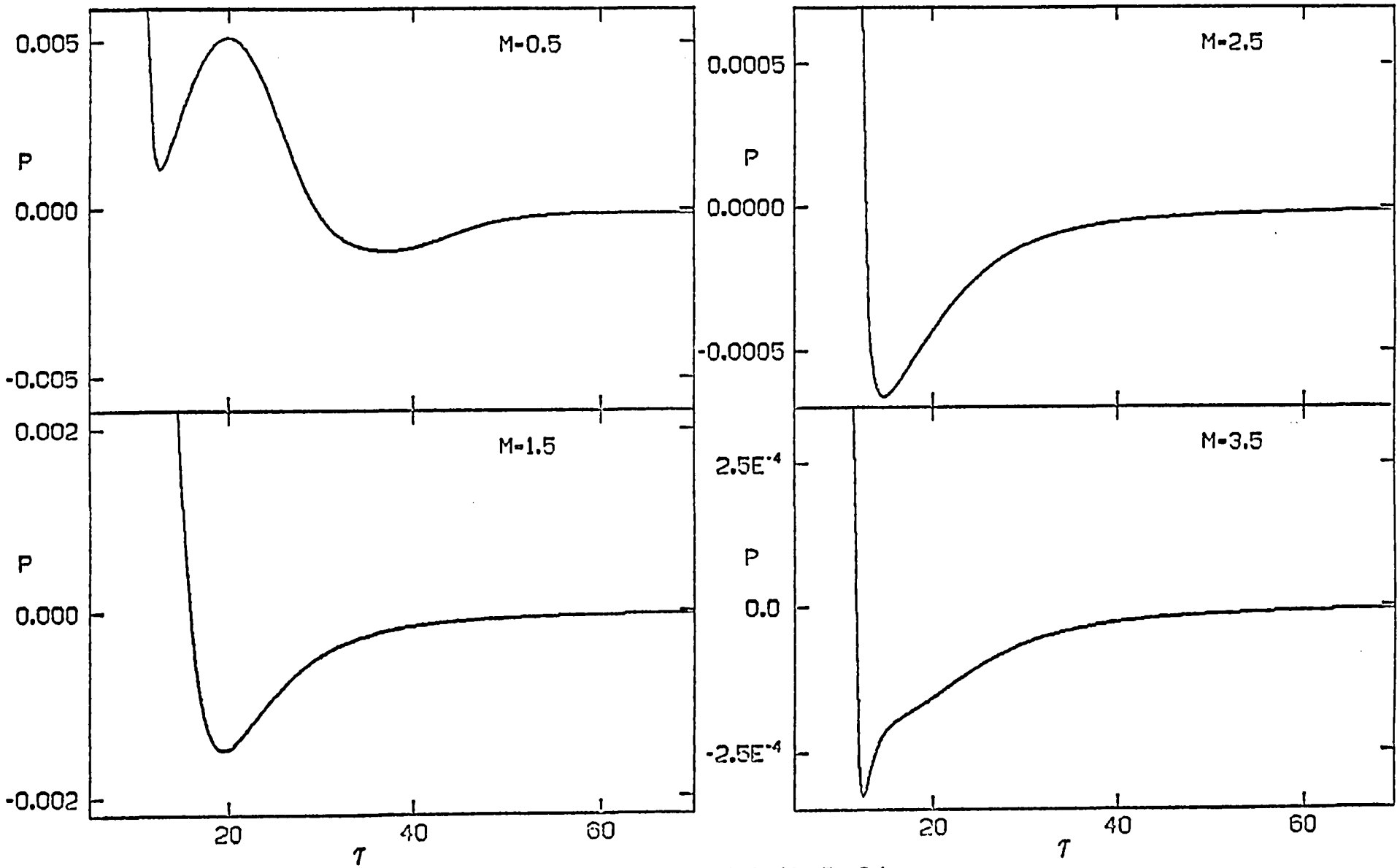

FIGURE VI-7: Z=5 R=10 R_S=0.1

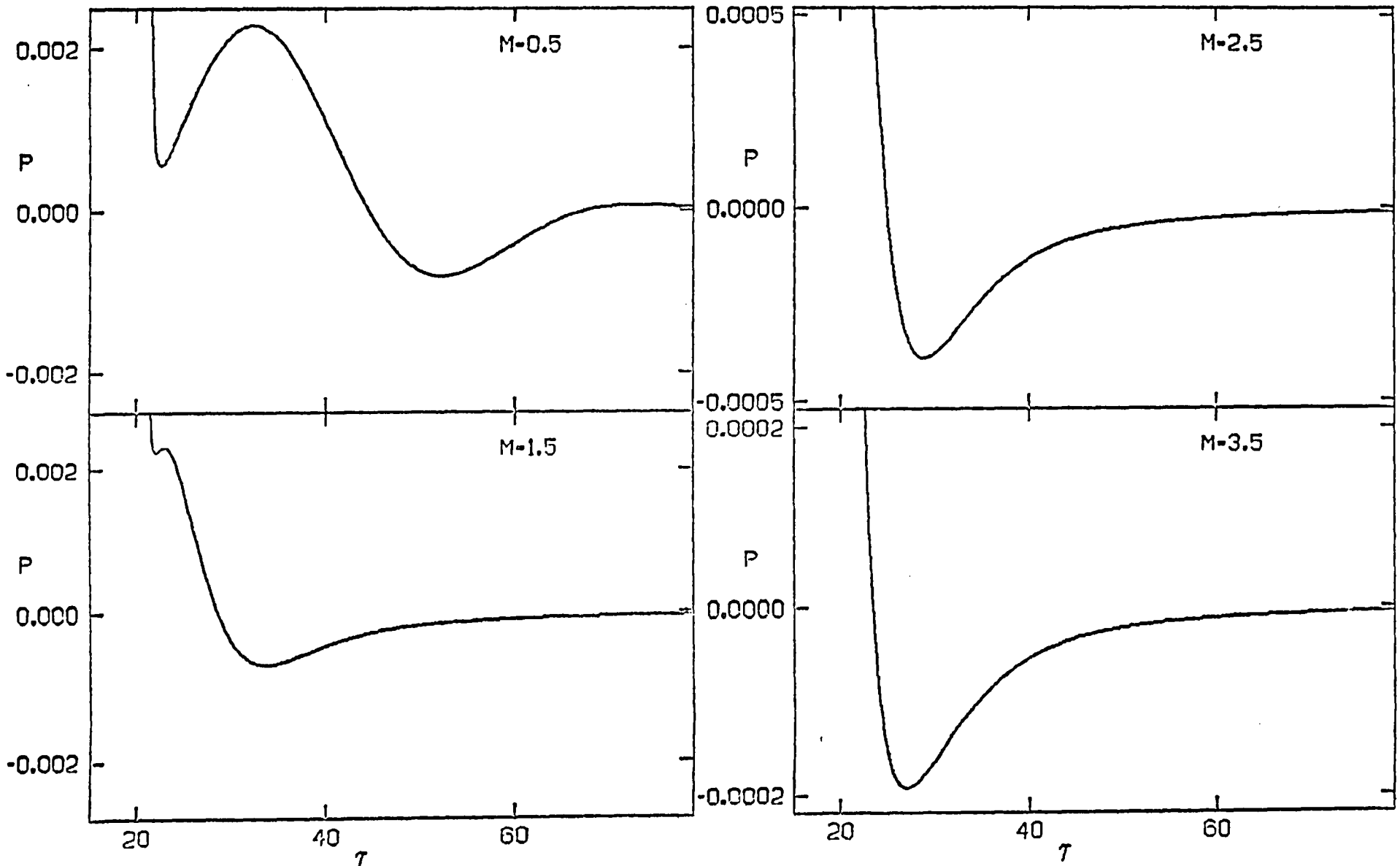

FIGURE VI-8 Z=5 R=20 R_0=0.1

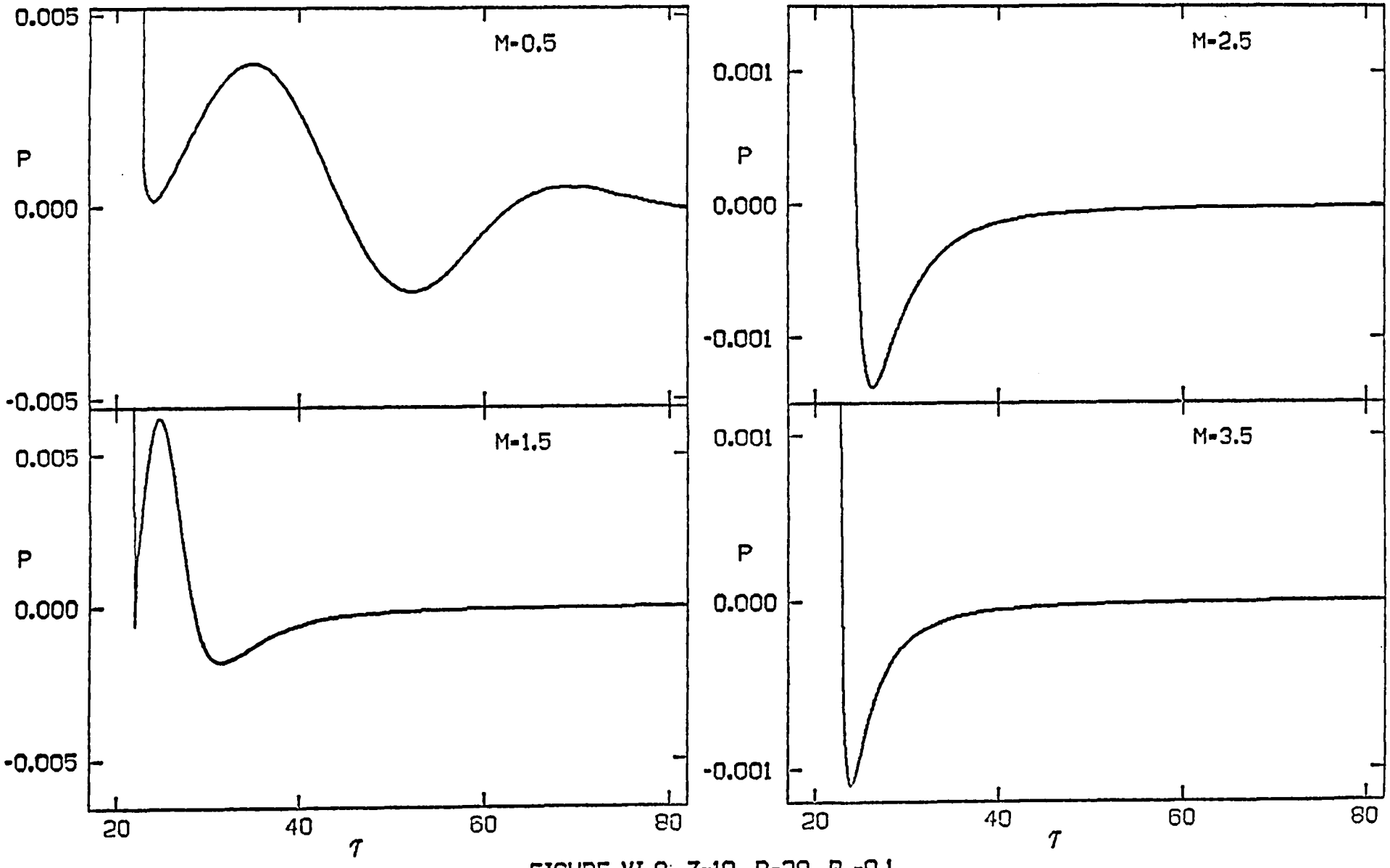

FIGURE VI-9: Z=10 R=20 R_S=0.1

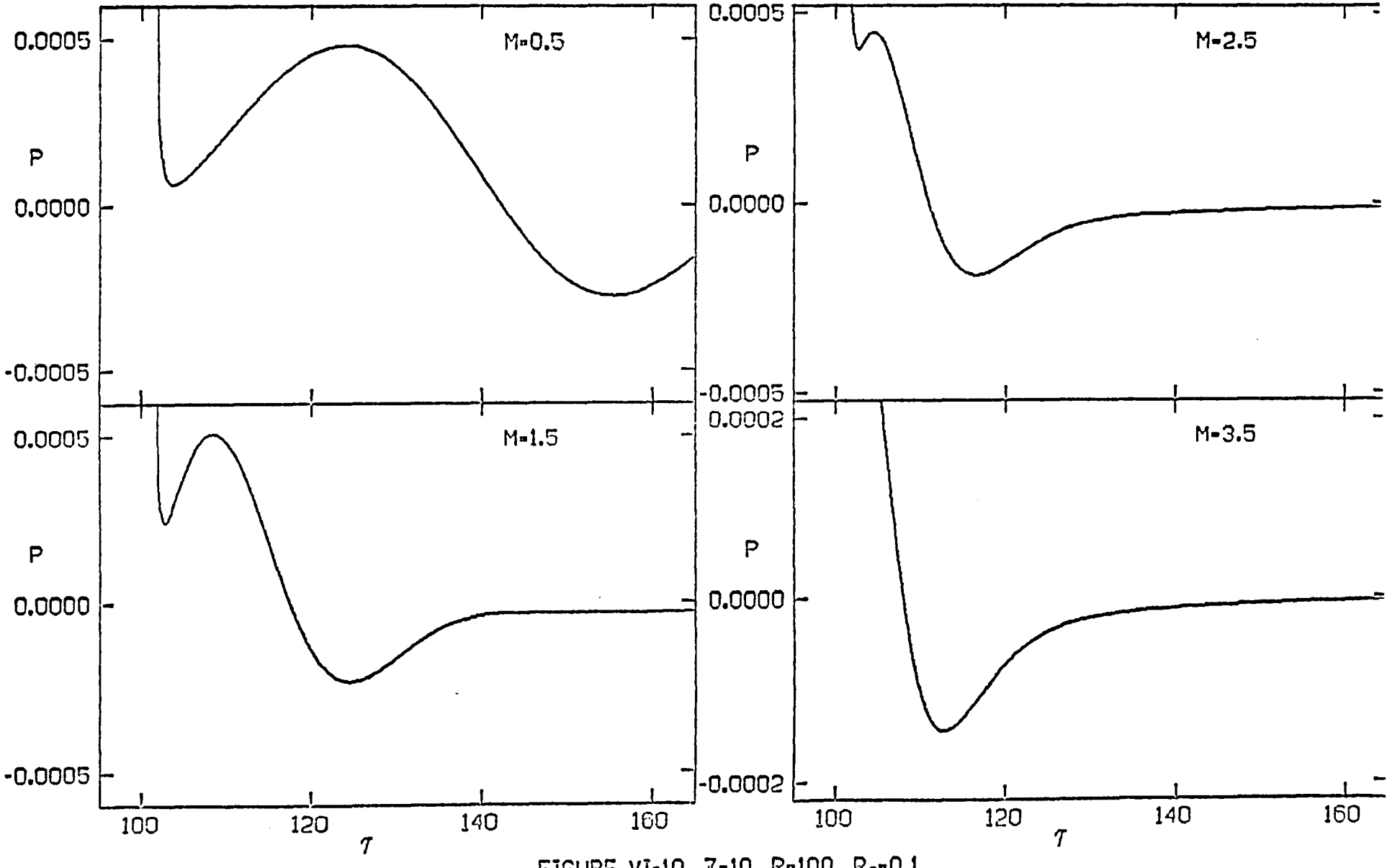

FIGURE VI-10 Z=10 R=100 R_S=0.1

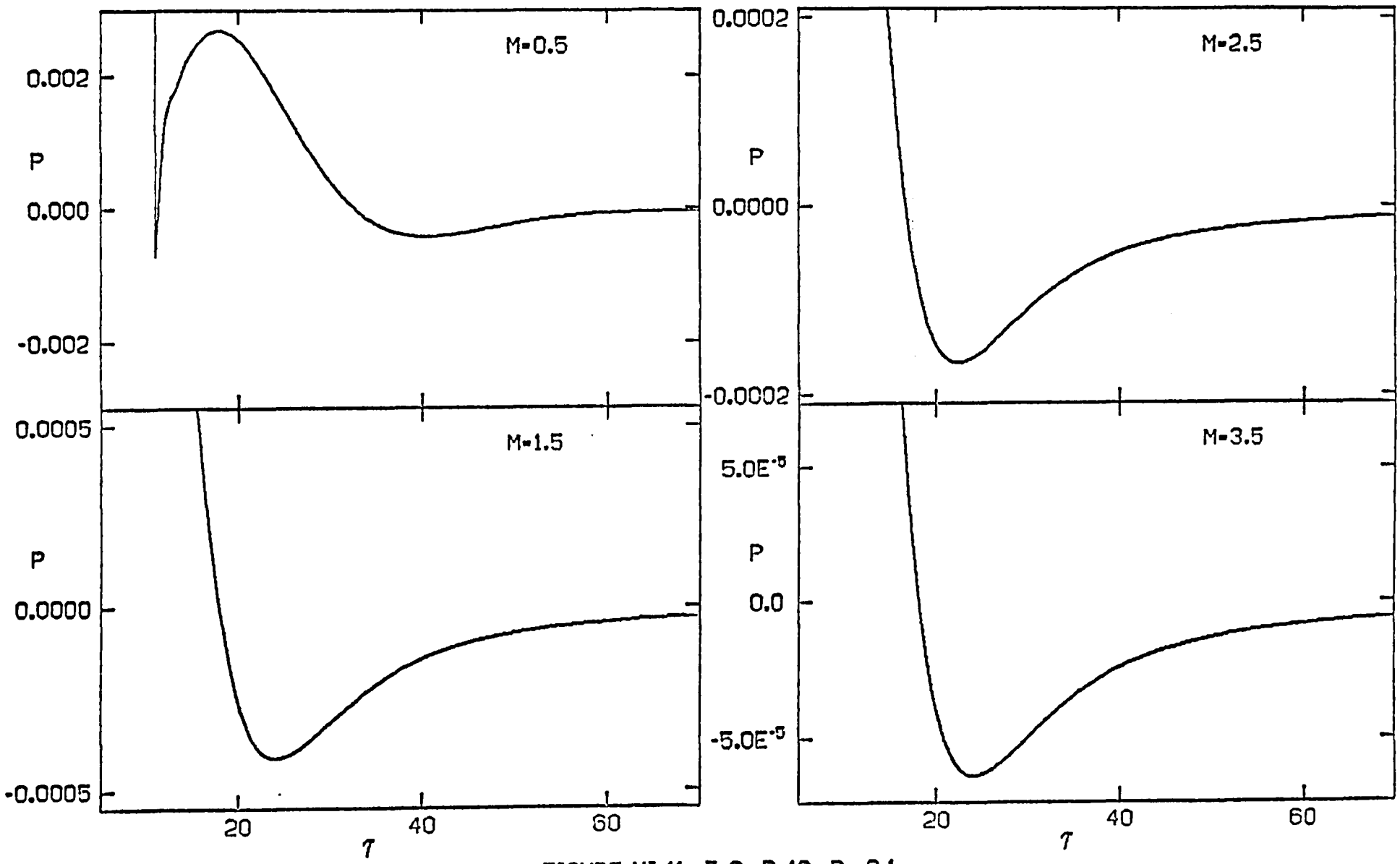

FIGURE VI-11. Z=0 R=10 R_g=0.1

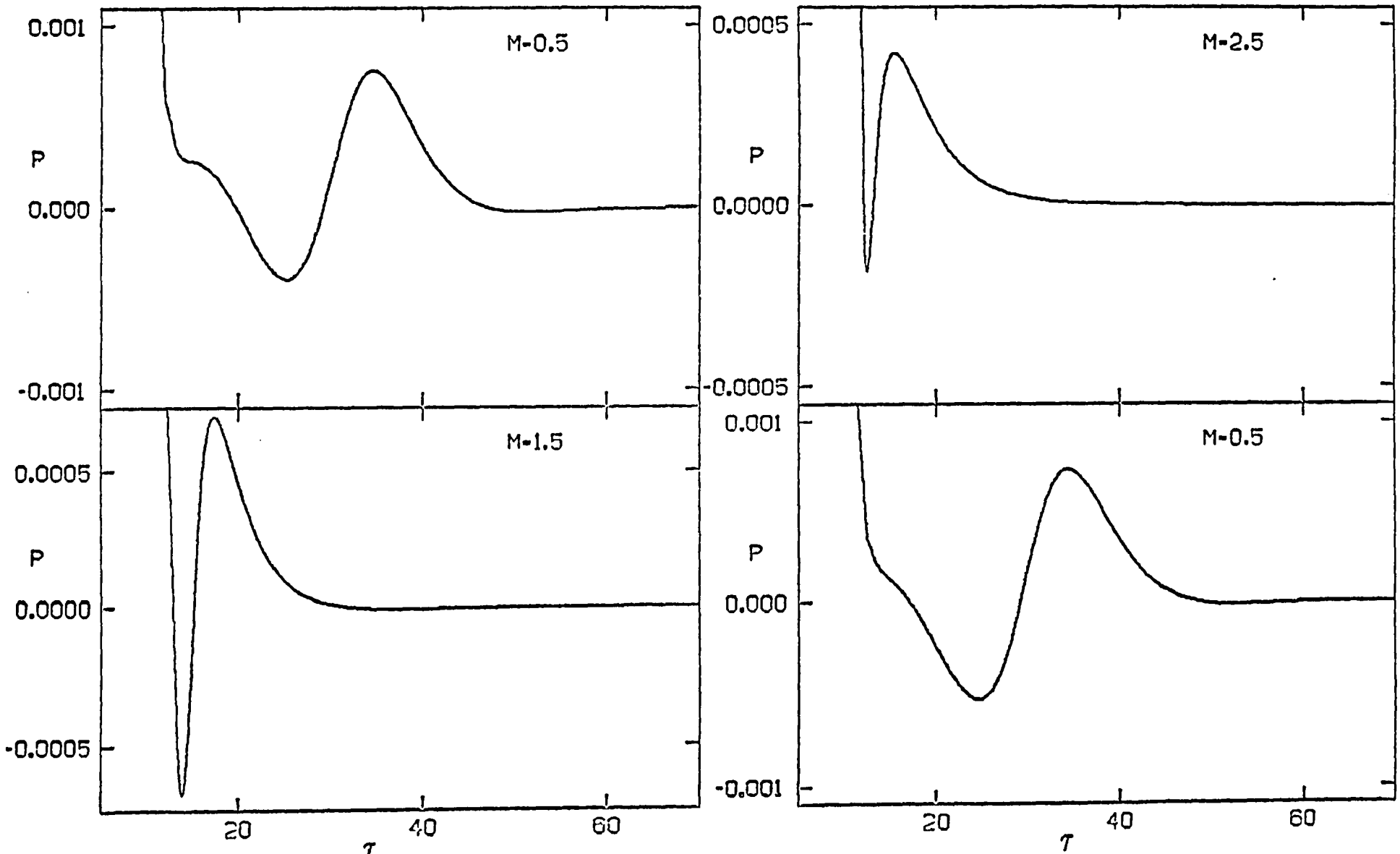

FIGURE VI-12 Z-5 R-10 R_S-0.5 EXCEPT LOWER RIGHT R_S-0.9

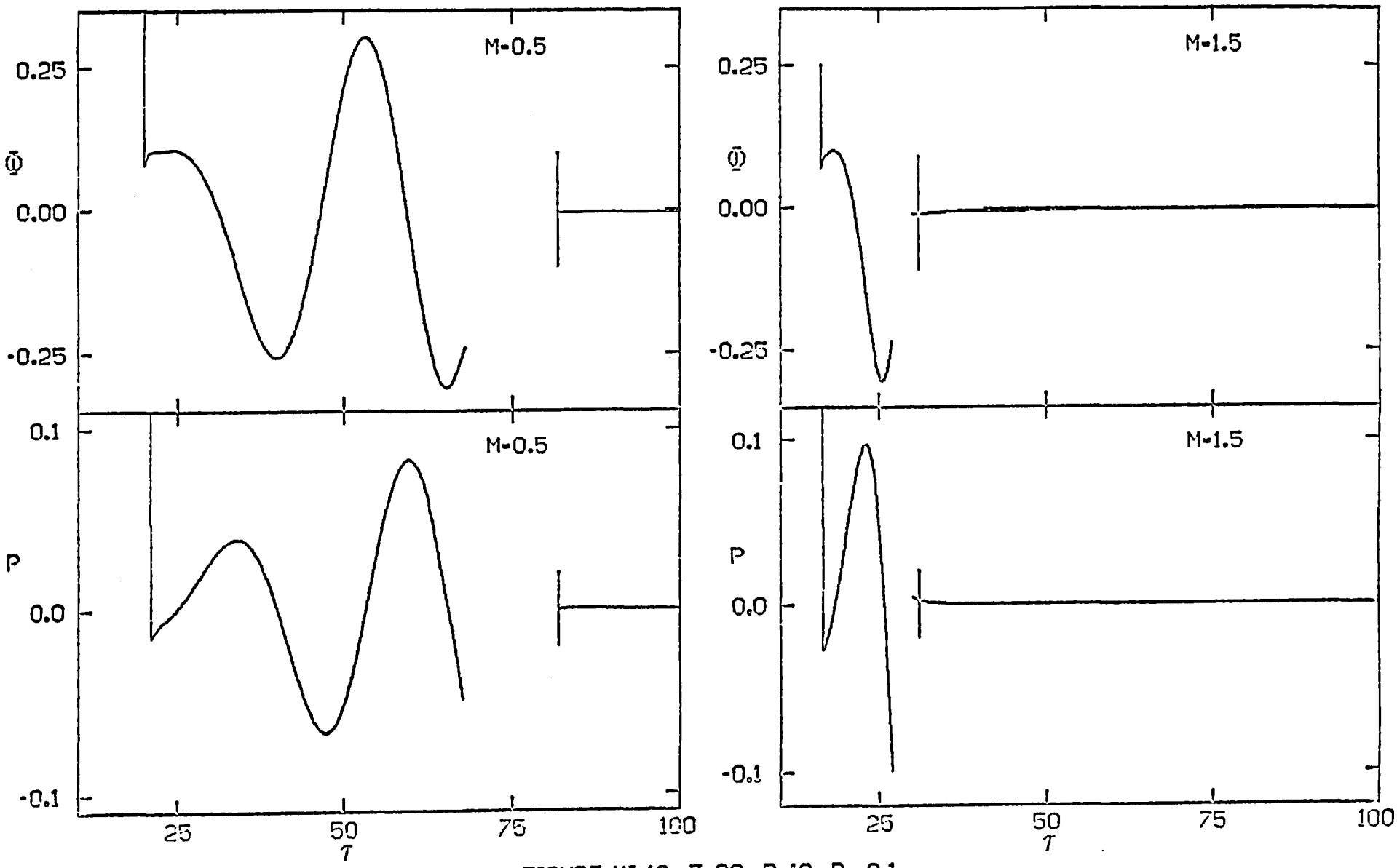

FIGURE VI-13 Z-20 R-10 R_S-0.1

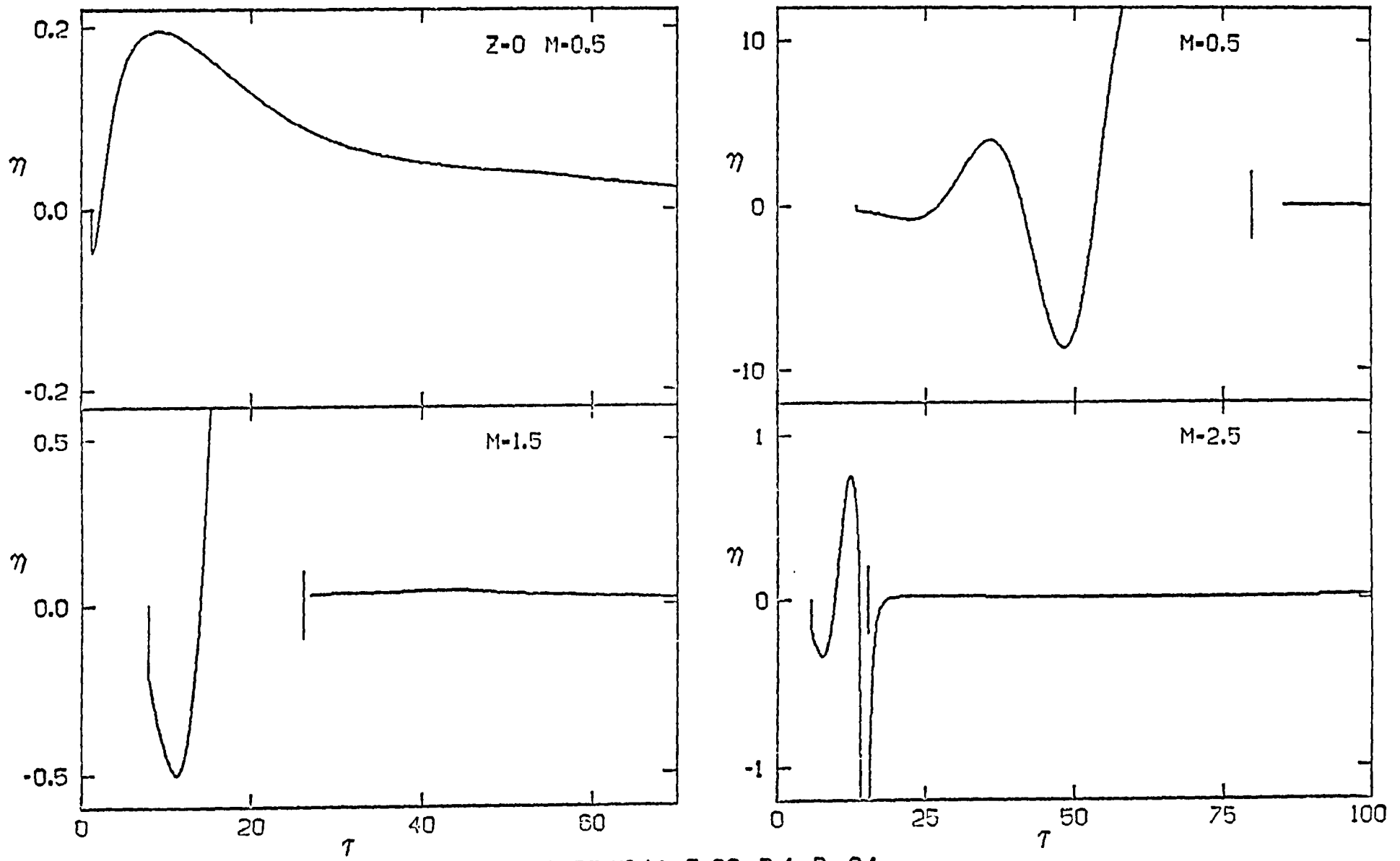

FIGURE VI-14 Z=20 R=1 R_S=0.1

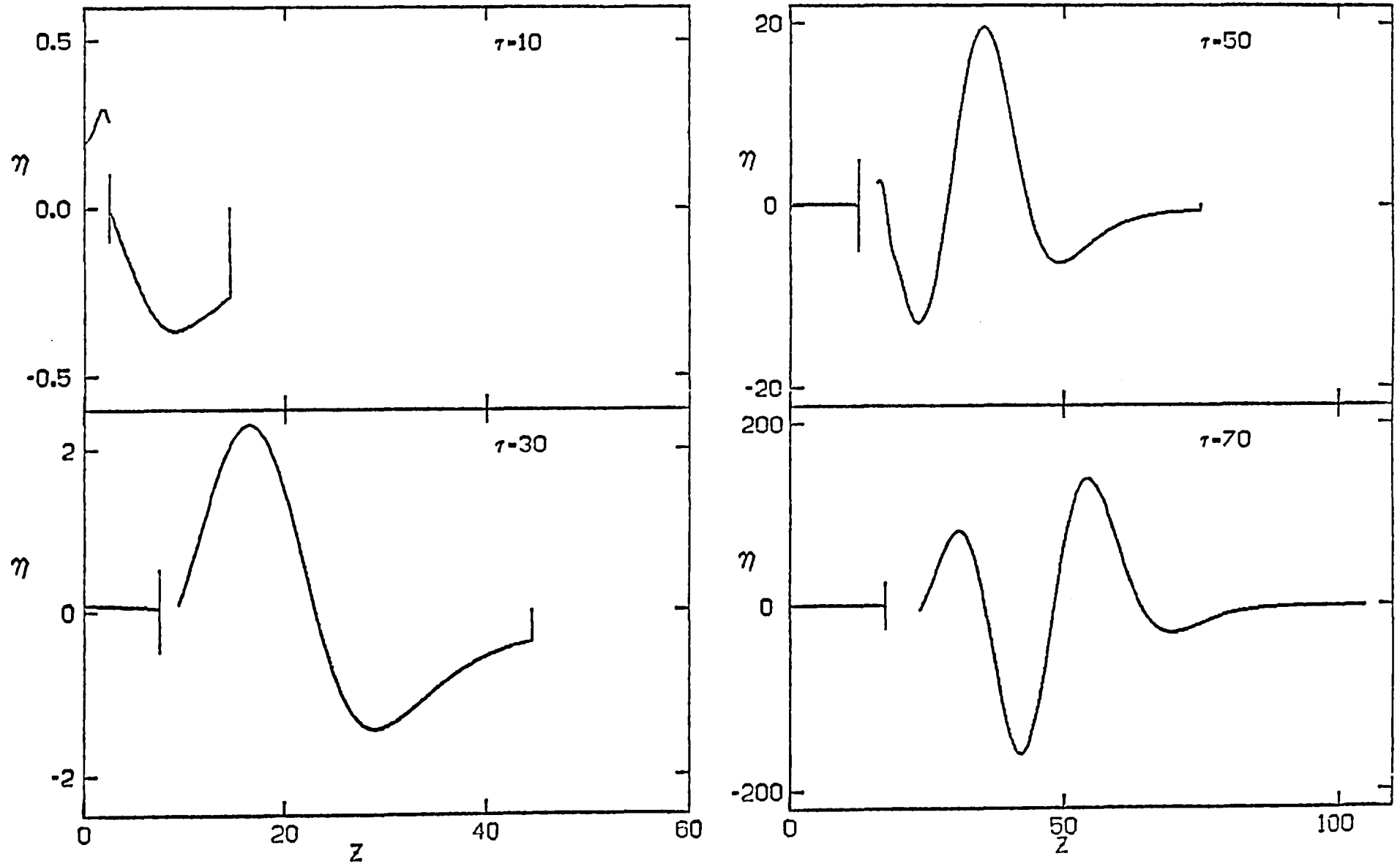

FIGURE VI-15 M=0.5 R=1 R_S=0.1

APPENDIX A. SINGULARITIES OF THE INTEGRAND

a. The zeros of $\Lambda_1 = (\Gamma_1 + \Gamma_2)(1 + \Gamma_1 \Gamma_2)$ have been determined in the plane vortex sheet problems as is evident in Eq. III-9, but they will be verified here for the sake of completeness. Recall

$$\Gamma_1 = (\xi^2 - 1)^{\frac{1}{2}} \quad , \quad \Gamma_2 = \left[(\xi - M)^2 - 1\right]^{\frac{1}{2}}$$

Now let

$$\Gamma_1 = \rho_1 e^{i\theta_1} = a_1 + ib_1$$
$$\Gamma_2 = \rho_2 e^{i\theta_2} = a_2 + ib_2 \qquad \text{(A-1)}$$

where b_1 and b_2 have the same sign. Then, $\Gamma_1 + \Gamma_2 = 0$ requires $a_1 + a_2 = 0$ and $b_1 + b_2 = 0$. The only possibility for satisfaction of the latter is if $b_1 = b_2 = 0$. As this translates to $\rho_1 \sin\theta_1 = -\rho_1 \sin\rho_2$, it requires either $\theta_1 = 0$ and $\theta_2 = \pi$ or vice versa. The condition $a_1 = -a_2$ means $\rho_1 \cos\theta_1 = -\rho_2 \cos\theta_2$ and it is clear from Fig. IV-1 that $\theta_1 = 0$ and $\theta_2 = \pi$ while $\rho_1 = \rho_2 = M/2$ only when $M > 2$. Thus, $\Gamma_1 + \Gamma_2$ has a single real zero at $\xi = \xi_3 = M/2$ for $M > 2$.

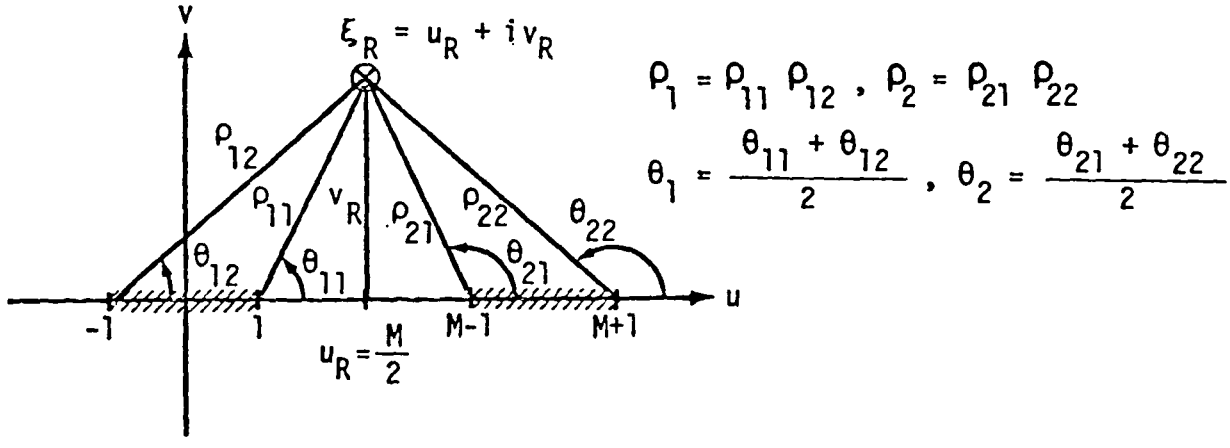

Figure IV-1

$1 + \Gamma_1\Gamma_2 = 0$ requires $a_1a_2 - b_1b_2 + 1 = 0$ and $a_1b_2 + a_2b_1 = 0$, from which $\cos(\theta_1 + \theta_2) = -\frac{1}{\rho_1\rho_2}$ and $\sin(\theta_1 + \theta_2) = 0$ are the consequences, leading to $\theta_1 + \theta_2 = \pi$ and $\rho_1\rho_2 = 1$. From Fig. IV-1, it is obvious that $\theta_1 + \theta_2 = \pi$ only if u_R, the real part of the zero $\xi_R = uR + iVR$, equals M/2. Then, $\rho_1 = \rho_2 = 1$ and v_R, the imaginary part of ξ_R, can be determined.

$$\rho_1 = \rho_{11}\ \rho_{12} = \sqrt{v_R^2 + (\frac{M}{2} - 1)^2}\ \sqrt{v_R^2 + (\frac{M}{2} + 1)^2} = 1$$

Square both sides and solve for v.

$$v_R^2 = -(M^2 + 1) \pm \sqrt{M^2 + 1}$$

The spurious negative root is discarded. Then,

$$v_R = \pm \left[\sqrt{M^2 + 1} - (\frac{M^2}{4} + 1)^{\frac{1}{2}}\right]^{\frac{1}{2}} \qquad \text{for } M < 2\sqrt{2}$$

$$= \pm \left[(\frac{M^2}{4} + 1) - \sqrt{M^2 + 1}\right]^{\frac{1}{2}} \qquad \text{for } M > 2\sqrt{2}$$

Thus, $1 + \Gamma_1\Gamma_2$ have two zeros, which for $M < 2\sqrt{2}$ are complex conjugates and for $M > 2\sqrt{2}$ are real. At $M = 2\sqrt{2}$, $v_R = 0$ and the two zeros collapse into a single value of M/2 which coincides with the zero of $\Gamma_1 + \Gamma_2$.

b. The zeros of $\Lambda_2 = i(\Gamma_1^2 - \Gamma_2^2)\ (1 - 3\Gamma_1\Gamma_2)/8$. The first part of $\Gamma_1^2 - \Gamma_2^2 = (\Gamma_1 + \Gamma_2)(\Gamma_1 - \Gamma_2)$ is examined in a). By making use of Eq. IV-1 again, $\Gamma_1 - \Gamma_2 = 0$ requires $\rho_1\cos\theta_1 = \rho_2\cos\theta_2$ and $\rho_1\sin\theta_1 = \rho_2\sin\theta_2$ and the only possibility of this is if $\theta_1 = \theta_2 = \pi/2$ and $\rho_1 = \rho_2$ when $M < 2$. The corresponding zero is then at M/2 as before, which is a point on the overlapped portion of the branch cuts.

Any zero of $1 - 3\Gamma_1\Gamma_2$ must satisfy the conditions $1 + 3(b_1b_2 - a_1a_2) = 0$ and $a_1b_2 = -a_2b_1$, which translates to $\cos\theta_1\sin\theta_2 = -\sin\theta_1\cos\theta_2$ or $\sin(\theta_1 + \theta_2) = 0$. Since b_1 and b_2 have the same sign as required by the way branch cuts are made, a_1 and a_2 similarly must have the same sign as well. This leads to $\theta_1 + \theta_2 = \pi$ and $\rho_1\rho_2 = -1/3$, which is not possible under any circumstances and therefore the conclusion is that $1 - 3\Gamma_1\Gamma_2$ does not have any zeros.

c. The zeros of L_+ and L_- are similar to the zeros of $\Gamma_1 + \Gamma_2$ and $\Gamma_1 - \Gamma_2$ but their presence and positions will depend on R_S and R. As R tends to become much larger than R_S, the zero of L_+ will move very closely to 0 on the branch cut of Γ_1, while that of L_- is likely to disappear.

d. The zeros that have been identifed thus far all fall in the ξ-plane and are functions of only the Mach number. The zeros of $K + \Lambda_2/(\Gamma_1\Gamma_2\Lambda_1)$ on the other hand are identifiable in both the ξ- and K-planes in addition to being Mach number dependent. Any zero in either plane is a function of the other variable and the resulting movement makes it rather difficult to handle. In the K-plane it is straightforward to recognize the zero as function of ξ_1 or $K = K_\xi = -\Lambda_2/(\Gamma_1\Gamma_2\Lambda_1)$. To find the corresponding zero as function of K in the ξ-plane is more elaborate and will require search by numerical means except for the limiting cases of $K \to 0$ and $K \to \infty$. However, as these are directly linked with instability, they will be treated in more details later.

The zeros of F and G have different physical interpretations so their treatment is given in the main text. In summary, all the zeros of Eqs. III-15 & 16 have been identified or pointed out. Those which are poles to the integrand will be shown to contribute to instability and resonance associated with the vortex layer model.

$$
\begin{aligned}
\xi_{1,\,2} &= \frac{M}{2} \pm i\left[\sqrt{M^2+1} - \left(\frac{M^2}{4}+1\right)\right]^{\frac{1}{2}} && M < 2\sqrt{2} \\
\xi_3 &= \frac{M}{2} && M > 2 \\
\xi_{4,\,5} &= \frac{M}{2} \pm \left[\left(\frac{M^2}{4}+1\right) - \sqrt{M^2+1}\right]^{\frac{1}{2}} && M > 2\sqrt{2}
\end{aligned}
\qquad \text{(A-2)}
$$

APPENDIX B. DERIVATION OF PRESSURE

From the linearlized momentum equation, the acoustic pressure p is related to the velocity potential by

$$p = - \rho \frac{\partial \phi}{\partial t} \tag{B-1}$$

In terms of non-dimensional quantities, this relationship reads,

$$P = \frac{r_o^3 p}{\rho a^2 Q} = - \frac{\partial \Phi}{\partial \tau} \tag{B-2}$$

where Φ and τ are defined in Section III.

Here, Eq. A-2 will be calculated for the specularly transmitted wave field. As $\Phi = \Phi_F + \Phi_G$, the total pressure field will also be the sum of P_F and P_G. This is expected to introduce some errors at the vicinity of arrival of P_G since the derivative of Φ_G is discontinuous there. Only the derivation for P_F will be demonstrated with the understanding that similar procedure applies to P_G. First write,

$$P_F = - \frac{\partial \Phi_F}{\partial \tau}$$

$$= \frac{1}{4\pi^3 \sqrt{R_S R}} \left\{ \mathrm{Re} \frac{\partial \xi_o}{\partial \tau} \frac{\partial}{\partial \xi_o} \left[2\pi i \frac{Q_F(\xi)}{\frac{dF}{d\xi}} \right]_{\xi=\xi_o} - \frac{\partial}{\partial \tau} \left[\Phi_{A12b} + \Phi_{B12b} \right] \right\} \tag{B-3}$$

Now, ξ_0 is such that, from Eq. III-16

$$F(\xi_o) = Z + \Gamma_1(\xi_o)(R - 1) + \Gamma_2(\xi_o)(1 - R_S) - \xi_o \tau = 0$$

and so

$$\tau = \frac{1}{\xi_o}\left[Z + \Gamma_1(\xi_o)\ (R - 1) + \Gamma_2(\xi_o)\ (1 - R_S)\right]$$

Thus,

$$\frac{\partial \tau}{\partial \xi_o} = \frac{\xi_o\left[\frac{\xi_o\ (R-1)}{\Gamma_1\ (\xi_o)} + \frac{(\xi_o - M)(1-R_S)}{\Gamma_2\ (\xi_o)}\right] - \left[Z + \Gamma_1(\xi_o)(R-1) + \Gamma_2(\xi_o)(1-R_S)\right]}{\xi_o^{\,2}} \qquad \text{(B-4)}$$

From Eq. IV-19

$$Q_F\ (\xi_o) = \frac{\xi_o(\xi_o - M)}{\Lambda_1\ (\xi_o)}$$

where

$$\Lambda_1(\xi_o) = (\Gamma_1 + \Gamma_2)\ (1 + \Gamma_1\Gamma_2)\Big|_{\xi=\xi_o}$$

Thus,

$$\frac{\partial}{\partial \xi_o} Q_F(\xi_o) = Q_F'(\xi_o) = \frac{\Lambda_1(\xi_o)(2\xi_o - M) - \xi_o\ (\xi_o - M)\ \Lambda_1'(\xi_o)}{\Lambda_1^{\,2}\ (\xi_o)} \qquad \text{(B-5)}$$

with

$$\Lambda_1'(\xi_o) = 2\left[\xi_o\Gamma_2(\xi_o) + (\xi_o - M)\,\Gamma_1(\xi_o)\right] + \xi_o(\xi_o - M)\left[\frac{(\xi_o - M)}{\Gamma_1(\xi_o)} + \frac{\xi_o}{\Gamma_2(\xi_o)}\right] \qquad \text{(B-5a)}$$

Next,

$$\left.\frac{dF}{d\xi}\right|_{\xi=\xi_o} = F'(\xi_o) = \frac{\xi_o\,(R-1)}{\Gamma_1(\xi_o)} + \frac{(\xi_o - M)(1 - R_S)}{\Gamma_2\ (\xi_o)} - \tau \qquad \text{(B-6)}$$

Then,

$$F''(\xi_o) = \frac{\Gamma_1(\xi_o)(R-1) - \dfrac{\xi_o^2(R-1)}{\Gamma_1(\xi_o)}}{\Gamma_1^2(\xi_o)} + \frac{\Gamma_2(\xi_o) - \dfrac{(\xi_o-M)^2(1-R_S)}{\Gamma_2(\xi_o)}}{\Gamma_2^2(\xi_o)} - \frac{\partial\tau}{\partial\xi_o} \qquad \text{(B-6a)}$$

Eqs. A-5 through 6a apply to the first term

$$\frac{\partial}{\partial\xi_o}\left[\left.\frac{Q_F(\xi)}{\frac{dF}{d\xi}}\right|_{\xi=\xi_o}\right] = \frac{F'(\xi_o)\,Q_F'(\xi_o) - Q_F(\xi_o)\,F''(\xi_o)}{F'(\xi_o)^2}$$

The second term of Eq. A-3 is made up of the sum of the time derivative of the two integrals Φ_{A12b} and Φ_{B12b}. As the two are identical in nature, it suffices to show the derivation of just the first part. From Eq. IV-32a,

$$\Phi_{A12b} = -\,i2\pi\int_{v_o}^{\infty} S_F(u_o + iv)\,dv$$

where

$$S_F(u_o + iv) = S_F(\xi) = \frac{i\xi(\xi-M)}{\Lambda_1} K_\xi\, e^{iK_\xi F}$$

and F is expressed in Eq. III-16. By Leibnitz's rule of differentiation,

$$\frac{\partial\Phi_{A12b}}{\partial\tau} = -\,i\,2\pi\int_{v_o}^{\infty}\frac{\partial\, S_F(u_o + iv)}{\partial\tau}\,du + i2\pi\; S_F(\xi_o)\frac{v_o}{\partial\tau} \qquad \text{(B-7)}$$

with

$$\frac{\partial S_F}{\partial \tau} = - i \xi K_\xi S_F (u_o + iv) \qquad \text{(B-7a)}$$

and

$$\frac{\partial v_o}{\partial \tau} = - i \frac{\partial \xi_o}{\partial \tau} \qquad \text{(B-7b)}$$

APPENDIX C. DERIVATION OF VORTEX LAYER DISPLACEMENT

The vortex layer displacement is related to the velocity potential through the kinematic boundary condition applied at the interface $r = r_0$,

$$\frac{\partial \phi_1}{\partial r} = \frac{\partial \eta}{\partial t}$$

Expressed in the Fourier transformed space,

$$\bar{\eta} = \frac{i}{\omega} \frac{\partial \psi_1}{\partial r}$$

By the use of Eq. II-19 for ψ_1,

$$\bar{\eta} = - i \frac{Q}{8\pi^3 r_o} \frac{\gamma_1 (\omega - Uk) J_o (\gamma_2 r_s) H_1^{(1)} (\gamma_1 r_o)}{S_J}$$

Then,

$$\eta = \int_{c_k} \int_{c_\omega} \bar{\eta} \; e^{-i(\omega t - kz)} \; d\omega \, dK$$

and this inverse can be evaluated in the exact manner as for Φ . Let $\xi = \omega/ka$, then

$$\eta = \frac{Q}{8\pi^3 r_o} \iint \frac{-i\Gamma_1(\xi - M) J_o (kr_s\Gamma_2) H_1^{(1)} (kr_o\Gamma_1)}{S_J'} e^{-ik(\xi at - z)} \, d\xi \, dK$$

In the development, Eqs. III-4 & 5 become,

$$J_o(kr_s\Gamma_2)H_1^{(1)}(kr_o\Gamma_1) = \frac{1}{\pi k \sqrt{r_o r_s \Gamma_1 \Gamma_2}} \left[D_1 e^{ik(r_o\Gamma_1 - r_s\Gamma_2)} \mp E_1 e^{ik(r_o\Gamma_1 + r_s\Gamma_2)} \right]$$

where

$$D_1 = \frac{1}{8k}\left(\frac{1}{r_s\Gamma_2} + \frac{3}{r_o\Gamma_1}\right) - i$$

$$E_1 = 1 - \frac{i}{8k}\left(\frac{1}{r_s\Gamma_2} - \frac{3}{r_o\Gamma_1}\right)$$

After some manipulations, the non-dimensional form becomes

$$\eta = \frac{nr_o^2}{Q} = \eta_F + \eta_G$$

$$= \frac{1}{4\pi^3\sqrt{R_s}}\ \mathrm{Re}\int_o^\infty\int_{c^+} \frac{i\Gamma_1(\xi-M)\left[1 + \frac{L_+}{K\Gamma_1\Gamma_2}\right]e^{iKF}}{\Lambda_1 + \frac{\Lambda_2}{\Gamma_1\Gamma_2K}}\ d\xi\ dK$$

$$+ \frac{1}{4\pi^3\sqrt{R_s}}\ \mathrm{Re}\int_o^\infty\int_{c^+} \frac{-\Gamma_1(\xi-M)\left[1 - \frac{L_-}{K\Gamma_1\Gamma_2}\right]e^{iKG}}{\Lambda_1 + \frac{\Lambda_2}{\Gamma_1\Gamma_2K}}\ d\xi\ dK$$

where now

$$F_G = Z + \Gamma_2\,(1 \mp R_S) - \xi\tau$$

$$L_\pm = \frac{i}{8}\left(\frac{1}{R_S} \pm 3\Gamma_2\right)$$

The above equation is then evaluated in the exact manner as described in Sections IV and VI.

APPENDIX D

```
C*************************************************
C     MAIN PROGRAM
C
C     R    -    RADIAL DISTANCE
C     RM   -    MACH NUMBER
C     B    -    RING SOURCE RADIUS.
C     A    -    TIME
C     X    -    DISTANCE IN THE DOWNSTREAM DIRECTION
C     ISP  -    1 BEFORE WAVE ARRIVAL. INITIAL INPUT
C          -    2 AFTER WAVE ARRIVAL. OUTPUT FROM ROOT FOR COMPLEX ROOT
C          -    3 SAME AS 2 BUT FOR REAL ROOT
C     NI   -    MAXIMUM NUMBER OF INTEGRATION SUBINTERVALS.
C     DI   -    ARRAY FOR ESTABLISHING SUBINTERVALS.
C     NL   -    NUMBER OF FUNCTION EVALUATIONS OF FUNCA OR B.
C     NG   -    NUMBER OF SUBINTERVALS NECESSARY TO ARRIVE AT
C               THE FINAL VALUE.
C     NT   -    NUMBER OF TIME INPUTS
C               MAXIMUM OF 30.  STOPS EXECUTION IF 0
C     NC   -    CASE NUMBER
C     NW   -    1 FOR VELOCITY POTENTIAL
C          -    2 FOR PRESSURE
C          -    3 FOR VORTEX LAYER DISPLACEMENT
C     FCR  -     0 FOR PHIA, -1 FOR PHIB
C     FCI  -    -1 FOR PHIA,  0 FOR PHIB
C     TIME -    SUBROUTINE FOR GENERATING TIME INPUTS
C     ROOT -    SUBROUTINE FOR FINDING THE ZERO OF F OR G
C     SMOD -    SUBROUTINE FOR CALCULATING MODIFIED FIELD IN THE
C               NEUTRAL INSTABILITY REGION, WHEN M > 2. FM ITS VALUE
C     SPEC -    SUBROUTINE FOR CALCULATING THE SPECULARLY
C               TRANSMITTED FIELD, AND FA ITS VALUE
C     LAG  -    SUBROUTINE WHICH PERFORMS GAUSS
C               INTEGRATIONS ON FUNCA OR FUNCB, AND FCB ITS VALUE.
C     F    -    THE TOTAL FIELD, PHI.
C
      IMPLICIT REAL*8(A-H,L,O-Z)
      DIMENSION T(30),DI(50)
      COMMON /CMA/ RM,R,B,A,X /CMB/ USP,FCR,FCI /CMC/ NW
      EXTERNAL FUNCA,FUNCB
      EPS=1.0D0
    5 EPS=EPS/2.0D0
      TOL1=1.0D0+EPS
      IF(TOL1.GT.1.0D0)GO TO 5
      PI=4.0D0*DATAN(1.0D0)
      READ 10,NI,NW
   10 FORMAT(2I2)
      READ 15,(DI(I),I=1,NI)
   15 FORMAT(7D10.2)
   20 READ 25,NC,NT,X,R,B,RM
   25 FORMAT(2I2,4D10.2)
      IF(NT.EQ.0)STOP
      NL=0
      NG=0
      RMM=RM*0.5D0
      DF=2.0D0*PI*DSQRT(B*R)
```

```
      CALL TIME(T,EPS,NT)
      PRINT 30,NC,RM,B,R,X
   30 FORMAT('-','CASE ',I2,', M= ',1PD12.5,', B= ',D12.5,', R= ',D12.5,
     +', X= ',D12.5//5X,'TIME',11X,'U',11X,'V',10X,'ABS',8X,'SPEC',8X,
     +'MODI',12X,'INTG',11X,'PHIA',8X,'PHIB',9X,'PHI'/)
      ISA=1
      ISP=1
      DO 85 I=1,NT
      FCR=0.0D0
      FCI=-1.0D0
      A=T(I)
      ISB=ISP
      ISP=ISA
      DO 70 J=1,2
      CALL ROOT(U,V,ISP,FS)
      USP=U
      FCB=0.0D0
      FA=0.0D0
      FM=0.0D0
      IF(B.LT.0.0D0)GO TO 45
      FM=SMOD(RMH)
      GO TO (60,45,55),ISP
   45 FA=SPEC(U,V)/PI
      GO TO (50,55,55),ISP
   50 FCB=LAG(FUNCA,NL,NG,U,NI,DI,ISP)/PI/8.0D0
      GO TO 60
   55 FCB=LAG(FUNCB,NL,NG,V,NI,DI,ISP)/PI/8.0D0
   60 F=(FCB+FA+FM)/DF
      B=-B
      GO TO (65,80),J
   65 FT=F
      FCR=-1.0D0
      FCI=0.0D0
      ISA=ISP
      ISP=ISB
   70 PRINT 75,A,U,V,FS,FA,FM,NL,FCB,NG,F
   75 FORMAT(' ',1PD12.5,5(2X,D10.3),2X,I3,1X,D10.3,1X,I2,2X,D10.3)
   80 FT=F+FT
   85 PRINT 90,U,V,FS,FA,NL,FCB,NG,F,FT
   90 FORMAT(' ',14X,4(1PD10.3,2X),12X,
     +I3,1X,D10.3,1X,I2,12X,2(2X,D10.3))
      GO TO 20
      END
C*******************************************************
      SUBROUTINE TIME(T,EPS,NT)
C
C     PROGRAM FINDS: WHEN NT=30, THE MINIMUM TIME OF TRAVEL FROM
C     SOURCE TO THE FIELD POINT, AND GENERATES 30 TIME STEPS FOR INPUT.
C     WHEN NT < 30, READS IN NT TIME STEPS FOR INPUT.
C     ZERO -   SUBROUTINE WHICH SOLVES FOR THE MINIMUM TIME
C     AMN  -   MINIMUM TIME
C
      IMPLICIT REAL*8(A-H,O-Z)
      DIMENSION T(30)
```

```
      COMMON /CMA/ RM,R,B,A,X /CTA/ AZ,S,RZ
      EXTERNAL FP
      IF(NT.NE.30)GO TO 50
      RZ=(R-1.0D0)**2
      NC=1
    2 AZ=1.0D0-B
      XZ=RM*AZ
      AU=AZ+DSQRT((X-XZ)**2+RZ)
      IF(X.LT.XZ)GO TO 10
      S=1.0D0
    5 AL=AZ
      AMN=ZERO(FP,AL,AU,1.0D-5,EPS)
      AMN=AMN+DSQRT((X-RM*AMN-S*DSQRT(AMN*AMN-AZ*AZ))**2+RZ)
      GO TO 20
   10 IF(RM.GT.1.0D0)GO TO 15
      S=-1.0D0
      GO TO 5
   15 AMN=AU
   20 IF(NC.EQ.2)GO TO 22
      T(2)=AMN
      T(1)=AMN-1.0D-4
      T(3)=AMN+1.0D-4
      B=-B
      NC=2
      GO TO 2
   22 T(5)=AMN
      T(4)=AMN-1.0D-4
      T(6)=AMN+1.0D-4
      T(7)=DINT(AMN+1.0D0)
      DO 25 I=8,13
   25 T(I)=T(I-1)+1.0D0
      DO 30 I=14,23
   30 T(I)=T(I-1)+2.0D0
      TE=T(23)
      EL=30.0DC
      DO 35 J=1,20
      IF(TE.LT.EL)GO TO 40
   35 EL=EL+5.0D0
   40 T(24)=EL
      DO 45 I=25,29
   45 T(I)=T(I-1)+5.0D0
      T(30)=T(29)+10.0D0
      B=-B
      RETURN
   50 READ 55,(T(I),I=1,NT)
   55 FORMAT(7D10.3)
      RETURN
      END
C*************************************************************
      FUNCTION FP(T)
C
C     FUNCTION EXTERNAL TO TIME AND CALLED BY ZERO
C
      IMPLICIT REAL*8(A-H,O-Z)
```

```
      COMMON /CMA/ RM,R,B,A,X /CTA/ AZ,S,RZ
      AA=DSQRT(T*T-AZ*AZ)
      AF=X-RM*T-S*AA
      FP=DSQRT(AF*AF+RZ)*AA-AF*(RM*AA+S*T)
      RETURN
      END
C*****************************************************
      SUBROUTINE ROOT(U,V,ISP,FS)
C
C     PROGRAM FINDS THE ROOT OF F OR G
C     FA,ZA  -  GAMMA ONE.   FB,ZB  -  GAMMA TWO
C     FS     -  VALUE OF F OR G AT THE ROOT
C
      IMPLICIT REAL*8(A,B,D-H,O-Y),COMPLEX*16(Z)
      COMPLEX*16 CDSQRT,CMPLX
      DIMENSION BM(5),FR(4),FI(4),FMA(4),FMB(4),FMS(4),XM(4)
      COMMON /CMA/ RM,R,B,A,X /CRA/ FA,FB /CRC/ JS /CRB/ ZA,ZB
      JS=0
      RMS=RM*RM
      BS=(1.0D0-B)**2
      AP=2.0D0*(RM*BS-X*A)
      AZ=X*X+BS*(1.0D0-RMS)
      AT=A*A-BS
      IF(R.EQ.1.0D0)GO TO 20
      RS=(R-1.0D0)**2
      AS=4.0D0*RS*BS
      AZ=AZ+RS
      AT=AT-RS
      BM(5)=AT*AT-AS
      BM(4)=(AP*AT+AS*RM)*2.0D0
      BM(3)=AP*AP+2.0D0*AZ*AT-(RMS-2.0D0)*AS
      BM(2)=2.0D0*(AP*AZ-AS*RM)
      BM(1)=AZ*AZ+AS*(RMS-1.0D0)
      CALL QUARTI(BM,FR,FI)
      JD=4
    5 MM=0
      DO 15 J=1,JD
      IF(FI(J).EQ.0.0D0)GO TO 10
      IF(FI(J).LT.0.0D0)GO TO 15
      Z=DCMPLX(FR(J),FI(J))
      ZA=CDSQRT(Z*Z-1.0D0)
      ZB=CDSQRT((Z-RM)**2-1.0D0)
      IF(DIMAG(ZA).LT.0.0D0)ZA=-ZA
      IF(DIMAG(ZB).LT.0.0D0)ZB=-ZB
      ZS=X+ZA*(R-1.0D0)+ZB*(1.0D0-B)-A*Z
      FS=CDABS(ZS)
      IF(FS.GT.1.0D-4)GO TO 15
      ISP=2
      U=FR(J)
      V=FI(J)
      RETURN
    8 FA=DSQRT(1.0D0-U*U)
      ZA=DCMPLX(0.0D0,FA)
      ZB=DCMPLX(FB,0.0D0)
```

```
      JS=1
      GO TO 12
   10 U=FR(J)
      FB=DSQRT((U-RM)**2-1.0D0)
      IF(U.LT.RM-1.0D0)FB=-FB
      IF(DABS(U).LT.1.0D0)GO TO 8
      FA=DSQRT(U*U-1.0D0)
      IF(U.LT.-1.0D0)FA=-FA
   12 FS=X+FA*(R-1.0D0)+FB*(1.0D0-B)-A*U
      IF(DABS(FS).GT.1.0D-4)GO TO 15
      MM=MM+1
      XM(MM)=U
      FMA(MM)=FA
      FMB(MM)=FB
      FMS(MM)=FS
   15 CONTINUE
      CALL SELECT(MM,XM,MN)
      FA=FMA(MN)
      FB=FMB(MN)
      U=XM(MN)
      V=0.0D0
      FS=FMS(MN)
      IF(ISP.EQ.2)ISP=3
      RETURN
   20 AA=AP*AP-4.0D0*AT*AZ
      SAD=-AP/AT*0.5D0
      IF(AA.LT.0.0D0)GO TO 25
      SAA=DSQRT(AA)/AT*0.5D0
      FR(1)=SAD+SAA
      FR(2)=SAD-SAA
      FI(1)=0.0D0
      FI(2)=0.0D0
      JD=2
      GO TO 5
   25 SAA=DSQRT(-AA)/AT*0.5D0
      FR(1)=SAD
      FR(2)=SAD
      FI(1)=SAA
      FI(2)=-SAA
      JD=2
      GO TO 5
      END
C*************************************************************
      FUNCTION SPEC(U,V)
C
C     CALCULATES THE SPECULARLY TRANSMITTED FIELD
C     U AND V ARE RESPECTIVELY THE REAL AND IMAGINARY PART OF PSI
C
      IMPLICIT REAL*8(A,B,D-H,O-Y), COMPLEX*16(C,Z)
      COMMON /CMA/ RM,R,B,A,X /CMB/ DUM,FR,FI /CMC/ NW /CRA/ FA,FB
      COMMON /CRC/ JS /CRD/ ZA,ZB
      RR=R-1.0D0
      BB=1.0D0-B
      IF(V.EQ.0.0D0.AND.JS.EQ.0)GO TO 10
```

```
      ZFAC=DCMPLX(FR,FI)
      Z=DCMPLX(U,V)
      ZG=(ZA+ZB)*(ZA*ZB+1.0D0)
      ZM=Z*(Z-RM)
      ZC=(Z-RM)*BB/ZB
      IF(NW.NE.3)ZC=ZC+Z*RR/ZA
      ZFN=ZM/ZG
      ZFD=ZC-A
      IF(NW.EQ.2)GO TO 5
      IF(NW.EQ.3)ZFN=-ZFN*ZA/Z
      SPEC=DREAL(ZFN/ZFD*ZFAC)
      RETURN
    5 NW=1
      ZMI=DCMPLX(0.0D0,-1.0D0)
      ZFG=X+ZA*RR+ZB*BB
      ZDT=Z*Z/(Z*ZC-ZFG)
      ZDG=2.0D0*(Z*ZB+(Z-RM)*ZA)+ZM*((Z-RM)/ZA+Z/ZB)
      ZDQ=(ZG*(2.0D0*Z-RM)-ZM*ZDG)/(ZG*ZG)
      ZDFD=(ZA-Z*Z/ZA)*RR/(ZA*ZA)-ZDT
     +     +(ZB-(Z-RM)*(Z-RM)/ZB)*BB/(ZB*ZB)
      SPEC=-DREAL((ZFD*ZDQ-ZFN*ZDFD)/(ZFD*ZFD)*ZFAC-ZMI*FUNCB(V))*ZDT
      NW=2
      RETURN
   10 FG=(FA+FB)*(FA*FB+1.0D0)
      FM=U*(U-RM)
      FC=(U-RM)*BB/FB
      IF(NW.NE.3)FC=FC+U*RR/FA
      FN=-FM/FG
      FD=FC-A
      IF(NW.EQ.2)GO TO 15
      IF(NW.EQ.3)FN=-FN*FA/U
      SPEC=FM/FD
      RETURN
   15 NW=1
      FFG=X+FA*RR+FB*BB
      FDT=U*U/(U*FC-FFG)
      FDG=2.0D0*(U*FB+(U-RM)*FA)+FM*((U-RM)/FA+U/FB)
      FDQ=(FG*(2.0D0*U-RM)-FM*FDG)/(FG*FG)
      FDFD=(FA-U*U/FA)*RR/(FA*FA)-FDT
     +     +(FB-(U-RM)*(U-RM)/FB)*BB/(FB*FB)
      SPEC=-FDT*((FDQ*FD-FDFD*FM)/(FD*FD)-FUNCA(U))
      NW=2
      RETURN
      END
C*******************************************************
      FUNCTION SMOD(U)
C
C     CALCULATES THE FIELD WHICH MODIFIES THAT OF THE
C     SPECULARLY TRANSMITTED WAVE
C     PRESENT BEHIND THE NEUTRAL STABILITY WAVE
C
      IMPLICIT REAL*8(A-H,O-Z)
      COMMON /CMA/ RM,R,B,A,X /CMC/ NW
      DATA TST/2.02842712474619D0/
```

```
      SMOD=0.0D0
      IF(RM.LT.2.0D0)RETURN
      IF(A.LT.RM*(R-B)/DSQRT(RM*RM-4.0D0))RETURN
      GA=DSQRT(U*U-1.0D0)
      GB=-GA
      PF=X+GA*(R-1.0D0)+GB*(1.0D0-B)-A*U
      IF(RM.GT.TST) GO TO 10
      IF(PF.GT.0.0D0) RETURN
      FAC=1.0D0
    5 GAB=GA*GB
      GPT=1.0D0+GAB
      QT=U*(U-RM)/(GPT*(U/GA+(U-RM)/GB)*8.0D0)
      IF(NW.EQ.3)QT=-QT*GA/U
      PS=(GA-GB)*(1.0D0-3.0D0*GAB)/GPT/GAB
      PSM=PS-GA/B+GB/R
      IF(NW.EQ.3)PSM=PS-GA/B-3.0D0*GB
      SMOD=PSM*QT*DEXP(-PS*PF/8.0D0)*FAC
      RETURN
   10 IF(PF.LT.0.0D0)RETURN
      FAC=-1.0D0
      GO TO 5
      END
C*********************************************************
      FUNCTION LAG(FUNC,IC,I,SP,NI,DI,ISP)
C
C     PERFORMS INTEGRATION OF FUNC OVER (SP,INF)
C     BY GAUSSIAN INTEGRATIONS.  IF SP < 0, THEN INTEGRATES
C     OVER (SP,-INF)
C     RANGE IS SPLIT INTO NI PARTS.  (SP,SP1), (SP1,SP2), .........
C     ........, (SP(NI-1),INF)
C     THE NUMBER OF GAUSS POINTS RANGE FROM
C     MINIMUM OF 2 TO MAXIMUM OF 16
C           SP(J)=SP(J-1)+DI(J)
C           SUPPLIED BY USER TO SUIT NEED
C     Y   - GAUSS    POINTS ARRAY LESS ALL ZEROS
C     V   - GAUSS    WEIGHTS ARRAY WITH THE ADDITION OF
C     VZ  - GAUSS    WEIGHTS ARRAY WHEN CORRESPONDING POINTS ARE 0.0D0
C     JRG - POINTER TO Y AND V
C     JZ  - POINTER TO VZ
C
      IMPLICIT REAL*8(A-H,L,O-Z)
      DIMENSION JRG(12),JZ(11),ID(5),V(39),Y(39),VZ(4),DD(80),E(5),DI(1)
      DATA JRG/1,2,3,5,7,10,13,17,21,26,32,40/
      DATA JZ/5,1,5,2,5,3,5,4,5,5,5/
      DATA Y/0.5773502691896260,0.7745966692414830,0.8611363115940530
     +      ,0.3399810435848560,0.9061798459386640,0.5384693101056830
     +      ,0.9324695142031520,0.6612093864662650,0.2386191860831970
     +      ,0.9491079123427590,0.7415311855993940,0.4058451513773970
     +      ,0.9602898564975360,0.7966664774136270,0.5255324099163290
     +      ,0.1834346424956500,0.9681602395076260,0.8360311073266360
     +      ,0.6133714327005900,0.3242534234038090,0.9739065285171720
     +      ,0.8650633666889850,0.6794095682990240,0.4333953941292470
     +      ,0.1488743389816310,0.9815606342467190,0.9041172563704750
     +      ,0.7699026741943050,0.5873179542866170,0.3678314989981800
```

```
     +      ,0.12523340851146900,0.98940093499165000,0.94457502307323300
     +      ,0.86563120238703200,0.75540440835500300,0.61787624402644000
     +      ,0.45801677765722700,0.28160355079260000,0.09501250933763700/
      DATA V/1.0D0              ,0.55555555555556000,0.34785485137454000
     +      ,0.65214515406254600,0.23692688505618900,0.47862867049936600
     +      ,0.17132449237917000,0.36076157304813900,0.46791393457269100
     +      ,0.12948496616887000,0.27970539148927700,0.38183005050511900
     +      ,0.10122853629037600,0.22238103445337400,0.31370664587788700
     +      ,0.36268378337036200,0.08127438836157400,0.18064816069405700
     +      ,0.26061069640293500,0.31234707704000300,0.06667134430868000
     +      ,0.14945134915058100,0.21908636251598200,0.26926671930999600
     +      ,0.29552422471475300,0.04717533638651200,0.10693932599531800
     +      ,0.16000328543346000,0.20316742672306600,0.23349253653835500
     +      ,0.24914704581340300,0.02715245941175400,0.06225352393864800
     +      ,0.09515851168249300,0.12462897125553400,0.14959598816577000
     +      ,0.16915651939500300,0.18260341504492400,0.18945061045507000/
      DATA VZ/0.88888888888889D0,0.56888888888888D0,
     +       ,0.47795918367346900,0.33023935500126000/
      SGN=1.0D0
      IF(ISP.EQ.1)SGN=DSIGN(1.0D0,SP)
      SV=SP
      IC=0
      DO 5 I=1,NI
    5 DD(I)=DI(I)
      KL=1
      KLS=1
      IS=1
      IL=NI
      GSD=0.0D0
   10 JS=1
      JP=0
      JML=1
      DO 55 I=IS,IL
      A=SP
      B=SP+DD(I)*SGN
      Q=0.5D0*(B+A)
      P=Q-A
      TB=0.0D0
      IB=0
      DO 25 J=JS,11
      GD=0.0D0
      JF=JRG(J)
      JL=JRG(J+1)-1
      JM=JZ(J)
      DO 15 K=JF,JL
      IB=IB+2
      PY=P*Y(K)
   15 GD=GD+V(K)*(FUNC(Q-PY)+FUNC(Q+PY))
      IF(JM.EQ.5)GO TO 20
      GD=GD+VZ(JM)*FUNC(Q)
      IB=IB+1
   20 TA=GD*P
      IF(DABS((TA-TB)/TA).LT.0.5D-3)GO TO 35
   25 TB=TA
```

```
      PRINT 30,I,TA
   30 FORMAT(' ','MAX',I2,'VAL',D10.3)
      ID(KL)=I
      E(KL)=A
      KL=KL+1
      GO TO 42
   35 GSA=GSB+TA
      IC=IC+IB
      IF(I.LT.15)GO TO 40
      IF(DABS((GSA-GSB)/GSA).LT.2.0D-3)GO TO 60
   40 GSB=GSA
   42 JT=J-JML
      IF(JT)45,47,50
   45 JS=J-3
      IF(JT.LT.-1)JS=J-2
      GO TO 52
   47 JS=J-3
      IF(JT.EQ.JP)JS=J-2
      GO TO 52
   50 JS=J+JT-2
      IF(JT.GT.2)JS=J+1
   52 JP=JT
      JML=J
      IF(JS.LT.1)JS=1
      IF(JS.GT.10)JS=10
   55 SP=B
   60 CONTINUE
      IF(KLS.EQ.KL)GO TO 70
      IP=ID(KLS)
      SP=E(KLS)
      DS=DD(IP)/1.0D1
      IS=I
      IL=I+9
      KLS=KLS+1
      DO 65 JJ=IS,IL
   65 DD(JJ)=DS
      GO TO 10
   70 LAG=GSA
      SP=SV
      RETURN
      END
C*******************************************************
      FUNCTION FUNCA(U)
C
C     INTEGRAL ALONG THE BRANCH CUT BEFORE WAVE ARRIVAL
C     U  -  ARGUMENT SUPPLIED BY FUNCTION LAG, REAL PART OF PSI
C
      IMPLICIT REAL*8(A-H,O-Z)
      COMMON /CMA/ RM,R,B,A,X /CMC/ MW
      PF=1.0D0
      GA=DSQRT(U*U-1.0D0)
      GB=DSQRT((U-RM)**2-1.0D0)
      IF(U.LT.-1.0D0)GA=-GA
      IF(U.LT.RM-1.0D0)GB=-GB
```

```
      GAB=GA*GB
      FP=(1.0D0+GAB)*GAB
      SP=(GA-GB)*(1.0D0-3.0D0*GAB)/FP
      IF(NW.EQ.2)PF=U*SP/8.0D0
      TP=U*(U-RM)/(GA+GB)
      SD=TP*SP/(1.0D0+GAB)
      IF(NW.EQ.1)TD=TP*(GB/R-GA/B)/FP
      IF(NW.EQ.3)TD=TP*GA/U*(3.0D0*GB+GA/B)/FP
      AM=SP*(X+GB*(1.0D0-B)-A*U)/8.0D0
      IF(NW.NE.3)AM=AM+SP*GA*(R-1.0D0)/8.0D0
      FUNCA=-(SD+TD)*DEXP(AM)*PF
      RETURN
      END
C*****************************************************
      FUNCTION FUNCB(V)
C
C     INTEGRAL ALONG THE BRANCH CUT AFTER WAVE ARRIVAL
C     V  -   ARGUMENT SUPPLIED BY FUNCTION LAG, IMAGINARY PART OF PSI
C     USP-   U0, STARTING POINT, REAL PART
C     FCR-   0 FOR PHIA, -1 FOR PHIB
C     FCI-  -1 FOR PHIA,  0 FOR PHIB
C
      IMPLICIT REAL*8(A,B,D-H,O-Y), COMPLEX*16(C,Z)
      COMMON /CMA/ RM,R,B,A,X /CMB/ USP,FCR,FCI /CMC/ NW
      ZPF=DCMPLX(1.0D0,0.0D0)
      ZFAC=DCMPLX(FCR,FCI)
      Z=DCMPLX(USP,V)
      IF(V.EQ.0.0D0)GO TO 10
      ZA=CDSQRT(Z*Z-1.0D0)
      ZB=CDSQRT((Z-RM)**2-1.0D0)
      IF(DIMAG(ZA).LT.0.0D0)ZA=-ZA
      IF(DIMAG(ZB).LT.0.0D0)ZB=-ZB
    5 ZAB=ZA*ZB
      ZFP=(1.0D0+ZAB)*ZAB
      ZSP=(ZA-ZB)*(1.0D0-3.0D0*ZAB)/ZFP
      IF(NW.EQ.2)ZPF=Z*ZSP/8.0D0
      ZTP=Z*(Z-RM)/(ZA+ZB)
      ZSD=ZTP*ZSP/(1.0D0+ZAB)
      IF(NW.NE.3)ZTD=ZTP*(ZA/B-ZB/R)/ZFP
      IF(NW.EQ.3)ZTD=-ZTP*ZA/Z*(3.0D0*ZB+ZA/B)/ZFP
      ZAM=ZSP*(X+ZB*(1.0D0-B)-A*Z)/8.0D0
      IF(NW.NE.3)ZAM=ZAM+ZSP*ZA*(R-1.0D0)/8.0D0
      FUNCB=DREAL(ZFAC*(ZSD-ZTD)*CDEXP(ZAM)*ZPF)
      RETURN
   10 FB=DSQRT((USP-RM)**2-1.0D0)
      IF(U.LT.RM-1.0D0)FB=-FB
      ZB=DCMPLX(FB,0.0D0)
      IF(DABS(USP).LT.1.0D0)GO TO 15
      FA=DSQRT(USP*USP-1.0D0)
      IF(U.LT.-1.0D0)FA=-FA
      ZA=DCMPLX(FA,0.0D0)
      GO TO 5
   15 FA=DSQRT(1.0D0-USP*USP)
      ZA=DCMPLX(0.0D0,FA)
```

```
      GO TO 5
      END
C*************************************************
      SUBROUTINE SELECT(M,XM,K)
C
C     PROGRAM FINDS THE ROOT EXTERIOR OF CF0 OR CG0
C
      IMPLICIT REAL*8(A-H,O-Z)
      DIMENSION XM(4),XN(4)
      COMMON /CRC/ JS
      IF(M.EQ.1)GO TO 30
      DO 5 I=1,M
    5 XN(I)=DABS(XM(I))
      GO TO (30,10,15,20), M
   10 XN(3)=0.0D0
   15 XN(4)=0.0D0
   20 X=DMAX1(XN(1),XN(2),XN(3),XN(4))
      IF(JS.EQ.1)X=DMIN1(XN(1),XN(2))
      DO 25 K=1,4
      IF(X.EQ.XN(K))RETURN
   25 CONTINUE
   30 K=1
      RETURN
      END
C*************************************************
      FUNCTION ZERO(F,AX,BX,TOL,EPS)
C
C     PROGRAM FINDS THE ZERO OF A FUNCTION F
C
      IMPLICIT REAL*8(A-H,O-Z)
      A = AX
      B = BX
      FA = F(A)
      FB = F(B)
      IF(DSIGN(1.0D0,FA).NE.DSIGN(1.0D0,FB))GO TO 20
      ZERO=A
      RETURN
   20 C=A
      FC = FA
      D = B - A
      E = D
   30 IF (DABS(FC) .GE. DABS(FB)) GO TO 40
      A = B
      B = C
      C = A
      FA = FB
      FB = FC
      FC = FA
   40 TOL1 = 2.0D0*EPS*DABS(B) + 0.5D0*TOL
      XM=0.5D0*(C-B)
      IF (DABS(XM) .LE. TOL1) GO TO 90
      IF (FB .EQ. 0.0D0) GO TO 90
      IF (DABS(E) .LT. TOL1) GO TO 70
      IF (DABS(FA) .LE. DABS(FB)) GO TO 70
```

```
      IF (A .NE. C) GO TO 50
      S = FB/FA
      P = 2.0D0*XM*S
      Q = 1.0D0 - S
      GO TO 60
   50 Q = FA/FC
      R = FB/FC
      S = FB/FA
      P = S*(2.0D0*XM*Q*(Q - R) - (B - A)*(R - 1.0D0))
      Q = (Q - 1.0D0)*(R - 1.0D0)*(S - 1.0D0)
   60 IF (P .GT. 0.0D0) Q = -Q
      P = DABS(P)
      IF ((2.0D0*P) .GE. (3.0D0*XM*Q - DABS(TOL1*Q))) GO TO 70
      IF (P .GE. DABS(0.5D0*E*Q)) GO TO 70
      E = D
      D = P/Q
      GO TO 80
   70 D = XM
      E = D
   80 A = B
      FA = FB
      IF (DABS(D) .GT. TOL1) B = B + D
      IF (DABS(D) .LE. TOL1) B = B + DSIGN(TOL1, XM)
      FB = F(B)
      IF ((FB*(FC/DABS(FC))) .GT. 0.0D0) GO TO 20
      GO TO 30
   90 ZERO=B
      RETURN
      END
C*********************************************************
      SUBROUTINE QUARTI (C,XR,XI)
C
C     PROGRAM FINDS ROOTS OF QUARTIC EQUATION
C     C(1) + C(2)*X + C(3)*X**2 + C(4)*X**3 + C(5)*X**4 = 0
C     REAL PARTS OF ROOTS ARE PLACED IN XR, IMAGINARY PARTS IN XI.
C
      IMPLICIT REAL*8 (A-H,O-Z)
      DIMENSION C(5), XR(4), XI(4), CU(5), YR(4), YI(4)
      Z=C(5)
      IF(Z.NE.0.0D0)GO TO 20
      CALL CUBIC(C,XR,XI)
      XR(4)=0.0D0
      XI(4)=0.0D0
      RETURN
   20 XI(1)=0.0D0
      XI(3)=0.0D0
      CU(5)=0.0D0
      CU(4)=1.0D0
      CU(3)=-C(3)/Z
      A0=C(1)/Z
      A12=C(2)/Z*0.5D0
      A32=C(4)/Z*0.5D0
      CU(2)=    (A32*A12-A0)*4.0D0
      CU(1)=    -(A12**2+A0*(A32**2+CU(3)))*4.0D0
```

```
      CALL CUBIC(CU,YR,YI)
      DO 40 I=1,3
      U12=   YR(I)*0.5D0
      T1=U12**2-A0
      IF(T1.LT. 0.0D0)GO TO 40
      T2=A32**2+U12+U12+CU(3)
      IF (T2.GE.0.0D0)GO TO 50
   40 CONTINUE
      XI(1)=-100.0D0
      RETURN
   50 T1=DSQRT(T1)
      T2=DSIGN(DSQRT(T2),A32*U12-A12)
   60 CQ=U12-T1
      BQ2=    (A32-T2)*0.5D0
      DISC=BQ2**2-CQ
      IF (DISC) 90, 80, 70
   70 DISC=DSQRT(DISC)
   80 XR(1)=-BQ2+DISC
      XR(2)=-BQ2-DISC
      GO TO 100
   90 XR(1)=-BQ2
      XR(2)=-BQ2
      XI(1)=DSQRT(-DISC)
  100 CQ=U12+T1
      BQ2=BQ2+T2
      DISC=BQ2**2-CQ
      IF (DISC) 130, 120, 110
  110 DISC=DSQRT(DISC)
  120 XR(3)=-BQ2+DISC
      XR(4)=-BQ2-DISC
      GO TO 150
  130 XR(3)=-BQ2
      XR(4)=-BQ2
      XI(3)=DSQRT(-DISC)
  150 XI(2)=-XI(1)
      XI(4)=-XI(3)
      RETURN
      END
C*************************************************
      SUBROUTINE CUBIC(C,XR,XI)
C
C     PROGRAM FINDS ROOTS OF CUBIC EQUATION
C     C(1) + C(2)*X + C(3)*X**2 + C(4)*X**3 = 0
C     REAL PART OF ROOTS ARE PLACED IN XR, IMAGINARY PART IN XI.
C
      IMPLICIT REAL*8 (A-H,O-Z)
      DIMENSION C(5),XR(4),XI(4)
      A=3.0D0
      Z=C(4)*3.0D0
      IF(Z.NE.0.0D0)GO TO 20
      XR(3)=0.0D0
      XI(3)=0.0D0
      C3=    C(3)*2.0D0
      CC=C(2)**2-    C(1)*C(3)*4.0D0
```

```
      IF(CC)10,50,90
   10 SC=DSQRT(-CC)
      XI(1)=SC/C3
      XI(2)=-XI(1)
      XR(1)=-C(2)/C3
      XR(2)=XR(1)
      RETURN
   50 XR(1)=-C(2)/C3
      XR(2)=0.0D0
  110 XI(1)=0.0D0
      XI(2)=0.0D0
      RETURN
   90 XR(1)=(-C(2)+DSQRT(CC))/C3
      XR(2)=(-C(2)-DSQRT(CC))/C3
      GO TO 110
   20 XI(1)=0.0D0
      XI(2)=0.0D0
      P3=C(3)/Z
      Q3=C(2)/Z
      PQ18=Q3*P3*0.5D0
      R2=C(1)*1.5D0/Z
      AMIN3=P3**2-Q3
      B2=AMIN3*P3-PQ18+R2
      DISC=B2**2-AMIN3**3
      IF (DISC) 80, 40, 30
   30 DISC=DSQRT(DISC)
   40 B2D=-B2+DISC
      SI=DSIGN(1.0D0,B2D)
      CAPA=SI*DABS(B2D)**(1.0D0/3.0D0)
      IF (CAPA.NE.0.0D0)GO TO 60
      CAPB=(-B2-B2)**(1.0D0/3.0D0)
      GO TO 70
   60 CAPB=AMIN3/CAPA
   70 XR(1)=CAPA+CAPB-P3
      XR(2)=-(CAPA+CAPB)*0.5D0-P3
      XR(3)=XR(2)
      XI(2)=DSQRT(A )    *(CAPA-CAPB)*0.5D0
      GO TO 100
   80 ROOT=DSQRT(AMIN3)
      PHI3=DARCOS(-B2/(ROOT*AMIN3))/3.0D0
      T1=DSQRT(A )*DSIN(PHI3)
      T2=DCOS(PHI3)
      XR(1)=T2*ROOT*2.0D0-P3
      XR(2)=ROOT*(-T2-T1)-P3
      XR(3)=ROOT*(-T2+T1)-P3
  100 XI(3)=-XI(2)
      RETURN
      END
```

REFERENCES

1. Abramowitz, M., and Stegun, I. A., "Handbook of Mathematical Functions," National Bureau of Standards, 1965.

2. Bachelor, G. K., and Gill, A. E., "Analysis for the Stability of Axisymmetric Jets," J. Fluid Mech., 1962, 14, pp. 529-551.

3. Chao, C. C., "Transmitted Sound Field Due to an Impulsive Line or Point Source Through a Plane Vortex Sheet," AIAA 4th Aeroacoustics Conference, 1977.

4. Crighton, D. G., "Radiation Properties of the Semi-Infinite Vortex Sheet," Proc. R. Soc., A 330, 1972, p. 185.

5. Crighton, D. G. and Leppington, F. G., "Radiation Properties of the Semi-Infinite Vortex Sheet: The Initial-Value Problem" J. Fluid Mech., 64, 1974, pp. 393-414.

6. Crow, S. C. and Champagne, F. H., "Orderly Structure in Jet Turbulence," J. Fluid Mech., 1971, 48(3), pp. 547-591.

7. Erdelyi, A. (Editor), "Tables of Integral Transforms," Bateman Manuscript Project, Vol. II, p. 134, McGraw-Hill, 1954.

8. Ffowcs Williams, J. E., "Aeroacoustics," Ann. Rev. Fluid Mech., 1977. pp. 447-468.

9. Friedland, A. B. and Pierce, A. D., "Reflection of Acoustic Pulses from Stable and Instable Interfaces Between Moving Fluids," The Physics of Fluids, 1969, Vol. 12, No. 6, pp. 1148-1159.

10. Graham, E. W. and Graham, B. B., "Effect of a Shear Layer on Plane Waves of Sound in a Fluid," J. Acoust. Soc. Am., 1968, 46, pp. 169-175.

11. Hardisty, N., "The Instability of Two Vortex Sheets Enclosing a Subsonic Jet Due to an Acoustic Point Source," Proc. R.S.E. (A), 71, 12, 1972/73, pp. 141-149.

12. Hardisty, N., "The Instability of Two Vortex Sheets Enclosing a Subsonic Jet Due to an Acoustic Point Source," Proc. R.S.E. (A), 73, 13, 1974/75, pp. 215-229.

13. Howe, M. S., "Transmission of an Acoustic Pulse Through a Plane Vortex Sheet," J. Fluid Mech., 1970, 43(2), pp. 353-367.

14. Jones, D. S. and Morgan, J. D., "The Instability Due to Acoustic Radiation Striking a Vortex Sheet on a Supersonic Stream," Proc. R.S.E. (A), 71, 11, 1972/73, pp. 121-140.

15. Jones, D. S. and Morgan, J. D., "The Instability of a Vortex Sheet on a Subsonic Stream under Acoustic Radiation," Proc. Camb. Phil. Soc., 1972, 72, pp. 465-488.

16. Jones, D. S., "The Reflexion of an Acoustic Pulse by a Plane Vortex Sheet," Proc. Camb. Phil. Soc., 1973, 74, pp. 349-364.

17. Jones, D. S., "The Scattering of Sound by a Simple Shear Layer," Phil. Trans. Roy. Soc., 1977, A 284, pp. 287-328.

18. Koutsoyannis, S. P., "Characterization of Acoustic Disturbances in Linearly Sheared Flows," J. Sound and Vibration, 1980, 68(2), pp. 187-202.

19. Landau, L., "Stability of Tangential Discontinuities in Compressible Fluid," Comptes Rendus (Doklady) de l'Academie des Sciences de l'URSS, 1944, Vol. XLIV, No. 4, pp. 139-141.

20. Lighthill, M. J., "On Sound Generated Aerodynamically. I. General Theory," Proc. R. Soc. Lond., A 211, pp 564-587.

21. Lush, P. A., "Measurements of Subsonic Jet Noise and Comparison with Theory," J. Fluid Mech., 1971, 46(3), pp. 477-500.

22. Mani, R., "A Moving Source Problem Relevant to Jet Noise," J. Sound and Vibration, 1972, 25(2), pp. 337-347.

23. Miles, J. W., "On the Reflection of Sound at an Interface of Relative Motion," J. Acoust. Soc. Am., 1957, 29, pp. 226-228.

24. Miles, J. W., "On the Disturbed Motion of a Plane Vortex Sheet," J. Fluid Mech., 1958, 4, pp. 538-552.

25. Miura, T., "Transmitted Sound Field due to an Impulsive Line Acoustic Source Bounded by a Rigid Plate Followed by a Vortex Sheet," Ph. D. Thesis, Stanford University, 1979.

26. Morgan, J. D., "The Interaction of Sound with a Subsonic Cylindrical Vortex Layer," Proc. R. Soc. Lond., A 344, 1975, pp. 341-362.

27. Munt, R. M., "The Interaction of Sound with a Subsonic Jet Issuing from a Semi-Infinite Cylindrical Pipe," J. Fluid Mech., 1977, 83(4), pp. 609-640.

28. Ribner, H. S., "Reflection, Transmission, and Amplification of Sound by a Moving Medium," J. Acoust. Soc. Am., 1957, 29, pp. 435-441.

29. Tam, C. K. W., "Directional Acoustic Radiation from a Supersonic Jet Generated by Shear Layer Instability," J. Fluid Mech., 1971, 46(4), pp. 757-768.

30. Watson, G. N., "A Treatise on the Theory of Bessel Functions," Cambridge University Press, 2nd Edition, 1958.